Theoretical Investigation of Ultrafast Energy Transport in Polymer Chains

An Abstract
Submitted On The Fourth Day of August, 2016
To The Department Of Chemistry
Of The Graduate School Of
Tulane University
In Partial Fulfillment Of The Requirements
For The Degree Of
Doctor Of Philosophy
By

Arkady A. Kurnosov

Approved:

Alexander Burin, Ph. D.
Chairman

Igor Rubtsov, Ph. D.

Michael Herman, Ph. D.

Russell Schmehl, Ph. D.

Abstract

In the present study a few approaches are developed for theoretical investigation of vibrational energy propagation in highly ordered polymers and linear atomic chains. Density matrix formalism applied to explain the transition between ballistic and diffusive regimes in polymers, the diffusive and ballistic regimes of energy transport are described in terms of asymptotic limits of exact solution of Liouville-Bloch equation. Energy bands theory is developed for oligomeric structures such as perfluoroalkane and alkane compounds, as an example, practical application for understanding experimental data for alkane is discussed. Also, purely electronic torsional mode in linear atomic chains, such as cumulene, is considered. The speed of up to 1000 km/s for electronic sound is predicted, the spectrum of quanta (*torsitons*) of torsional electronic mode in cumulene is obtained.

Theoretical Investigation of Ultrafast Energy Transport in Polymer Chains

A Dissertation
Submitted On The Fourth Day of August, 2016
To The Department Of Chemistry
Of The Graduate School Of
Tulane University
In Partial Fulfillment Of The Requirements
For The Degree Of
Doctor Of Philosophy
By

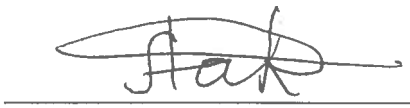

Arkady A. Kurnosov

Approved: 

Alexander Burin, Ph. D.
Chairman

Igor Rubtsov, Ph. D.

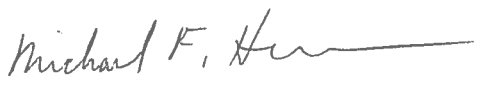

Michael Herman, Ph. D.

Russell Schmehl, Ph. D.

Acknowledgments

It is my pleasure to use this opportunity to thank my research adviser Dr. Alexander Burin for his support, encouragement and patience throughout my graduate studies, and also for his hospitality, especially during my first year of the program, especially in the middle of the unusually cold for New Orleans winter of 2009–2010.

I would like to thank Prof. Igor Rubtsov for being my unofficial second adviser and for creating a friendly environment of scientific discussion and interaction with theoreticians in his experimental group.

I express my thanks to Prof. Herman for his interest in my research and readiness to find time to help despite a busy schedule. Also, I'm very grateful to Prof. Russel Schmehl for accepting a membership on my dissertation committee and carefully reading my work despite very late notice.

I also appreciate a company of my fellow grad students in the Chemistry Department and my co-authors, Andrii Maksymov, Layla Qasim, Joel Ledger, Robert Mackin, Dr. Natalia Rubtsova, and Ross Zaenglein.

And the most important acknowledgment is to my parents, who have always encouraged my curiosity in science since kindergarten.

This work was supported by the National Science Foundation (CHE-1462075).

Contents

Introduction **1**

1 Quantum mechanical description of vibrational energy transport through highly ordered polymer chains. Liouville-Bloch equation. **3**

1.1 Overview 3

1.2 The model and solution 5

1.3 Discussion 9

2 Electronic torsional mode in linear polymers. **16**

2.1 Overview 16

2.2 The system 20

2.3 Electronic torsional mode 20

2.4 Electronic moment of inertia 23

2.5 Torsional stiffness calculation 25

2.6 Quantum mechanical approach 26

2.7 Effect of zero-point atomic vibrations 32

2.8 Experiment suggestions 35

2.9 Conclusion 36

3 Vibrational energy bands in oligomers **37**

3.1 Overview 37

3.2 Dispersion equation 38

3.3 Special solutions of the dispersion equation. Acoustic bands 44
3.4 Acoustic velocity 49
3.5 Long-order interaction 51
3.6 Numerical calculation of symmetry parameters 52
3.7 Energy bands theory application for ballistic energy transport in alkane oligomers 54
3.8 Conclusion 58

Appendices **59**

A Derivations for the Liouville-Bloch equation **60**

A.1 White noise in the quantum Liouville - Bloch equation 60
A.2 Derivation of the exact solution 65
A.2.1 General approach 65
A.2.2 Purely ballistic transport 68
A.2.3 Purely Diffusive transport (approximate solution) 69
A.2.4 Diffusive transport (exact solution) 70
A.3 Asymptotic limits of the solution 73
A.3.1 Ballistic component 73
A.3.2 Diffusive component 78

B Derivations for electronic sound through cumulene chain **81**

B.1 Derivation of the hydrogen torsional mode frequency as a function of molecule length 81
B.2 Zero-point atomic vibrations 85
B.2.1 Analytical derivation of energy correction 85
B.2.2 Numerical estimate of the gap 89

List of Figures

1.1 Log – Log representation of T_{max} vs distance 11

1.2 Log - Log representation of P_{max} vs distance 12

1.3 T_{max} vs decoherence rate 13

1.4 P_{max} vs decoherence rate 15

2.1 Carbyne modifications: (a) cumulene; (b) polyyne 18

2.2 Cumulene molecule torsionally strained along primary axis 19

2.3 Linear density of the electronic inertia moment 24

2.4 Frequency of the torsional mode vs molecule length 27

2.5 Energy of the 1st excited state 30

2.6 A schematic experiment set up 36

3.1 Perfluoroalkane chain 39

3.2 Alkane chain 55

3.3 Optical energy bands in alkane chain 57

A.1 Bessel function approximation 74

A.2 Log-Log representation of Bessel function maximum 76

List of Tables

1.1 Characteristics of three vibrational energy transport regimes 14

B.1 The list of frequencies and the third-order anharmonic constants for H_2=C_5=H_2 91

Introduction

The development of new materials with unique energy transport landscapes has attracted broad interest. Nanomaterials, such as nanowires [1, 2], layered semiconductor structures [3], nanocomposites, and self-assembled monolayer junctions [4–7] featuring controlled thermal conductivity, have been designed. The thermal conductivity of ordered polyethylene fibers exceeds that of many pure metals [8, 9] whereas disordered polyethylene is a poor thermal conductor. Because of their low density, oligomeric materials are attractive candidates for energy dissipation in molecular electronics devices [10]. Nanostructured materials often consist of several components, and the energy transport within each component and between them has to be understood. Detailed knowledge of the energy transport properties can lead to optimization of reaction rates and to finding ways of controlling such reactions [11–13].

Two mechanisms, ballistic and diffusive, describe the limiting regimes of the vibrational energy transport. Diffusive energy transport involves Brownian-like energy exchange steps and was observed in numerous molecular compounds including peptides, helices, and small molecules [14–17]. Ballistic energy transport involves free propagation of the vibrational wave packet and can be very fast and efficient [10, 18–21]. It requires vibrational states delocalized over the region of transport; thus, it benefits from having an ordered oligomeric molecular structure.

In the present work we develop some theoretical methods and approaches to investigation of vibrational energy transport in ordered oligomeric structures and linear atomic chains.

In Chapter 1 we consider ballistic and diffusive vibrational energy transport and crossover between those two regimes using density matrix quantum formalism. We introduce a model, solve Liouville – Bloch equation, and show how its solution and asymptotic limits correspond to different energy propagation regimes. Most of the results of Chapter 1 have been published in Ref. [22]: "Arkady A. Kurnosov, Igor V. Rubtsov, Alexander L. Burin, Communication: Fast transport and relaxation of vibrational energy in polymer chains, *J. Chem. Phys*, 142, 011101 (**2015**)".

In Chapter 2 we consider purely electronic torsional sound in cumulene chains. The results of Chapter 2 have been recently published in Ref. [23]: "Arkady A. Kurnosov, Igor V. Rubtsov, Andrii O. Maksymov, Alexander L. Burin, Electronic torsional sound in linear atomic chains: chemical energy transport at 1000 km/s, *J Chem Phys*, 145, 034903 (**2016**)".

In Chapter 3 we apply semi-classical approach based on oligomer structure and DFT-calculations, develop energy bands theory and determine speed of energy transport as group velocity of different modes. Application for alkane chain [20] is also discussed.

Some detailed derivations for Chapters 1, 2 can be found in Appendices A and B respectively.

Chapter 1

Quantum mechanical description of vibrational energy transport through highly ordered polymer chains. Liouville-Bloch equation.

1.1 Overview

The transport on a molecular scale is usually associated with coherent and incoherent mechanisms. The coherent transport is characterized by energy and phase conservation and absence of environment disturbance. In the event of semi-classical motion with no under-barrier tunneling such transport also can be called a *ballistic* transport. Both coherent and incoherent transport and transition between them have been a long term focus for the scientific community. Such transitions were studied for electronic, [2, 24, 25] exciton [26, 27] and, more recently, vibrational energy transport [16, 19, 28–32].

In the *ballistic* regime, the energy is transferred via a free-propagating vibrational wavepacket, formed by vibrational states delocalized over the whole transport

region; such transport can be very efficient and fast [8, 9]. The *ballistic* transport can be expected in polymeric molecules composed of nearly identical units, where the normal modes are formed by superposition of many excited monomer states; otherwise the *diffusive* mechanism is mostly prevalent.

The *diffusive* energy transport is a result of intramolecular *vibrational energy redistribution* (IVR), which involves energy hopping between vibrational states. Diffusive transport is expected to occur in molecules lacking periodic structure [33] with the normal modes localized at the length comparable to inter-atomic distances. A single IVR event, serving as a driving force of *diffusive* energy transport, is characterized by a change of three or more quantum numbers of the involved spatially overlapping vibrational modes, and requires anharmonic coupling of these modes.

In oligomers normal vibrational modes can be substantially delocalized because of the translational symmetry. Therefore one can expect observing *ballistic* transport in such systems. Indeed, this transport has been observed in bridged azulene-anthracene compounds,[29] polyethylene glycol oligomers,[32] alkanes [31] and perfluoroalkanes [16] and the theory describing it has been suggested [18, 34, 35].

In Ref. [36] energy transport via highly ordered perfluoroalkane chains was studied by a relaxation-assisted two-dimensional infrared spectroscopy method [37, 38]. *Ballistic* transport with a speed of 385 m/s was found and the transport time showed strong temperature dependence.[36] To interpret the observations, the authors developed a simple model describing the *ballistic* transport and its decoherence caused by dynamic fluctuations of the environment. The strong temperature dependence has been interpreted by assuming that the transition from the *ballistic* regime to the *diffusive* regime takes place with the temperature increase.

In this study we describe the model for the *ballistic* transport and decoherence in greater detail and derive its analytical solution in the space-time representation

extending the earlier results of Haken and Strobl [26] and Schwartzer [27] to the practical regime of interest [8, 9, 16, 18, 33–36]. To the best of our knowledge the solution of the problem within the space-time representation has never been reported.

Then we consider asymptotic limits that describe different transport mechanisms, including *ballistic*, *diffusive* and *directed diffusive* regimes, as well as the crossovers between them.

Most of the results of this chapter were published in Ref. [22]. For reader's convenience most of the corresponding mathematical derivations are placed in Appendix A.

1.2 The model and solution

Consider a polymer chain composed of N identical monomers with the only one relevant vibrational mode (for example C-F stretching or F-F bending modes in perfluoroalkanes) on each site forming an optical phonon band. The Hamiltonian can be expressed as

$$\hat{\boldsymbol{\mathcal{H}}} = \sum_{m=1}^{N} \hbar\omega_m \hat{b}_m^\dagger \hat{b}_m + \frac{\hbar\Delta}{2} \sum_{m=1}^{N-1} \left(\hat{b}_m^\dagger \hat{b}_{m+1} + \hat{b}_m \hat{b}_{m+1}^\dagger \right) \tag{1.1}$$

where ω_m is the average vibration frequency on the m-th site and Δ is the coupling of the neighboring sites. We assume that the average site frequencies are the same for each site,

$$< \omega_m >= \omega_0 \tag{1.2}$$

and their fluctuations are delta-correlated:

$$< \delta\omega_m(t_1)\delta\omega_n(t_2) >= \frac{W}{2}\delta_{mn}\delta(t_1 - t_2) \tag{1.3}$$

where δ_{mn} is the Kronecker delta. The assumption of Eq. (1.2) is justified by the high ordering of perfluoroalkane chains. The assumption of Eq. (1.3) is the standard approximation, which treats the site frequencies as uncorrelated, while introducing the decoherence rate of $W/2$ for each site [26, 39, 40].

We consider the low temperature case, $k_B T \ll \hbar\omega$, so that the thermal excitations of vibrational states can be neglected and the only excitation in the chain is caused by an external laser pulse. The time evolution of this excitation can be described in terms of the density matrix ρ_{mn}. The density matrix satisfies the quantum *Liouville - Bloch equation* [26, 27, 40]

$$\frac{\partial \boldsymbol{\rho}}{\partial t} = -\frac{i}{\hbar}\left[\hat{\boldsymbol{\mathcal{H}}}, \boldsymbol{\rho}\right] - \hat{\boldsymbol{\mathcal{W}}}\boldsymbol{\rho} - \gamma\boldsymbol{\rho} \tag{1.4}$$

$$\left(\hat{\boldsymbol{\mathcal{W}}}\boldsymbol{\rho}\right)_{mn} = W(1-\delta_{mn})\rho_{mn} \tag{1.5}$$

where W is the decoherence for all off-diagonal elements and γ stands for the pure dissipation rate, e. g. relaxation to the solvent.[1] We assume that the decoherence rate is much larger than the dissipation rate. This agrees with the experimental data analysis [36] and common sense expectation, because the decoherence comes from the energy fluctuations while the dissipation requires a real transition.

The probability to observe excitation on the n-th site, which is referred to as a signal intensity, is given by the diagonal density matrix element ρ_{nn}. To characterize the excitation transport we consider the simplest model of infinite chain, $N = \infty$, and assume that initially only a single site with $n = 0$ is populated, so the initial

[1]The relaxation term can be determined also by interaction with the thermal bath of low-frequency modes even without solvent.

condition is $\rho_{mn}(0) = \delta_{0m}\delta_{0n}$ and we are to solve the system of equations:

$$\frac{\partial \rho_{mn}}{\partial t} = -i\Delta\left\{\rho_{m-1n} + \rho_{m+1n} - \rho_{mn-1} - \rho_{mn+1}\right\} - (W+\gamma)\rho_{mn} + W\delta_{mn}\rho_{mn} \quad (1.6)$$

In general the white noise in off diagonal elements can also be considered. With delta correlated fluctuations of the coupling $\langle \delta\Delta_{nn+1}(t_1)\delta\Delta_{n+1n}(t_2)\rangle = (\tilde{W}/2)\delta(t_1 - t_2)$ Eq. (1.6) gains two additional terms $-2\tilde{W}(1-\delta_{mn})\rho_{mn}$ and $\tilde{W}\delta_{mn}\{\rho_{m+1m+1} - 2\rho_{mm} + \rho_{m-1m-1}\}$. The first term can be included into decoherence rate as $W \longrightarrow W + 2\tilde{W}$. The second term creates an additional diffusion channel. Since we are interested in the situation where ballistic transport is significant, this suggests $W \ll \Delta$, so that the channel with $\tilde{W}$ is not important compared to the weakly scattered coherent transport contribution and we can neglect it. The detailed derivation of how white noise in energy fluctuations leads to Eq. (1.6) can be found in Appendix A.1.

The solution of Eq. (1.6) for the diagonal elements of the density matrix can be obtained in the exact form in the continuous limit, $N \gg 1$. This limit is equivalent to evaluation of the *inverse Fourier transform* of the solution in the momentum representation obtained in Ref. [26]. Importantly this solution can be evaluated in the analytical form in the space-time representation.

Applying the *Fourier transform* and *Laplace transform* to Eq. (1.6) we can represent the density matrix in terms of its diagonal part as

$$\tilde{\rho}(p,k;z) = \frac{1 + W\tilde{P}(p-k;z)}{z + i2\Delta\left[\cos(pa) - \cos(ka)\right] + W + \gamma} \quad (1.7)$$

where $\tilde{P}(q)$ is the *Fourier transform* of the site-diagonal density matrix characterizing transport of the excitation density and a is the average distance between two adjacent monomers, and $2\Delta\cos(pa)$ describes the spectrum of optical phonons within the band. The group velocity for the specific wave vector p is given by $2a\Delta\sin(pa)$. The

maximum velocity corresponds to $p = \pi/(2a)$ and is given by $v_{max} = 2a\Delta$. We will show below that this is the actual velocity of the *ballistic* transport.

From Eq. (1.7) one can derive an expression for $\tilde{P}(q;z)$ as

$$\tilde{P}(q;z) = \frac{1}{\sqrt{[z+W+\gamma]^2 + [4\Delta\sin(qa/2)]^2} - W} \tag{1.8}$$

To obtain the probability of finding excitation on the n-th site, $P_n(t) = \rho_{nn}(t)$, we need to apply the *inverse Fourier transform* and the *inverse Laplace transform* to Eq. (1.8). Before doing that we will split Eq. (1.8) into two components, $\tilde{P} = \tilde{P}_B + \tilde{P}_D$, defined below in Eqs. (1.9) and (1.10) and discuss their physical meaning.

The first component

$$\tilde{P}_B(q;z) = \frac{1}{\sqrt{[z+W+\gamma]^2 + [4\Delta\sin(qa/2)]^2}} \tag{1.9}$$

is responsible for the *ballistic* transport. Indeed, if we consider transport to large distances so that q is small and $\sin(qa/2) \simeq qa/2$, then Eq. (1.9) corresponds to the running wavepacket with the group velocity $v = 2a\Delta$ and dumping rate $W + \gamma$. The *diffusive* part takes the form

$$\tilde{P}_D(q;z) = \frac{W\tilde{P}_B(q;z)}{\sqrt{[z+W+\gamma]^2 + [4\Delta\sin(qa/2)]^2} - W} \tag{1.10}$$

In the case of energy conservation and long distance - long time limit, it can be expressed in the form of a diffusion pole $\tilde{P}_D(q;z) \sim 1/(z+Dq^2)$, where $D = 4a^2\Delta^2/W$ is a diffusion coefficient.

The probability of finding the excitation on the n-th site is given by the exact

expression

$$P_n(t) = e^{-(W+\gamma)t}\Bigg\{ \mathrm{J}_n^2(2\Delta t) + \frac{W}{4\Delta}\Bigg[\mathrm{I}_0\left(W\sqrt{t^2 - \frac{n^2}{4\Delta^2}}\right) + \mathrm{L}_0\left(W\sqrt{t^2 - \frac{n^2}{4\Delta^2}}\right)\Bigg]\theta\left(t^2 - \frac{n^2}{4\Delta^2}\right)\Bigg\} \quad (1.11)$$

where J_n (corresponds to the *ballistic* component) is the n-th order Bessel function, I_0 and L_0 (correspond to the *diffusive* component) are the zero-order modified Bessel and Struve functions respectively [41]. The detailed derivation of Eq. (1.11) can be found in the Appendix A.2.

1.3 Discussion

To reveal how Eq. (1.11) describes *ballistic* and *diffusive* regimes we need to consider the asymptotic limits and discuss transitions between them. Experimentally and computationally, the energy transport time can be characterized by the dependence $T_{max}(n)$, which is the time required for the intensity on the n-th monomer to reach its maximum [16]. Another interesting characteristic of the energy propagation is P_{max}, which is the maximal intensity at site n taken at the time T_{max}. Though our model is discreet, it is convenient to introduce a spatial coordinate $x = na$ so that $P_n(t) \longrightarrow P(x,t)$ in the asymptotic limit. We also introduce the characteristic velocity $v = 2a\Delta$, which represents the maximum group velocity of the optical phonon. The summary of the results is given in Table 1.1. The detailed mathematical evaluation of asymptotic limits can be found in Appendix A.3.

The *ballistic* transport dominates at short times, $t < 1/(W+\gamma)$, where the decoherence can be neglected. For $n \gg 1$ it can be shown [41–44] that the Bessel function, $\mathrm{J}_n(a)$, has its first maximum at $n \approx a$ and the function amplitude $\mathrm{J}_n(n) \propto n^{-1/3}$. Then the energy transport time and the maximal intensity can be estimated

as a function of distance, x,

$$T_{max}(x) = \frac{x}{v}; \quad P_{max}(x) \propto x^{-2/3} e^{-\frac{W+\gamma}{v}x} \tag{1.12}$$

indicating that the wavepacket in the *ballistic* regime moves with the maximum group velocity (see dashed green lines in FIGs. 1.1, 1.2 and Table 1.1).

The second limit, $W^{-1} < t < \gamma^{-1}$, corresponds to the *diffusive* behavior (the *ballistic* component is suppressed exponentially in this regime, while the dissipation is still not significant). Using the expansion for the Bessel and Struve functions [41] the standard diffusive behavior can be reproduced as

$$T_{max}(x) = x^2/D; \quad P_{max}(x) \propto x^{-1} e^{-\frac{\gamma}{D}x^2} \tag{1.13}$$

where $D = v^2/W$. One can describe the transport in this regime using the time varying instantaneous velocity $\dot{x}(t) = \sqrt{D/(4t)}$. (red dotted lines in FIGs. 1.1, 1.2 and Table 1.1).

In the case of strong dissipation, $\gamma^{-1} < t$, the asymptotics changes resulting in a new regime of "directed diffusion" affected by dissipation, where the linear dependence of the energy transport time on distance is restored

$$T_{max}(x) = \frac{x}{\sqrt{2\gamma D}}; \quad P_{max}(x) \propto x^{-1/2} e^{-\frac{\tilde{v}}{D}x} \tag{1.14}$$

and $\tilde{v} = \sqrt{2\gamma D}$ is a new speed of the energy propagation. In this regime the straight transport is more efficient than the random walk because of the high chance of absorption for longer paths.

All three regimes are illustrated in FIGs. 1.1, 1.2 in a logarithmic scale. The blue solid line corresponds to the exact expression Eq. (1.11), where we set $a = 1$,

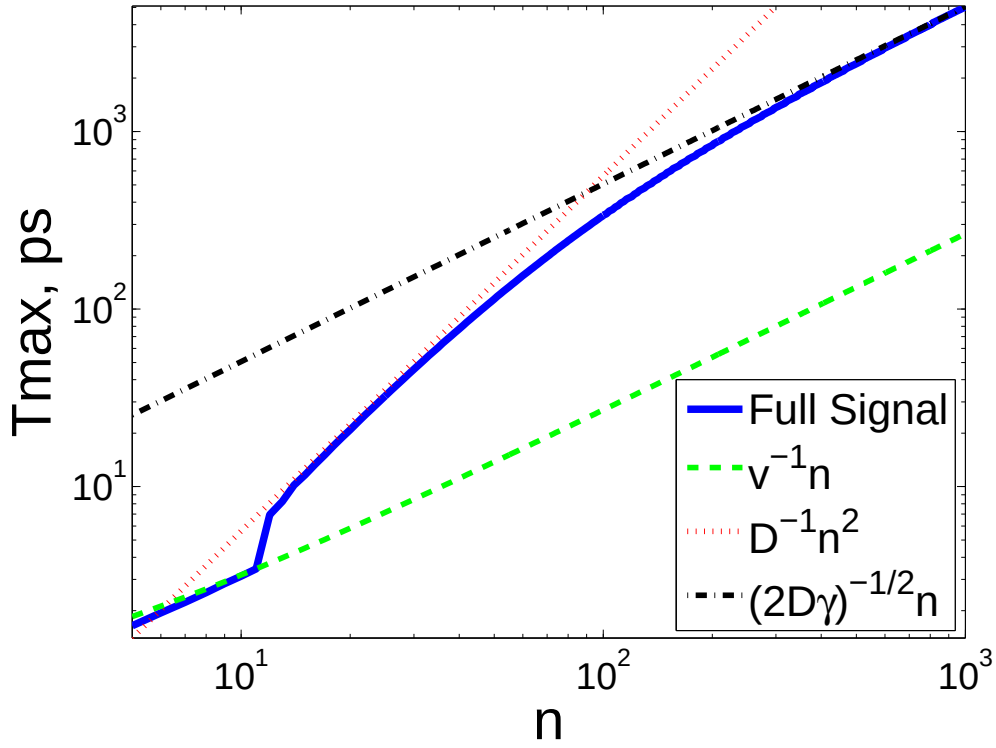

Figure 1.1: Log – Log representation of the energy transport time, T_{max}, as a function of distance expressed in site numbers with the key asymptotics from Eqs. (1.12), (1.13), (1.14), also shown in Table 1.1, associated with the *ballistic* (green dashed line), *diffusive* (red dotted line) and *directed diffusion* (black dash-dotted line) regimes, respectively. $\Delta = 10$ cm^{-1}, $W = 0.8$ ps^{-1}, $\gamma = 0.001$ ps^{-1}.

$\alpha = [\gamma/(4\pi^2 D)]^{1/4}$, $\beta = \tilde{v}/(2D)$, $\lambda = (2/9)^{1/3}/\Gamma(2/3)$. The selection of the coupling, $\Delta = 10$ cm^{-1}, while somewhat arbitrary, provides qualitative agreement with the experimental data of Ref. [36]. Different W and γ parameters were selected for convenience of illustrating clearly the transitions between the regimes (1 cm^{-1} $\sim$ 0.19 ps^{-1}). It is interesting to analyze how the energy transport time depends on the decoherence rate, W (Fig. 1.3). The dissipation rate does not affect the transition between the *ballistic* and *diffusive* regimes, as long as $\gamma \ll W$, while at $\gamma \sim W$ the transition becomes smooth. For the sake of simplicity the results computed with $\gamma = 0$ are shown. The reported site number, $n = 25$, is chosen to satisfy the condition $n \gg 1$.

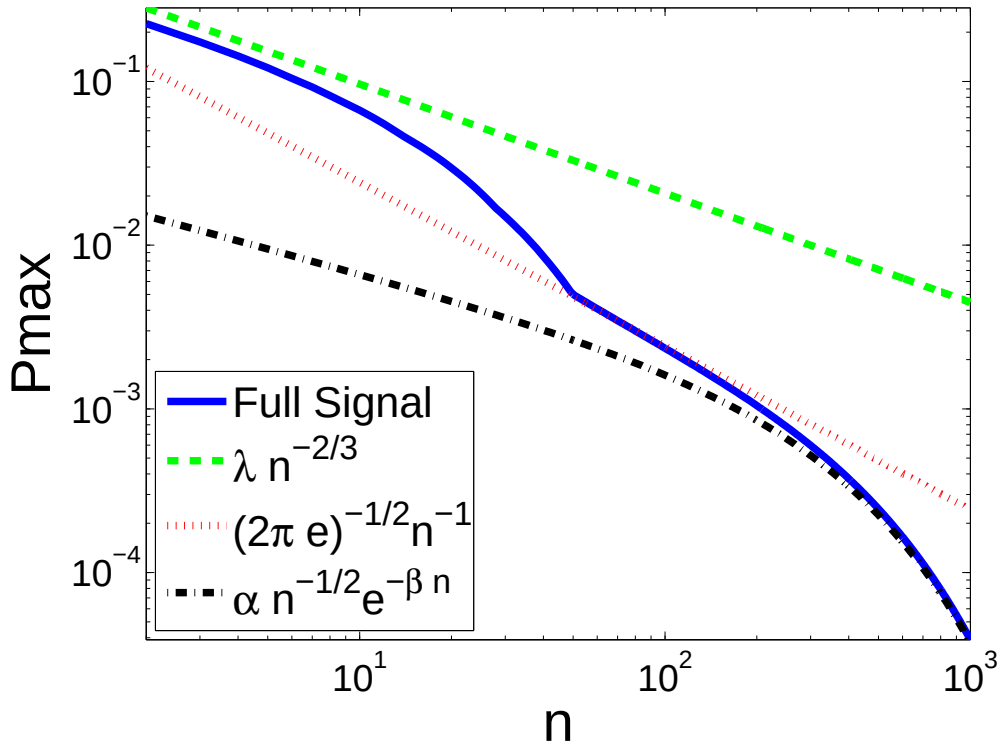

Figure 1.2: Log - Log representation of the maximal intensity, P_{max}, as a function of distance expressed in site numbers with the key asymptotics from Eqs. (1.12), (1.13), (1.14), also shown in Table 1.1, associated with the *ballistic*(green dashed line), *diffusive* (red dotted line) and *directed diffusion* (black dash-dotted line) regimes respectively. $\Delta = 10$ cm^{-1}, $W = 0.2$ ps^{-1}, $\gamma = 0.0003$ ps^{-1}.

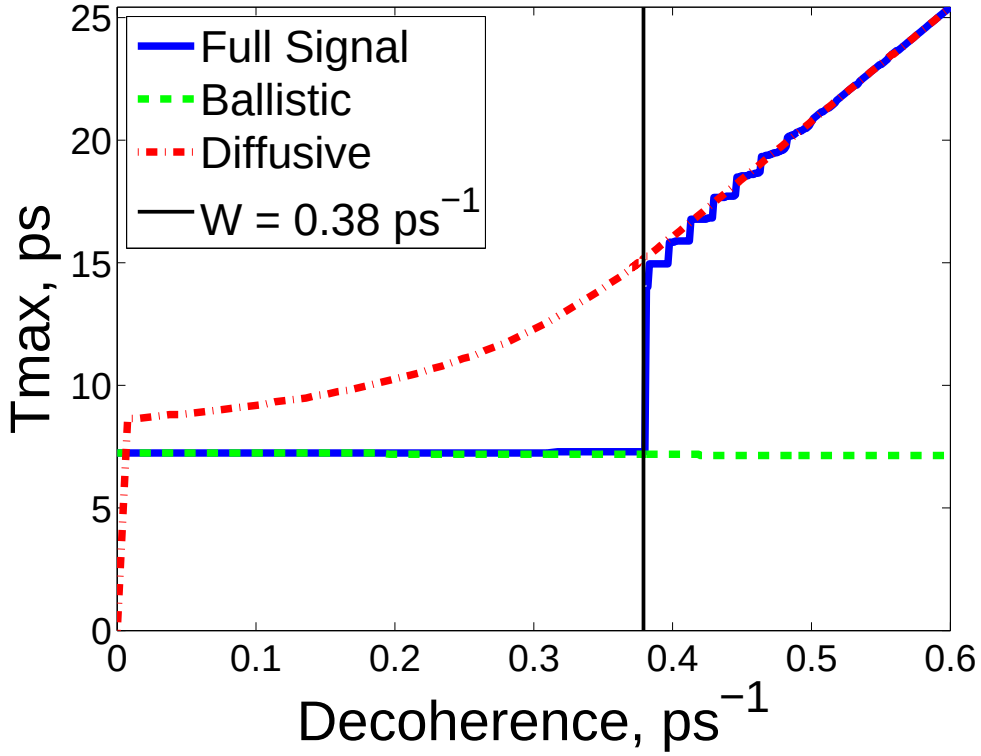

Figure 1.3: Energy transport time at the 25-th site as a function of the decoherence rate W; $\Delta = 10$ cm^{-1}, $\gamma = 0$ ps. The sharp transition between the *ballistic* (green dashed line) and *diffusive* (red dash-dotted line) regimes occurs at the decoherence rate $W = 0.38$ ps^{-1}.

One can see that the sharp transition occurs on the 25-th site at the decoherence rate $W = 0.38$ ps^{-1}. This transition is also illustrated in Fig. 1.4, where the intensity at the 25-th site is shown as a function of time. The signal intensity reaches its maximum twice: at 7 ps when the maximum of the *ballistic* wave-packet is arriving and at 15 ps when the *diffusive* component at this particular site reaches its highest value. While the *ballistic* energy transport is associated with propagation of spatially localized wave-packet, the *diffusive* transport reflects energy "spilling" from the origin so the definition of the diffusive wave front has to be clarified. In accord with the experimental definition [36] we define that the diffusive front reaches the certain point x when the amplitude of the diffusive energy transport reaches maximum.

Table 1.1: Characteristics of three vibrational energy transport regimes: *ballistic*, *diffusive* and *directed diffusive*. (Note that $D = 4a^2\Delta^2/W$, $\lambda = (2/9)^{1/3}/\Gamma(2/3)$, $\alpha = [\gamma/(2\pi^2 D)]^{1/4}$)

Transport mechanism	**Time range**	**Velocity**	$\mathbf{T_{max}}$	$\mathbf{P_{max}}$
Ballistic	$0 < t < W^{-1}$	$v = 2a\Delta$	$\frac{x}{2a\Delta}$	$\lambda x^{-2/3} e^{-\frac{W+\gamma}{v}x}$
Diffusive	$W^{-1} < t < \gamma^{-1}$	$\dot{x}(t) = \sqrt{\frac{D}{4t}}$	$\frac{x^2}{D}$	$(2\pi e)^{-1/2} x^{-1} e^{-\frac{\gamma}{D}x^2}$
Directed diffusion	$t > \gamma^{-1}$	$\tilde{v} = \sqrt{2\gamma D}$	$\frac{x}{\sqrt{2\gamma D}}$	$\alpha x^{-1/2} e^{-\frac{\tilde{v}}{D}x}$

At shorter distances the *ballistic* transport dominates, while at longer distances the *diffusion* becomes more important (FIGs. 1.1, 1.2). The crossover occurs therefore in discontinuous manner when the two mechanisms provide similar intensity contributions. The signature of such crossover was observed in the temperature dependence of the energy transport time in perfluoroalkanes [36]. The oscillations of energy excess at site 25, seen in Fig. 1.4 near the crossover, are in contrast to the experimental data and numerical analysis of Ref. [36]. The small dissipation rate, taken for illustrative purposes for these calculations, is the reason of the discrepancy. Decay of the ballistic amplitude can also smear out the coherent oscillations, while the qualitative picture of transport does not change very much.

In conclusion, in this study we obtained the exact solution for the space-time represented vibrational energy *ballistic* transport affected by decoherence in the quasi-continuous limit. We described various asymptotic analytical regimes of interest, all subject to experimental verification. We predict a sharp transition between the *ballistic* and *diffusive* transport regimes in a qualitative agreement with the recent experimental data [36]. Many questions need to be addressed, including identification of a specific vibrational mode responsible for the energy transport in a particular oligomer and accurate analysis of decoherence and dissipation for various chain structures.

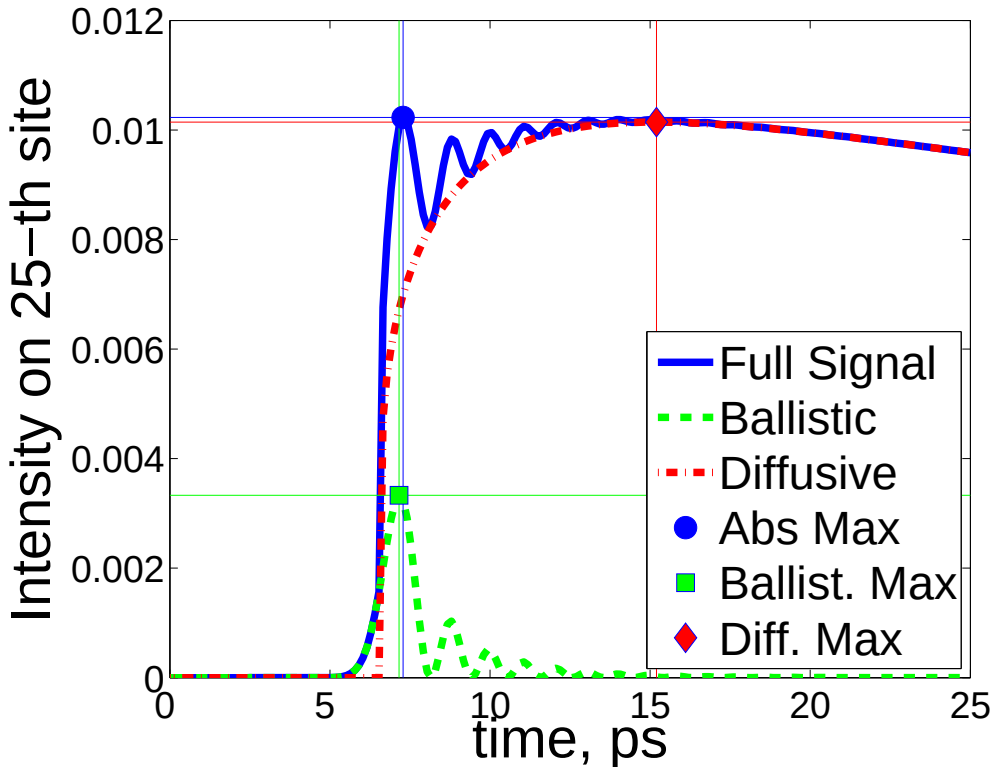

Figure 1.4: Intensity on the 25-th site as a function of time at the decoherence rate $W = 0.38$ ps^{-1}; $\Delta = 10$ cm^{-1}, $\gamma = 0$ ps. The full signal (blue solid line) has two equal maxima associated with the *ballistic* (7 ps) and *diffusive* (15 ps) components.

Chapter 2

Electronic torsional mode in linear polymers.

2.1 Overview

Highly efficient and fast vibrational energy transport on a molecular scale has been a subject of theoretical and experimental investigations in recent decades. The possible applications in biochemistry, organic chemistry and nanotechnology include development of efficient cooling in microscopic and nanoscopic molecular systems, such as nanowires [18] and optical limiters, designing efficient energy transport schematics for energy signaling, [32] as well as optimizing and even promoting chemical reactions by concentrating the excess energy at the reaction center [12, 45]. It is suggested that quantum vibrational excitations can be manipulated similarly to electrons and photons, thus enabling controlled heat transport. Moreover, delocalized excitations (phonons) can be used to carry and process quantum information [46–48]. The highest transport speed was found in alkanes (1.44 km/s) [20].

Possible candidates capable to maintain fast and efficient energy transport are oligomers because of their periodic structure [21]. In such systems vibrational states can be substantially delocalized because of the strong interaction of equiva-

lent site states, so that ballistic energy transport takes place as a free-propagating wavepacket. The ballistic constant-speed transport has been observed in bridged azulene-anthracene compounds [29], polyethylene glycol oligomers [32], alkanes [20, 21, 31], and perfluoroalkanes [16, 36] and the theory describing this transport and its possible breakdown due to decoherence has been suggested [18, 22, 34, 35].

Phonon wavepackets in carbon based polymer chains can propagate with the group velocity as high as 10 km/s because of a high strength of covalent bonds [8, 9]. Yet the maximum energy of singly excited vibrations does not exceed ca. 3000 cm^{-1}, as the motion is associated with displacements of rather heavy nuclei. Thus, the ballistically transferred energy is much smaller than a typical bond energy exceeding 1 eV ($\sim 10^4$ cm^{-1}). Involvement of multi-phonon transport to increase the amount of transferred energy is expected to enhance the energy relaxation/dissipation. Much larger energy can be carried by excitons, delocalized electronic states [49]. However molecular excitons are usually strongly coupled to the environment resulting in incoherent energy transport (see e. g. exciton transport in DNA [50, 51]).

Here we propose to exploit the special vibrational modes of entirely electronic nature capable of efficient delivery of energies in the eV ($\sim 10^4$ cm^{-1}) range. Such modes can exist in molecules having all atoms aligned along the single axis (see Fig. 2.1) and they are formed by propagating torsional oscillations of electronic nature. Nuclei do not participate in these oscillations because their rotation about the axis they located on is degenerate.

Considering a linear molecule as an elastic rod, four gapless phonon branches are expected based on symmetry, including longitudinal, two transverse, and one torsional modes [52, 53]. The longitudinal and torsional oscillations of frequency ω and wavevector q are characterized by an acoustic spectrum $\omega = cq$, with the relatively high speed of sound, c. As opposed to an elastic rod, a molecular chain

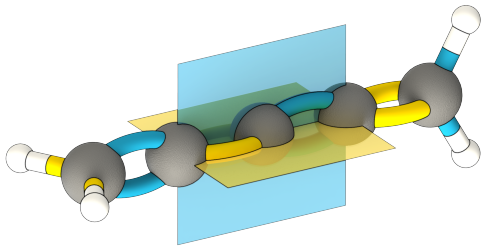

(a) cumelene

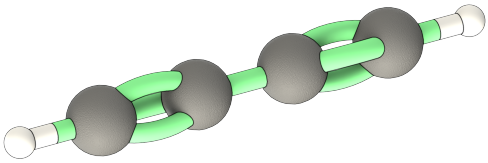

(b) polyyne

Figure 2.1: Carbyne modifications: (a) cumulene molecule with orthogonal double bonds; (b) polyyne molecule with alternating single and triple bonds

with all atoms located on the same axis has no nuclear contribution to the torsional vibrations, since the chain is completely linear. Nevertheless, the system can possess a remarkable torsional stiffness due to anisotropic arrangement of its electronic clouds. Such situation is found in cumulenes, featuring a chain of carbon atoms coupled to each other by double bonds [54], where the anisotropy results from the π-bond anisotropy between carbon atoms (see Fig.s 2.1(a), 2.2). Similar conditions can be realized in transition metals where atoms can form chain bridges between junctions [55–57].

The torsional sound should exist in such systems and we expect it to be of a purely electronic nature because nuclei are positioned along the primary axis and cannot participate in the torsional motion. Since electrons are much lighter than atoms it is natural to expect the speed and a single quantum energy to be much higher than those for nuclei vibrations.

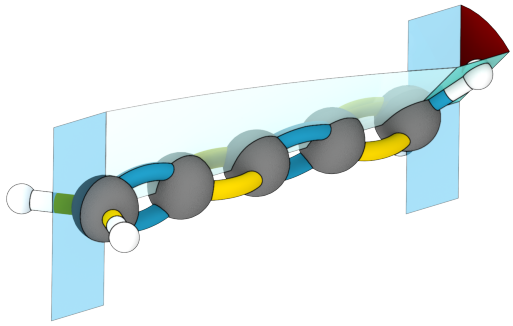

Figure 2.2: Cumulene molecule torsionally strained along primary axis

In the present study we performed a first principle investigation of the electronic torsional waves in cumulene chains. We found that the speed of sound in cumulenes to be as high as 1000 km/s and a maximum energy of the quantum as high as 10 eV.

Because this type of motion is not related to the vibrations of nuclei the corresponding quantum quasi-particle is not a usual phonon. As a collective motion of electrons it can be associated with a plasmon with a specific symmetry and a gapless spectrum, though its symmetry properties differ drastically from Langmuir waves in plasma and typical translational plasmons in conjugated systems. To avoid confusion and emphasize the symmetry properties we call a quantum of torsional electronic oscillations a *torsiton*.

The axial symmetry is exact in case of classical treatment of nuclei, while the quantum vibrations of the nuclei violate this symmetry. These vibrations result in a small *torsiton* spectral gap of the order of 0.02 eV. The possible ways to observe *torsitons* experimentally are discussed.

We consider the torsional oscillations of a cumulene in a dielectric environment, so the electronic excitations can be neglected. Although the metallic behavior of cumulene was predicted theoretically [54, 58] it has not been confirmed experimentally

[59, 60], so the nature of electronic excitations remains unclear. Here we ignore electronic excitations assuming that there is significant spectral gap (cf. Ref. [59]). Most of the results of this chapter were published in Ref. [23]. For reader's convenience most of the corresponding mathematical derivations are placed in Appendix B.

2.2 The system

A linear cumulene chain is a compound containing a sequence of n carbon atoms with $(n-1)$ double bonds between them R=C=(C=)$_{n-2}$C=R [61]. Quantum chemistry calculations were performed for the simplest termination of cumulene chain by two hydrogen atoms on each side; an example of cumulene molecule $H_2C{=}(C{=})_3CH_2$ is shown schematically in Fig. 2.1(a). One can see that orthogonal π-bonds between carbon atoms can provide rigidity with respect to twisting with remarkable torsional stiffness, while much smaller stiffness is expected in another carbyne modification, polyyne, which is a chain of carbon atoms with alternating single and triple bonds between them (see Fig. 2.1(b)). For cumulene molecules the shortened notation $H_2C_nH_2$ (without bond type specification) will be used.

2.3 Electronic torsional mode

To estimate the speed of sound for electronic torsional wave we consider a model of elastic rod (torsion spring) which can be described by the Lagrangian

$$\mathcal{L}_e = \frac{1}{2}\int_{z_l}^{z_r} dz \left\{ j_e \left(\frac{d\theta}{dt}\right)^2 - \kappa \left(\frac{\partial\theta}{\partial z}\right)^2 \right\} \tag{2.1}$$

where dynamical variable $\theta(z,t)$ is a twisting angle of the rod along z-axis as a function of coordinate along prime axis and time (Fig. 2.2); two neighboring cross-sections at points z and $z+dz$ will rotate with respect to each other with a relative angle

$d\theta = (\partial\theta/\partial z)\, dz$ [62]. Here $z_{l,r} = \mp L/2$, L - molecule length, κ stands for torsional stiffness and j_e is an average linear density of electronic moment of inertia with respect to z-axis.

We estimate parameters of interest as $j_e = 1.73\ m_e \cdot$ Å $(0.95 \cdot 10^{-3}$ u·Å) and torsional stiffness $\kappa = 10.6$ eV·Å as described in the next two sections. Our estimate for the torsional stiffness is consistent with the previous estimate of 10.3 eV·Å reported in Ref. [54].

With the angle $\theta(z,t)$ and the related angular velocity $d\theta/dt$ considered as dynamical variables Eq. (2.1) leads to the Euler equation

$$j_e \frac{\partial^2\theta}{\partial t^2} = \kappa \frac{\partial^2\theta}{\partial z^2} \tag{2.2}$$

which is a wave equation with the dispersion relation $\omega(q) = q\sqrt{\kappa/j_e}$ and the speed of the *torsiton* wave

$$c = \frac{d\omega}{dq} = \sqrt{\frac{\kappa}{j_e}} \simeq 1.0 \cdot 10^6\,\mathrm{m/s} \tag{2.3}$$

using j_e evaluated below. This velocity exceeds the typical phonon propagation velocity in polymers by two or three orders of magnitude. Next we also estimate the maximum energy transfered by the electronic torsional mode.

The dispersion relation for longitudinal vibration in a uniform chain with nearest neighbor coupling and the lattice period a has the standard form $\omega(q) = \omega_* \sin(aq/2)$ [63].

It should be a good approximation for the torsional mode under consideration because the interaction responsible for the torsional stiffness is due to short range covalent bonding. In the long wavelength limit $q \longrightarrow 0$ we estimate maximum energy of the *torsiton* as

$$\hbar\omega_* = 2\frac{\hbar c}{a} \simeq 10.5\,\mathrm{eV} \tag{2.4}$$

(the lattice period in cumulenes is given by $a = 1.28$ Å) [64]. This value corresponds to the typical electronic excitations energy range.

Though *torsiton* spectrum is gapless in the infinite chain limit if atomic vibrations are neglected, $\omega(0) = 0$, the energy of the first excited *torsiton* mode in the cumulene of finite chain length, L, corresponds to the minimum wavevector $q_{min} = \pi/L$. For sufficiently long molecules the *torsiton* spectrum acquires the gap due to zero-point atomic vibrations $\Delta\varepsilon \sim 0.1$ eV, which is smaller than typical electronic excitation energies (see also Sec. 2.7).

We can also roughly estimate the *torsiton* mean free path. While a precise analysis of dephasing in cumulene is beyond the scope of the present study, for an estimate we use the reported data for electronic dephasing in several organic systems. The coherence time of electronic excitations in FMO complexes ranges from 300 to 660 fs,[65, 66] the electron-phonon scattering rate in bilayer graphene,[67] another carbon allotrope, is saturated at 5 ps^{-1}, which corresponds to coherence time of 200 fs. Assuming coherence time for the *torsiton* as $T \gtrsim 100$ fs, one can estimate its mean free path as $l_0 = cT \gtrsim 100$ nm, which exceeds a length of any realistic cumulene chain. This estimate is valid for *torsiton* energies not matching other electronic excitations in cumulene. Otherwise the strong scattering will be expected.

Thus we found the electronic torsional sound wave velocity and energy unprecedentedly high compared to typical phonon parameters which makes this system very attractive for energy transport applications. The energy transferred by a single quantum is sufficiently large for chemical applications: bond making-bond breaking, energy release, and energy transfer to reaction center.

Below we derive our estimates for electronic moment of inertia and for torsional stiffness, discuss the limitations of our result due to zero point atomic vibrations and propose the way to observe the ultrafast energy transport due to electronic torsional

sound.

2.4 Electronic moment of inertia

The linear density of electronic moment of inertia is defined as

$$j_e(z) = \iint \rho(x, y, z) \left(x^2 + y^2\right) dxdy \tag{2.5}$$

where ρ is the electronic density. We calculated the linear density of electronic moment of inertia for cumulene molecule using density functional theory (DFT) with `B3LYP` hybrid functional and `6-31(d, p)` basis sets, as implemented in a Gaussian 09 software package [68]. The electron density as a function of coordinates is extracted with the uniform grid of 0.1 Bohr radius (0.0529 Å), the symmetric limits in X-Y plane (the plane perpendicular to the prime axis) were chosen ±6.5 Bohr radius (±3.44 Å). Either doubling of the limits or decrease of the grid by the same factor change the result by less than 1%.

To estimate the accuracy of the numerical result we tested the same approach on the hydrogen atom. The theoretical value of the moment of inertia of hydrogen electron cloud in the ground state can be calculated using the electron wave-function [69] as $J_0 = 2m_e a_0^2$, where m_e is electron mass and a_0 is the Bohr radius. The result of numerical calculations obtained using the same method as for cumulene is $J_{num} = 1.90 m_e a_0^2$, which is within 5% accuracy.

In Fig. 2.3 we show dependence $j_e(z)$ obtained from DFT-calculations for $H_2C_{11}H_2$. One can see that $j_e(z)$ is a smooth function weakly deviating from its average J_e/L ($\sim 5\%$), so for simplicity coordinate dependent moment of inertia density $j_e(z)$ can be replaced with the constant $j_e \simeq J_e/L \simeq 1.73\ m_e \cdot$ Å ($0.95 \cdot 10^{-3}$ u·Å). As shown in Fig. 2.3, we define molecular length L as a distance between the second left and second right carbon atoms, where $j_e(z)$ is still not affected by boundaries.

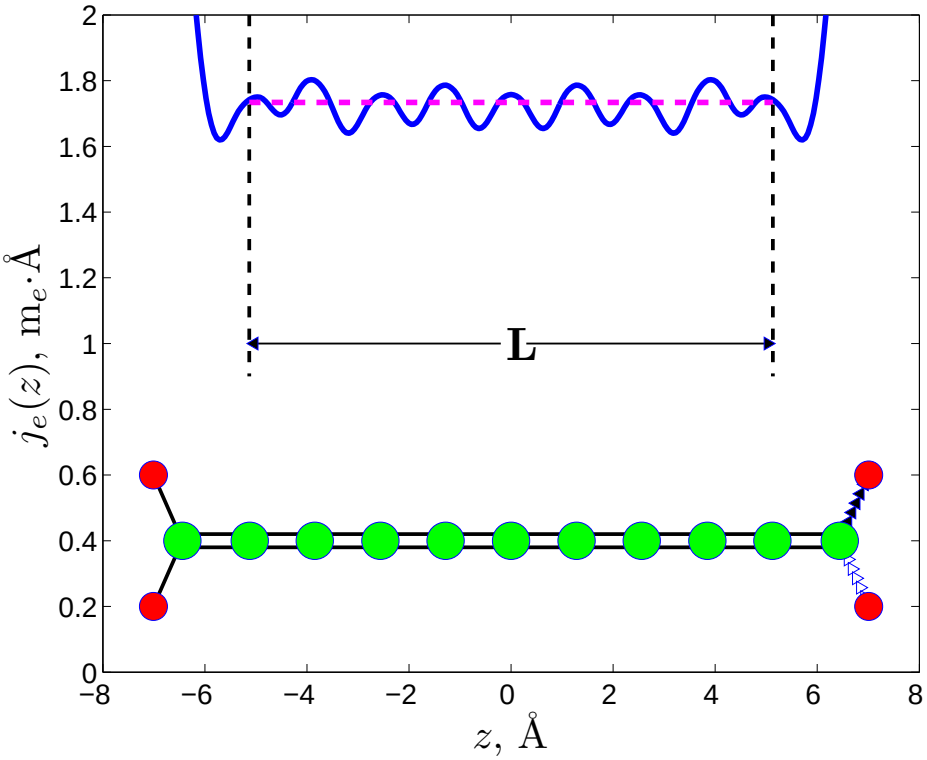

Figure 2.3: Linear density of the electronic inertia moment $j_e(z)$ as a function of coordinate along primary axis z (blue solid line). The corresponding molecule $H_2C_{11}H_2$ is represented below. One can see that $j_e(z)$ is a smooth function with low deviations from the average (magenta dash-line), except of the boundaries. The effective length L is defined as a distance between second left and second right carbon atoms.

2.5 Torsional stiffness calculation

Combining the proposed model with the first principles calculations of the hydrogen atom torsional vibrational mode associated with the relative torsional oscillations of pair of hydrogen atoms ("whiskers", see Fig. 2.2), we introduce Lagrangian

$$\mathcal{L} = \frac{J_l}{2}\left(\frac{d\Phi_l}{dt}\right)^2 + \frac{J_r}{2}\left(\frac{d\Phi_r}{dt}\right)^2 - \int_{-L/2}^{+L/2} dz \frac{\kappa}{2}\left(\frac{\partial\theta}{\partial z}\right)^2 \tag{2.6}$$

where $\Phi_l(t)$, $\Phi_r(t)$ are the angles of the "whiskers" deviation from equilibrium on the left and right side, $J_l = J_r = J/2$ are moments of inertia of the whiskers, J is the entire atomic moment of inertia along primary axis, defined by 4 hydrogen atoms. $\theta(z,t)$ is the same as in Eq. (2.1) with boundary conditions $\theta(\mp L/2) = \Phi_{l,r}$.

In this model the potential energy is originated from the torsional strain of the electronic spring and kinetic energy is entirely defined by the motion of hydrogen atoms, so long as the kinetic energy of electrons is neglected. The latter assumption is justified as long as $J_e \ll J$ (0.028 vs 3.43 u·Å for $n = 25$).

The torsional energy has a minimum at constant torsional angle gradient $(\partial\theta/\partial z) = (\Phi_r - \Phi_l)/L$ suggesting that electrons adiabatically follow atomic motion. For the only hydrogen torsional oscillator mode one can assume antisymmetric condition $-\Phi_l = \Phi = \Phi_r$. Then the Euler equation for Lagrangian (2.6) is

$$\frac{d^2\Phi}{dt^2} = -\frac{4\kappa}{JL}\Phi \tag{2.7}$$

This equation describes the harmonic oscillator with the frequency defined as[1]

$$\omega_\tau^2 = \frac{4\kappa}{J}\frac{1}{L} \tag{2.8}$$

Using the same DFT calculation, from harmonic vibrational analysis one can find ω_τ of $H_2C_nH_2$ for different n. In Fig. 2.4 we presented the related frequency ω_τ for $n = 5, 6, 8, 10, 12, 16, 24, 25$. Since the choice of length L includes some arbitrariness (our choice is illustrated in Fig. 2.3), the correct fit should include some length parameter $B \sim a$, so that $\omega_\tau^2 = A/(B+L)$. Using optimum fitting analysis we found $B = 4.22$ Å and the torsional stiffness is given by $\kappa = AJ/4 \simeq 2.89 \cdot 10^6$ cm^{-2}·u·Å^3 $\simeq 10.6$ eV·Å (u stands for the atomic mass unit), while atomic moment of inertia J is defined by end groups only and does not depend on n. These estimates were used to evaluate the speed of *torsitons*. Below we discuss the quantum approach to the problem and analyze the effect of zero-point atomic vibrations on the *torsiton* spectrum.

2.6 Quantum mechanical approach

In Sec. 2.3 we treated cumulene electronic torsional oscillations classically. Here we consider the quantum mechanical aspects of the problem.

Using periodicity of the system one can arrange all the electrons into "blocks" or unit cells. In cylindrical coordinates position of each electron in the n-th block is described by sets $\{\theta_i, r_i, z_i\}$, $i = 1..N$, where N is number of electrons in the block. One can introduce new coordinates using the average angles ϕ_n for description of the torsional angle of the whole block (double bond). Then we suggest to represent the

---

[1]More accurate detailed derivation of Eq. (2.8) for the hydrogen torsional mode can be found in Appendix B.1.

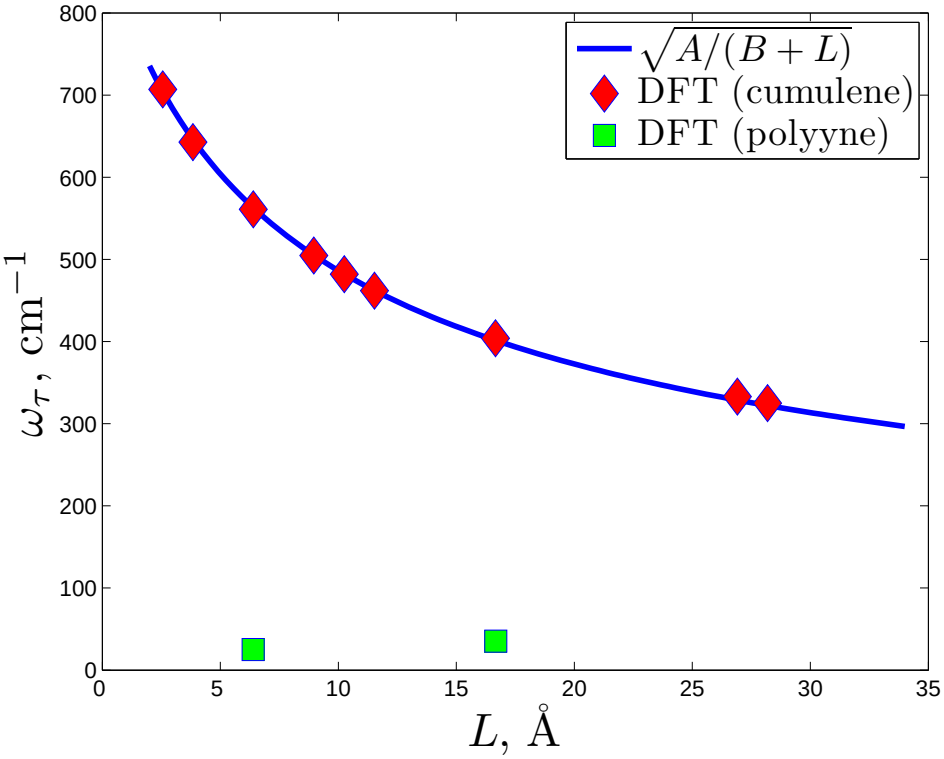

Figure 2.4: Frequency of the torsional mode ω_t as a function of cumulene molecule length calculated using $A = 3.37$ cm^{-2}·Å, $B = 4.22$ Å. Atomic moment of inertia $J = 3.43$ u·Å^2. From Eq. (2.8) $\kappa = 2.89 \cdot 10^6$ cm^{-2}·u·Å^3. In addition, torsional mode frequency for polyyne $H_3C{-}(C{\equiv}C{-})_mCH_3$, $m = 3, 11$, are shown (green squares); one can see that its torsional stiffness is small and does not follow Eq. (2.8)

kinetic energy related to these collective variables ϕ_n as

$$\hat{\mathcal{K}} = \sum_n \frac{\hat{\xi}_n^2}{2J_n} \tag{2.9}$$

where $\hat{\xi}_n = -i\hbar\frac{\partial}{\partial\phi_n}$ is the operator of the z-axis projection of the electron angular momentum in the n-th block, and J_n is a corresponding electronic moment of inertia of the block. Such expression leads to the right behavior for the overall rotation corresponding to the $q = 0$ mode. Indeed, one can rewrite Eq. (2.9) as

$$\hat{\mathcal{K}} = -\frac{1}{2J_nN}\sum_q \hat{\mathcal{M}}_q^2 \tag{2.10}$$

where $\hat{\mathcal{M}}_q = \sum_p e^{iqp}\hat{\xi}_p$ is defined in the manner that $\hat{\mathcal{M}}_0$ corresponds to the total angular momentum and J_nN is the total moment of inertia of the molecule with respect to the z-axis. For the long wavelength modes $qa \ll 1$ we expect that one can use the limit of $q \longrightarrow 0$.

The potential energy can be derived solving the corresponding Born – Oppenheimer problem. The expected form would be a sum like

$$\hat{\mathcal{U}} = \sum_{nk} U_{nk}\left(\hat{\phi}_n - \hat{\phi}_k\right) \tag{2.11}$$

satisfying the axial symmetry requirements, where $\{U_{nk}\}$ are functions of the previously introduced angles $\{\phi_n\}$; more complicated constructions than binary interactions can also be included, but they will not affect our further consideration. It is assumed that all high energy ("fast") degrees of freedom are excluded, while the low energy ("slow") degrees of freedom left, which are related to the long wavelength *torsitons* possessing a small energy compared to the other electronic excitations. Leaving only the nearest neighbor interactions and making expansion near the minimum we

come up with the quadratic Hamiltonian (cf. Eq. (2.1)):

$$\hat{\boldsymbol{\mathcal{H}}} = -\frac{\hbar^2}{2j_e a}\sum_n \left[\frac{\partial^2}{\partial\phi_n^2} + \frac{\kappa}{2a}(\phi_n - \phi_{n+1})^2\right] \tag{2.12}$$

where the moment of inertia on the n-th block can be taken as $J_n \simeq j_e \cdot a$, where a is a distance between two adjacent atoms and κ/a is a torsional stiffness per unit cell (see also Sec. 2.4). This Hamiltonian has a spectrum [70]

$$\varepsilon_q = \hbar\omega_q = \frac{2\hbar}{a}\sqrt{\frac{\kappa}{j_e}}\sin\left(\frac{aq}{2}\right) \tag{2.13}$$

This prediction is consistent with the results of time-dependent density functional theory (TD DFT) calculations of the first excited electronic state (see Fig 2.5). Indeed, the energy of this state scales as the inverse molecular length, in agreement with Eq. (2.13) for $q = \pi/L$. The obtained energy is also consistent with the estimate based on the electronic stiffness. We do not expect that this mode is associated with the electron delocalization since in that case a $1/L^2$ dependence for the minimum energy is expected, similarly to the particle in the box problem.[69]

In Fig 2.5 we present the results of TD DFT calculations with `B3LYP` hybrid functional and `6-31(d, p)` basis sets, as implemented in a Gaussian 09 software package [68] (see also Sec. 2.4) for the first excited singlet electronic state in cumulene (red diamonds) and polyyne (green squares) with their fit based on the theoretical predictions (Eq. 2.13, Ref.[70]). The determined speed of sound is very close to that obtained with Eq. (2.3). The result deviates from the nearest neighbor model Eq. (2.12) at small molecular length, which is probably a consequence of the next neighbor interactions. We also did the calculations for polyyne and found the saturation of minimum energy at about 1.27 eV, which estimates the gap in the electronic spectrum there.

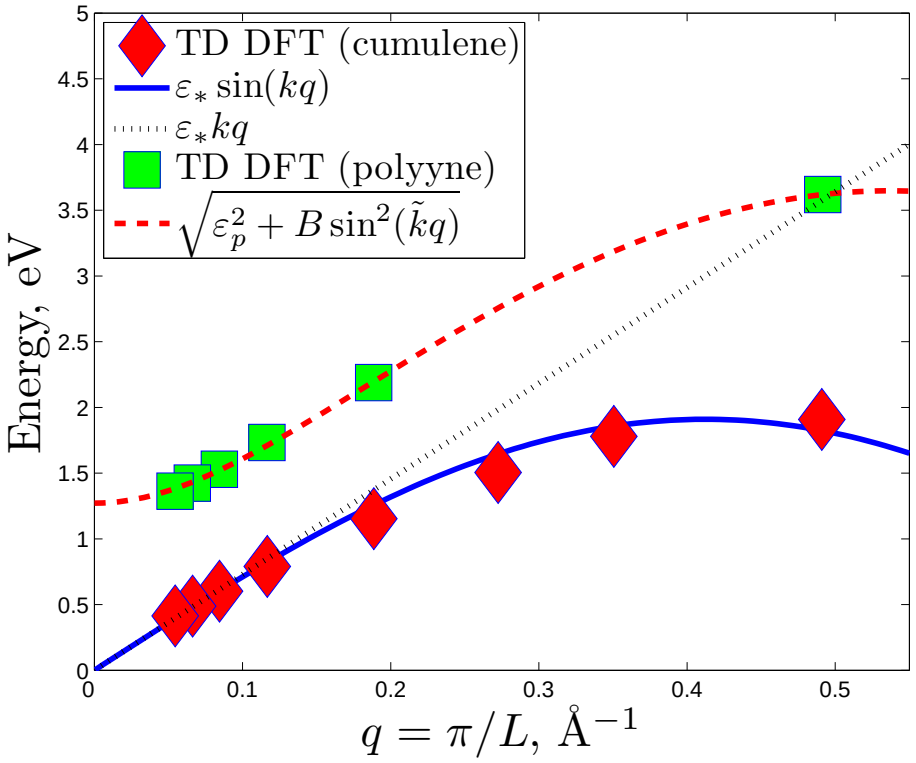

Figure 2.5: Energy of the 1st excited electronic singlet state as a function of the inverse molecule length. Red diamond markers correspond to TD DFT calculations for cumulene C_nH_4 with $n = 8, 10, 12, 16, 24, 32, 40, 48$ carbon atoms; blue solid line is the model spectrum, $\hbar\omega(q) = \varepsilon_* \sin(kq)$, $k = 3.49\,\text{Å}$, $\varepsilon_* = 1.91$ eV; the slope at $q = 0$ (black dotted line) corresponds to the group velocity $c = \varepsilon_* k/\hbar = 1.01 \cdot 10^6$ m/s; green squares correspond to TD DFT calculations for polyyne C_nH_6 with $n = 8, 16, 24, 32, 40, 48$ carbon atoms; red dashed line shows the fit to the optical band spectrum [70] $\varepsilon = \sqrt{\varepsilon_p^2 + B\sin^2(\tilde{k}q)}$ with the gap $\varepsilon_p = 1.27$ eV, $B = 11.7$ eV, $\tilde{k} = 2.92\,\text{Å}$.

To explain the qualitative difference in the cumulene and polyyne spectra we matched our model to the well investigated model of the Josephson junction array:[71]

$$\hat{\boldsymbol{\mathcal{E}}} = -\frac{E_C}{2}\sum_n \frac{\partial^2}{\partial\phi_n^2} - E_J\sum_n \cos(\phi_{n+1}-\phi_n) \tag{2.14}$$

The kinetics energy in this model is associated with the Coulomb repulsion of superconducting granules, while the cosine term describes the Josephson coupling between granules. The parameters of the matching model consistent with our model for cumulene are $E_C = \hbar^2/(j_e a) = 3.45$ eV, $E_J = \kappa/a = 8.28$ eV. This model shows a quantum phase transition between superconducting state with a weakly oscillating phase difference between granules and the insulating state with weakly correlated phases of granules at $G_c = E_J/E_C = 1.23$. In our case this is the phase transition between an ordered ground state (cumulene) having gapless torsional mode (*torsiton*) and an uncorrelated state with the gap in the spectrum realized in polyyne. Indeed, in the first case corresponding to cumulene ($E_J/E_C = 2.40 > G_c$) the system has a continuous spectrum of gapless excitations (*torsitons* in our case) while in the second case there is the gap $\varepsilon_p = 1.27$ eV in the spectrum as we found in polyyne (see Fig 2.5). In polyyne the interaction between bond orientations is much weaker than that in cumulene because the triple and single bonds are almost axially symmetric. Therefore this system is likely on the "insulating" gapped side of the quantum phase transition. Quantum phase transition in one dimensional systems takes place at zero temperature only. Since our system is finite and and the thermal energy $k_B T$ is small compared to electronic interaction energies the zero temperature consideration should be still applicable.

In spite of our quantum mechanical derivation is not rigorous we believe that being considered together with TD DFT simulation results and classical arguments of Sec. 2.3 it supports our expectations of the existence of the electronic sound spectral

branch, i. e. *torsitons*.

2.7 Effect of zero-point atomic vibrations

In our description of the electronic torsional mode we implicitly used Born-Oppenheimer approximation, considering electronic motion in an axially symmetric field of motionless nuclei, positioned along the z-axis. This axial symmetry is reflected by the symmetry of the Lagrangian in Eq. (2.1) with respect to the change of the function $\theta(z)$ by arbitrarily constant.

In reality, the nuclei participate in zero-point vibrations in the ground state, which does not possess an axial symmetry because this ground state is adjusted to the electronic ground state where this symmetry is broken (see Fig. 2.2). Indeed, to find this ground state, one needs to consider interacting nuclei in the field of electronic cloud with already calculated anisotropic electronic density.

Thus, the potential energy depends on the angle θ even in the absence of torsion and the energy minimum is realized at some angle θ_0 which we can set to zero. The potential energy can be expanded over the small displacement from this minimum as $\alpha\theta^2/2$. This term incorporated to the Lagrangian in Eq. (2.1) as $-\alpha\theta^2/(2L)$ leads to the gap in the spectrum of torsional waves. Correcting Eq. (2.2) by $-\alpha\theta/(j_e L)$ term in the right hand side, we obtain a new dispersion relation

$$\omega^2(q) = \frac{\kappa}{j_e} q^2 + \frac{\alpha}{j_e L} \tag{2.15}$$

Since $\omega(0) \neq 0$ the mode is not exactly acoustic due to the gap $\Delta\omega = \sqrt{\alpha/j_e L}$.

To estimate the parameter α consider the change of classical energy $\delta E(\theta) = \left\langle \hat{\boldsymbol{\mathcal{H}}}(\theta) - \hat{\boldsymbol{\mathcal{H}}}(0) \right\rangle_g$, where $\hat{\boldsymbol{\mathcal{H}}}$ is the atomic chain quantum Hamiltonian and $\langle \dots \rangle_g$ is an

average over the ground state of carbon atoms considering their zero-point vibrations.[2]

All the normal modes of carbon atoms in the molecule, which don't include motion of hydrogen atoms with respect to the adjacent carbon atoms, can be either longitudinal or transverse. For D_{2d} symmetry point group with coordinate system defined above there are only two possible second order invariants: z^2 and x^2+y^2 , so the transverse modes of the harmonic Hamiltonian of the atomic chain are expected to be double-degenerate and the corresponding eigenfunctions possess axial symmetry [72]. Practically, this degeneracy is observed in DFT-calculated IR spectra of $H_2C_nH_2$ for odd n, while for even n all energy levels are split, because such molecules belong to D_{2h} symmetry group. Indeed, the splitting is entirely an effect of sides, because in even n molecules the side CH_2 groups lie in the same plane (while in odd n they are orthogonal), so X-Z and Y-Z plane become distinguishable, while for an infinite chain this effect would disappear.

The break of axial symmetry takes place in the third order anharmonic interaction. To express potential energy in normal modes representation introduce notations u_{x_i} and u_{y_i} for transverse modes with energy $\hbar\omega_{x_i} = \hbar\omega_{y_i} = \hbar\omega_i$ and u_{z_k} for $k-th$ longitudinal mode. Thus the third order anharmonic energy is expressed by

$$\hat{\boldsymbol{\nu}}_3 = \sum_k \left\{ \frac{1}{2} \sum_i V_{iiz_k} \left(u_{x_i}^2 - u_{y_i}^2 \right) + \sum_{i<j} V_{ijk} \left(u_{x_i} u_{x_j} - u_{y_i} u_{y_j} \right) \right\} u_{z_k} \tag{2.16}$$

where it is assumed that $V_{x_i x_j z_k} = -V_{y_i y_j z_k} = V_{ijz_k}$ for any i, j.

With $\hat{\boldsymbol{\nu}}_3$ as a perturbation, a meaningful correction to the ground state in the

---

[2]The detailed derivations of energy correction due to zero-point vibrations and description of the spectrum gap numerical calculations can be found in Sec. B.2

first order of perturbation theory is given by

$$|\psi_0\rangle = |0\rangle - \frac{1}{4\hbar}\sum_k\sum_i \frac{V_{iiz_k}}{2\omega_i+\omega_{z_k}}\Big(|2_i^x 1_k^z\rangle - |2_i^y 1_k^z\rangle\Big) - \\ \frac{1}{\hbar\sqrt{2}}\sum_k\sum_{i<j}\frac{V_{ijz_k}}{\omega_i+\omega_j+\omega_{z_k}}\Big(\big|1_i^x 1_j^x 1_k^z\big\rangle - \big|1_i^y 1_j^y 1_k^z\big\rangle\Big) \quad (2.17)$$

The rotation of electronic cloud about the z-axis by an angle θ changes the energy in diabatic approximation by

$$\delta\hat{\boldsymbol{\mathcal{H}}}(\theta) = -\sum_k\left\{\sum_i V_{iiz_k}\big(u_{x_i}^2 - u_{y_i}^2\big) + 2\sum_{i<j}V_{ijz_k}\big(u_{x_i}u_{x_j} - u_{y_i}u_{y_j}\big)\right\}u_{z_k}\sin^2\theta \quad (2.18)$$

Assuming for the small displacement from the minimum $\sin\theta \simeq \theta$, one can find $\delta E(\theta) = \langle\psi_0|\,\delta\hat{\boldsymbol{\mathcal{H}}}(\theta)\,|\psi_0\rangle = \alpha\theta^2/2$, with α given by

$$\alpha = \sum_k\left\{\sum_i\frac{|V_{iiz_k}|^2}{\hbar(2\omega_i+\omega_{z_k})} + \sum_{i<j}\frac{4|V_{ijz_k}|^2}{\hbar(\omega_i+\omega_j+\omega_{z_k})}\right\} \quad (2.19)$$

Using anharmonic frequency analysis of $H_2C_5H_2$ we calculated third-order anharmonicity constants [68, 73]. To exclude effect of hydrogen atoms we considered the only transverse and longitudinal normal modes with the nearest integer of reduced mass greater or equal 2 atomic units. Applying Eq. (2.19) we found $\alpha = 119$ cm^{-1}, so that the energy gap can be estimated using Eq. (2.15) as $\Delta\varepsilon \simeq 890$ cm^{-1} (see also Sec. B.2.2).

To answer a question how crucial is the described effect for the acoustic mode, one can find the length L of a cumulene chain where this energy becomes comparable to the minimum *torsiton* energy, which can be estimated as

$$\hbar\omega_{min} \simeq \hbar c q_{min} = \hbar c\frac{\pi}{L} \quad (2.20)$$

Thus the length required to make the gap value of the same order as $\hbar\omega_{min}$ is $L_* \simeq \hbar\pi c/\Delta\varepsilon \simeq 20$ nm, that is sufficiently larger than the real molecule length [74].

Axial symmetry can be violated also by the forth-order anharmonic interaction, however its contribution into the energy gap does not change qualitatively the presented estimate.

2.8 Experiment suggestions

As shown above, the electronic torsional mode features an unprecedented speed of 1000 km/s = 1 nm/fs and can transfer energy up to 10 eV, which is comparable to the energies of the strongest chemical bonds (C=C, N≡N, etc.). Such high transferred energy brings an opportunity of performing chemistry at distances, including chemical bond breaking reactions. Fig. 2.6 shows a schematic of the compound suitable for the proof of principle experiment on remote chemistry initiation. The compound features two surface-anchored end-groups connected by a cumulene chain. Laser initiated bond breaking at the initiation (left) end-group can result in generation of a strong torque at the chain which will propagate as a wave-packet along the chain and can result in bond breaking at another end group, the target. The energy released by the initiation end-group can be tuned by selecting convenient functional groups. Spectroscopic observation of the transported energy can aim at detecting the formation of the products at the target or detection of the excess energy at the target. In the latter case a longer cumulene chain is required as for the chain length of 50 carbon atoms the transport time is only ca. 5 fs. Compounds with such long chains have been synthesized for polyynes [75] and we hope that this should be possible for cumulenes as well.

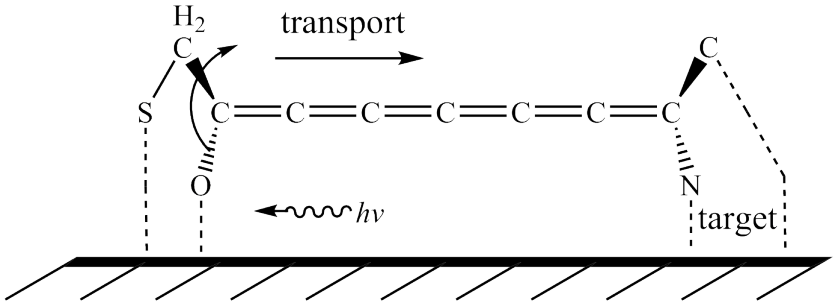

Figure 2.6: A schematic experiment set up on remote chemistry initiation. The compound features two surface-anchored end-groups connected by a cumulene chain. Laser initiated bond breaking at the initiation (left) end-group can result in generation of a strong torque at the chain which will propagate as a wave-packet along the chain and can result in bond breaking at another end group, the target.

2.9 Conclusion

In this chapter we considered electronic torsional waves in cumulene chains (*torsitons*) which are torsional sound waves of entirely electronic nature. We evaluated the speed of *torsiton* propagation as high as 1000 km/s. Single *torsiton* can carry energy from almost 0 to 10 eV. Similar waves should exist in other atomic chain with anisotropic bonds including recently discovered transition metal linear chains. While the largest band energy computed for cumulenes at 10 eV, the computations neglected electronic excitation, which will likely be contributing at such high energies. It will be interesting to see how the ground electronic state *torsitons* are perturbed by electronic excitations at higher *torsiton* band energies and how the quasi-particles of two types, *torsitons* and excitons, interact. Nevertheless, the presented band calculations are expected to be free of electronic excitation effects at smaller energies. Importantly, the transport speed supported by the lower half of the *torsiton* band is similar to that of the full band (with small corrections due to the *torsiton*-vibron coupling).

Chapter 3

Vibrational energy bands in oligomers

3.1 Overview

In this chapter we will discuss another semi-classical approach to investigation of ballistic transport in oligomers. The idea of the method to perform DFT-calculations for geometry optimization and harmonic analysis of well-ordered polymer compound with periodic structure and to use the results quantum mechanical calculations in classical equations of atomic motion. This approach allows to consider the speed of ballistic energy transport as group velocities corresponding to acoustic and optical energy bands and modes of different geometry. The application of this method was recently discussed in Refs. [20, 21].

In Sec. 3.2 – 3.6 we will develop energy bands theory assuming ideal polymer chains possessing special set of symmetries using perfluoroalkane compound as an example. In a section 3.7 we will briefly deduce some practical application for alkane chains.

3.2 Dispersion equation

Consider an ideal pefluoroalkane (alkane) chain with C_2F_4 (C_2H_4) as a monomer (Figs. 3.1, 3.2). The main idea of such consideration is that any of those six atoms can be "replicated" by to consequent operations: translation along primary axis z by distance a and rotation along this axis by angle θ. Actually, the periodicity of the alkane chain does not include rotation (pure translational symmetry), however we will just assume a trivial case of rotation by angle $\theta = 0$ for alkane chain and develope general approach. Using of word *ideal* implies consideration of infinite chain (no boundary effects) built of described unit cells and that the Hessian (matrix of the force constants - second derivatives of the potential) possesses the same symmetry. Later we will discuss the effect of deviation from the ideal geometry (Sec. 3.3) and how the parameters a and θ can be obtained numerically from the results of DFT calculation.

Introduce $\boldsymbol{r}_k$ - 18-dimensional displacement vector for atoms into k-th unit cell (6 atoms $\times$ 3 Cartesian coordinates = 18 degrees of freedom). The next unit cell displacement vector $\boldsymbol{r}_{k+1}$ is obtained form $\boldsymbol{r}_k$ by symmetry operation

$$\boldsymbol{r}_{k+1} = \hat{\boldsymbol{\mathcal{U}}}\boldsymbol{r}_k + a\boldsymbol{e}_z \tag{3.1}$$

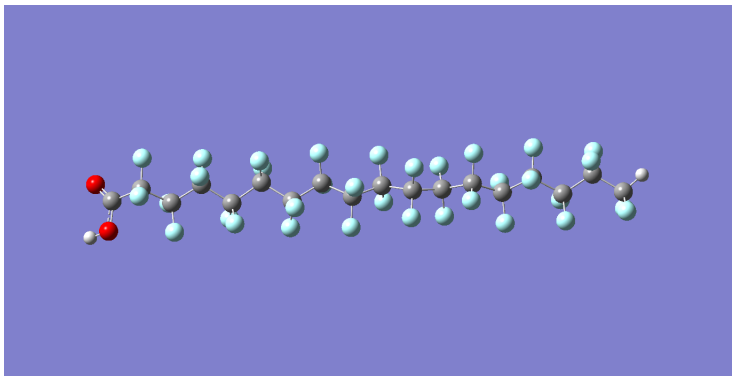

(a) projection on X-Z plane

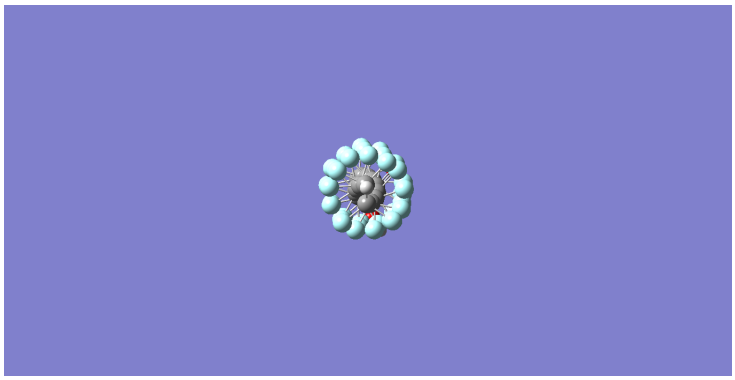

(b) projection on X-Y plane

Figure 3.1: Perluoroalkane compound C_{16} with CO_2H and CF_2H complexes on the ends: (a) projection on X-Z plane, (b) projection on X-Y plane.

where $\hat{\boldsymbol{\mathcal{U}}}$ is 6×3 unitary[1] matrix - generator of rotation along z-axis[2] by angle θ:

$$\hat{\boldsymbol{\mathcal{U}}} = \begin{pmatrix} \hat{\boldsymbol{u}} & \cdots & 0 \\ 0 & \ddots & 0 \\ 0 & \cdots & \hat{\boldsymbol{u}} \end{pmatrix}, \quad \hat{\boldsymbol{u}} = \begin{pmatrix} \cos\theta & \sin\theta & 0 \\ -\sin\theta & \cos\theta & 0 \\ 0 & 0 & 1 \end{pmatrix} \tag{3.2}$$

and $\boldsymbol{e}_z$ is a 18×1 unit vector directed along z-axis:

$$\boldsymbol{e}_z = \frac{1}{\sqrt{6}} \begin{pmatrix} 0 \\ 0 \\ 1 \\ \vdots \\ 0 \\ 0 \\ 1 \end{pmatrix} \tag{3.3}$$

The Hessian of the system can be split into blocks $\hat{\boldsymbol{H}}_{kn}$, 18-by-18 matrices corresponding to harmonic interaction between k-th and n-th unit cells. As long as Hessian is a hermitian matrix,

$$\hat{\boldsymbol{H}}_{kn} = \hat{\boldsymbol{H}}_{nk}^{\dagger} \tag{3.4}$$

and from translation-rotational symmetry

$$\hat{\boldsymbol{H}}_{k+1,n+1} = \hat{\boldsymbol{\mathcal{U}}} \hat{\boldsymbol{H}}_{kn} \hat{\boldsymbol{\mathcal{U}}}^{\dagger} \tag{3.5}$$

---

[1] $\hat{\boldsymbol{\mathcal{U}}}^{-1} = \hat{\boldsymbol{\mathcal{U}}}^{\dagger}$

[2] it is also called Kronecker (or tensor) product of of 6×6 identity matrix $\hat{\boldsymbol{\mathcal{E}}}$ by matrix $\hat{\boldsymbol{u}}$: $\hat{\boldsymbol{\mathcal{U}}} = \hat{\boldsymbol{\mathcal{E}}} \otimes \hat{\boldsymbol{u}}$.

In the nearest-neighbor approximation the harmonic Hamiltonian can be represented as

$$\hat{\boldsymbol{\mathcal{H}}} = \frac{1}{2}\sum_k \left\{ \boldsymbol{p}_k^\dagger \hat{\boldsymbol{M}}^{-1} \boldsymbol{p}_k + \boldsymbol{r}_k^\dagger \hat{\boldsymbol{H}}_{kk} \boldsymbol{r}_k + \boldsymbol{r}_k^\dagger \hat{\boldsymbol{H}}_{kk-1} \boldsymbol{r}_{k-1} + \boldsymbol{r}_k^\dagger \hat{\boldsymbol{H}}_{k+1k} \boldsymbol{r}_{k+1} \right\} \tag{3.6}$$

where $\hat{\boldsymbol{M}}$ is 18×18 diagonal matrix of atomic masses

$$\hat{\boldsymbol{M}} = \begin{pmatrix} m_1 & 0 & 0 & \cdots & 0 & 0 & 0 \\ 0 & m_1 & 0 & \cdots & 0 & 0 & 0 \\ 0 & 0 & m_1 & \cdots & 0 & 0 & 0 \\ \cdots & \cdots & \cdots & \ddots & \cdots & \cdots & \cdots \\ 0 & 0 & 0 & \cdots & m_6 & 0 & 0 \\ 0 & 0 & 0 & \cdots & 0 & m_6 & 0 \\ 0 & 0 & 0 & \cdots & 0 & 0 & m_6 \end{pmatrix}$$

and $\boldsymbol{p}_k$ is 18×1 momentum vector, following the same symmetry operation as $\boldsymbol{r}_k$ in Eq. (3.1). By the nearest-neighbor approximation here we assume non-zero interaction between atoms inside one unit cell and between atoms into the neighbor unit cells, i. e. $\hat{\boldsymbol{H}}_{k,k+m} \equiv 0$ for any $|m| > 1$. Practically, this assumption is not necessarily justified, we use it for the sake of derivation simplicity, though terms of the long-order interaction can be added into Eq. (3.6) (see Sec. 3.5).

Introduce the following notations for the Hessian blocks:

$$\begin{aligned} \hat{\boldsymbol{\mathcal{A}}} &= \hat{\boldsymbol{H}}_{kk} \\ \hat{\boldsymbol{\mathcal{B}}} &= \hat{\boldsymbol{H}}_{kk+1} \end{aligned} \tag{3.7}$$

From Eqs. (3.4), (3.5):

$$\hat{\boldsymbol{H}}_{kk-1} = \hat{\boldsymbol{H}}^{\dagger}_{k-1k} = \left(\hat{\boldsymbol{U}}^{\dagger}\hat{\boldsymbol{H}}_{kk+1}\hat{\boldsymbol{U}}\right)^{\dagger} = \hat{\boldsymbol{U}}^{\dagger}\hat{\boldsymbol{H}}^{\dagger}_{kk+1}\hat{\boldsymbol{U}} = \hat{\boldsymbol{U}}^{\dagger}\hat{\boldsymbol{B}}^{\dagger}\hat{\boldsymbol{U}} \tag{3.8}$$

so that Hessian matrix can be visualized as

$$\begin{pmatrix}
\cdots & & & & & & & & & & & \\
0 & \cdots & 0 & \ddots & \ddots & \ddots & 0 & 0 & 0 & 0 & \cdots & 0 \\
0 & \cdots & 0 & 0 & \hat{\boldsymbol{U}}^{\dagger 2}\hat{\boldsymbol{B}}^{\dagger}\hat{\boldsymbol{U}}^{2} & \hat{\boldsymbol{U}}^{\dagger}\hat{\boldsymbol{A}}\hat{\boldsymbol{U}} & \hat{\boldsymbol{U}}^{\dagger}\hat{\boldsymbol{B}}\hat{\boldsymbol{U}} & 0 & 0 & 0 & 0 & \cdots & 0 \\
0 & \cdots & 0 & 0 & 0 & \hat{\boldsymbol{U}}^{\dagger}\hat{\boldsymbol{B}}^{\dagger}\hat{\boldsymbol{U}} & \hat{\boldsymbol{A}} & \hat{\boldsymbol{B}} & 0 & 0 & 0 & \cdots & 0 \\
0 & \cdots & 0 & 0 & 0 & 0 & \hat{\boldsymbol{B}}^{\dagger} & \hat{\boldsymbol{U}}\hat{\boldsymbol{A}}\hat{\boldsymbol{U}}^{\dagger} & \hat{\boldsymbol{U}}\hat{\boldsymbol{B}}\hat{\boldsymbol{U}}^{\dagger} & 0 & 0 & \cdots & 0 \\
0 & \cdots & 0 & 0 & 0 & 0 & 0 & \ddots & \ddots & \ddots & 0 & \cdots & 0 \\
\cdots & & & & & & & & & & & &
\end{pmatrix}$$

Eq. (3.6) can be rewritten as

$$\hat{\boldsymbol{\mathcal{H}}} = \frac{1}{2}\sum_{k}\left\{\boldsymbol{p}_k^{\dagger}\hat{\boldsymbol{M}}^{-1}\boldsymbol{p}_k + \boldsymbol{r}_k^{\dagger}\hat{\boldsymbol{A}}\boldsymbol{r}_k + \boldsymbol{r}_k^{\dagger}\hat{\boldsymbol{U}}^{\dagger}\hat{\boldsymbol{B}}^{\dagger}\hat{\boldsymbol{U}}\boldsymbol{r}_{k-1} + \boldsymbol{r}_k^{\dagger}\hat{\boldsymbol{B}}\boldsymbol{r}_{k+1}\right\} \tag{3.9}$$

Introducing "weighted" vectors and matrices

$$\begin{aligned}
\tilde{\boldsymbol{r}}_k &= \hat{\boldsymbol{M}}^{1/2}\boldsymbol{r}_k \\
\tilde{\boldsymbol{p}}_k &= \hat{\boldsymbol{M}}^{-1/2}\boldsymbol{p}_k \\
\hat{\boldsymbol{A}}_W &= \hat{\boldsymbol{M}}^{-1/2}\hat{\boldsymbol{A}}\hat{\boldsymbol{M}}^{-1/2} \\
\hat{\boldsymbol{B}}_W &= \hat{\boldsymbol{M}}^{-1/2}\hat{\boldsymbol{B}}\hat{\boldsymbol{M}}^{-1/2} \\
\hat{\boldsymbol{U}}_W &= \hat{\boldsymbol{M}}^{1/2}\hat{\boldsymbol{U}}\hat{\boldsymbol{M}}^{-1/2}
\end{aligned} \tag{3.10}$$

we obtain the equation of motion for k-th unit cell as

$$\frac{d^2\tilde{\boldsymbol{r}}_k}{dt^2} = -\hat{\boldsymbol{\mathcal{A}}}_W\tilde{\boldsymbol{r}}_k - \hat{\boldsymbol{\mathcal{B}}}^\dagger_W\tilde{\boldsymbol{r}}_{k-1} - \hat{\boldsymbol{\mathcal{B}}}_W\tilde{\boldsymbol{r}}_{k+1} \tag{3.11}$$

To solve this equation one can switch over to frequency domain by Fourier Transform

$$\tilde{\boldsymbol{r}}_k(t) = \sum_q \boldsymbol{\xi}_k(q)\exp\{-i\omega(q)t\} \tag{3.12}$$

where q is one-dimensional wave-vector, and to apply the Bloch theorem ansatz[3]

$$\boldsymbol{\xi}_k(q) = \exp\{iaqk\}\hat{\boldsymbol{\mathcal{U}}}^k_W\boldsymbol{\xi}(q) \tag{3.13}$$

Applying Eqs. (3.12), (3.13) to Eq. (3.11) we obtain equation

$$\omega^2(q)\boldsymbol{\xi} = \hat{\boldsymbol{\mathcal{G}}}(q)\boldsymbol{\xi} \tag{3.14}$$

where

$$\hat{\boldsymbol{\mathcal{G}}}(aq) = \hat{\boldsymbol{\mathcal{A}}}_W + \left(\hat{\boldsymbol{\mathcal{B}}}_W\hat{\boldsymbol{\mathcal{U}}}_W + \hat{\boldsymbol{\mathcal{U}}}^\dagger_W\hat{\boldsymbol{\mathcal{B}}}^\dagger_W\right)\cos(aq) + i\left(\hat{\boldsymbol{\mathcal{B}}}_W\hat{\boldsymbol{\mathcal{U}}}_W - \hat{\boldsymbol{\mathcal{U}}}^\dagger_W\hat{\boldsymbol{\mathcal{B}}}^\dagger_W\right)\sin(aq) \tag{3.15}$$

and a is the previously defined lattice period. From Eq. (3.14) *dispersion relations* $\omega_i = \omega_i(q)$, $i = 1..18$, can be obtained as square roots of eigenvalues of hermitian matrix $\hat{\boldsymbol{\mathcal{G}}}(q)$.

The dispersion equation Eq. (3.14) is to be solved numerically, the solutions split into two groups: *acoustic bands* with[4] $\omega(0) = 0$ and *optical bands* with $\omega_i(0) \neq 0$,

---

[3] As we have mentioned above, the effect of boundaries is neglected, so for the sake of simplicity we can choose periodic boundary condition.

[4] As it shown in Sec. 3.3 it can be also a band with $\omega(\theta) = 0$.

$(d\omega_i/dq)|_{q=0} = 0$. The speed of energy propagation by acoustic band is characterized by group velocity $v = (d\omega_i/dq)|_{q=0}$, while for optical bands one can estimate it by the mean group velocity corresponding to whole i-th[20]

$$\frac{1}{\pi}\int_0^{\pi/a} |v_i(q)|dq \tag{3.16}$$

In the next section we will discuss how exactly the existence of the acoustic bands follows from the symmetry properties of the Hessian and matrix $\hat{\boldsymbol{\mathcal{G}}}$.

3.3 Special solutions of the dispersion equation. Acoustic bands

Defined in Eq. (3.15) matrix $\hat{\boldsymbol{\mathcal{G}}}(\phi) = \hat{\boldsymbol{\mathcal{A}}}_W + \hat{\boldsymbol{\mathcal{B}}}_W\hat{\boldsymbol{\mathcal{U}}}_W e^{i\phi} + \hat{\boldsymbol{\mathcal{U}}}_W^{\dagger}\hat{\boldsymbol{\mathcal{B}}}_W^{\dagger}e^{-i\phi}$ has two zero eigenvalues for $\phi = 0$ and one for $\phi = \theta$ on $0 < \phi < \pi$. This fact follows from the two properties the Hessian:

- Translational symmetry

$$\left[\hat{\boldsymbol{\mathcal{A}}} + \hat{\boldsymbol{\mathcal{B}}} + \hat{\boldsymbol{\mathcal{U}}}^{\dagger}\hat{\boldsymbol{\mathcal{B}}}^{\dagger}\hat{\boldsymbol{\mathcal{U}}}\right]\boldsymbol{\eta} = \mathbf{0} \tag{3.17}$$

  where $\boldsymbol{\eta}$ is any 18×1 vector. Indeed, the translational symmetry of Hessian $\hat{\boldsymbol{H}}$ requires $\boldsymbol{E}_{\alpha}^{\dagger}\hat{\boldsymbol{H}}\boldsymbol{E}_{\beta} = 0$, for any α, $\beta = \{x, y, z\}$, and by introducing vector $\boldsymbol{I}_N$, vector of length equal to number of atoms N, consisting of ones, we define $\boldsymbol{E}_{\alpha}$

in $3 \times N$ Cartesian space as[5]

$$\boldsymbol{E}_x = \frac{1}{\sqrt{N}} \boldsymbol{I}_N \otimes \begin{pmatrix} 1 \\ 0 \\ 0 \end{pmatrix}; \quad \boldsymbol{E}_y = \frac{1}{\sqrt{N}} \boldsymbol{I}_N \otimes \begin{pmatrix} 0 \\ 1 \\ 0 \end{pmatrix}; \quad \boldsymbol{E}_z = \frac{1}{\sqrt{N}} \boldsymbol{I}_N \otimes \begin{pmatrix} 0 \\ 0 \\ 1 \end{pmatrix} \tag{3.18}$$

By our assumption only $\hat{\boldsymbol{H}}_{kk} = \hat{\boldsymbol{\mathcal{A}}}$, $\hat{\boldsymbol{H}}_{kk+1} = \hat{\boldsymbol{\mathcal{B}}}$, $\hat{\boldsymbol{H}}_{kk-1} = \hat{\boldsymbol{\mathcal{U}}}^\dagger \hat{\boldsymbol{\mathcal{B}}}^\dagger \hat{\boldsymbol{\mathcal{U}}}$ are non-zeros, so Eq. (3.17) takes place.

- Rotational symmetry

$$\hat{\boldsymbol{\mathcal{A}}} \Big[\boldsymbol{e}_z \times \boldsymbol{r} \Big] + \hat{\boldsymbol{\mathcal{B}}} \Big[\boldsymbol{e}_z \times \Big(\hat{\boldsymbol{\mathcal{U}}} \boldsymbol{r} \Big) \Big] + \hat{\boldsymbol{\mathcal{U}}}^\dagger \hat{\boldsymbol{\mathcal{B}}}^\dagger \hat{\boldsymbol{\mathcal{U}}} \Big[\boldsymbol{e}_z \times \Big(\hat{\boldsymbol{\mathcal{U}}}^\dagger \boldsymbol{r} \Big) \Big] = \boldsymbol{0} \tag{3.19}$$

where cross-product is defined as

$$\boldsymbol{e}_z \times \boldsymbol{r} = \begin{pmatrix} -y_1 \\ x_1 \\ 0 \\ \vdots \\ -y_6 \\ x_6 \\ 0 \end{pmatrix} \tag{3.20}$$

---

[5] compare to Eq. (3.3)

Indeed, Eq. (3.19) just reflects $\hat{\boldsymbol{H}}\boldsymbol{R} = \boldsymbol{0}$ for

$$\boldsymbol{R} = \begin{pmatrix} \vdots \\ \boldsymbol{e}_z \times \left(\hat{\boldsymbol{\mathcal{U}}}^{\dagger}\boldsymbol{r}\right) \\ \boldsymbol{e}_z \times \boldsymbol{r} \\ \boldsymbol{e}_z \times \left(\hat{\boldsymbol{\mathcal{U}}}\boldsymbol{r}\right) \\ \vdots \end{pmatrix} \tag{3.21}$$

Using Eq. (3.10) one can rewrite Eqs. (3.17), (3.19) in "weighted" values:

$$\begin{cases} \left[\hat{\boldsymbol{\mathcal{A}}}_W + \hat{\boldsymbol{\mathcal{B}}}_W + \hat{\boldsymbol{\mathcal{U}}}_W^{\dagger}\hat{\boldsymbol{\mathcal{B}}}_W^{\dagger}\hat{\boldsymbol{\mathcal{U}}}_W\right]\boldsymbol{\eta} = \boldsymbol{0} \\ \hat{\boldsymbol{\mathcal{A}}}_W\left[\boldsymbol{e}_z \times \tilde{\boldsymbol{r}}\right] + \hat{\boldsymbol{\mathcal{B}}}_W\left[\boldsymbol{e}_z \times \left(\hat{\boldsymbol{\mathcal{U}}}_W\tilde{\boldsymbol{r}}\right)\right] + \hat{\boldsymbol{\mathcal{U}}}_W^{\dagger}\hat{\boldsymbol{\mathcal{B}}}_W^{\dagger}\hat{\boldsymbol{\mathcal{U}}}_W\left[\boldsymbol{e}_z \times \left(\hat{\boldsymbol{\mathcal{U}}}_W^{\dagger}\tilde{\boldsymbol{r}}\right)\right] = \boldsymbol{0} \end{cases} \tag{3.22}$$

1. Special solution $\hat{\boldsymbol{\mathcal{G}}}(0)\tilde{\boldsymbol{e}}_z = \boldsymbol{0}$,

   where $\tilde{\boldsymbol{e}}_z = \hat{\boldsymbol{M}}^{1/2}\boldsymbol{e}_z$. Vector $\boldsymbol{e}_z$ is an eigenvector of $\hat{\boldsymbol{\mathcal{U}}}$ so that $\hat{\boldsymbol{\mathcal{U}}}\boldsymbol{e}_z = \boldsymbol{e}_z$. Thus

   $$\hat{\boldsymbol{\mathcal{U}}}_W\tilde{\boldsymbol{e}}_z = \hat{\boldsymbol{M}}^{1/2}\hat{\boldsymbol{\mathcal{U}}}\hat{\boldsymbol{M}}^{-1/2}\hat{\boldsymbol{M}}^{1/2}\boldsymbol{e}_z = \hat{\boldsymbol{M}}^{1/2}\boldsymbol{e}_z = \tilde{\boldsymbol{e}}_z$$

   Therefore

   $$\hat{\boldsymbol{\mathcal{G}}}(0)\tilde{\boldsymbol{e}}_z = \left[\hat{\boldsymbol{\mathcal{A}}}_W + \hat{\boldsymbol{\mathcal{B}}}_W\hat{\boldsymbol{\mathcal{U}}}_W + \hat{\boldsymbol{\mathcal{U}}}_W^{\dagger}\hat{\boldsymbol{\mathcal{B}}}_W^{\dagger}\right]\tilde{\boldsymbol{e}}_z = \left[\hat{\boldsymbol{\mathcal{A}}}_W + \hat{\boldsymbol{\mathcal{B}}}_W + \hat{\boldsymbol{\mathcal{U}}}_W^{\dagger}\hat{\boldsymbol{\mathcal{B}}}_W^{\dagger}\hat{\boldsymbol{\mathcal{U}}}_W\right]\tilde{\boldsymbol{e}}_z = \boldsymbol{0} \tag{3.23}$$

2. Special solution for $\phi = \theta$.

   Vector $\boldsymbol{\xi} = \boldsymbol{e}_x - i\boldsymbol{e}_y$ is also eigenvector of $\hat{\boldsymbol{\mathcal{U}}}$ so that $\hat{\boldsymbol{\mathcal{U}}}\boldsymbol{\xi} = e^{-i\theta}\boldsymbol{\xi}$ and therefore

$\hat{\boldsymbol{\mathcal{U}}}_W\boldsymbol{\xi} = e^{-i\theta}\boldsymbol{\xi}$, $\boldsymbol{\xi} = \tilde{\boldsymbol{e}}_x - i\tilde{\boldsymbol{e}}_y$. Indeed,

$$\hat{\boldsymbol{\mathcal{U}}}\Big(\boldsymbol{e}_x - i\boldsymbol{e}_y\Big) = \Big(\boldsymbol{e}_x\cos\theta - \boldsymbol{e}_y\sin\theta\Big) - i\Big(\boldsymbol{e}_x\sin\theta + \boldsymbol{e}_y\cos\theta\Big) = e^{-i\theta}\Big(\boldsymbol{e}_x - i\boldsymbol{e}_y\Big)$$

Thus

$$\hat{\boldsymbol{\mathcal{G}}}(\theta)\boldsymbol{\xi} = \Big[\hat{\boldsymbol{\mathcal{A}}}_W + \hat{\boldsymbol{\mathcal{B}}}_W\hat{\boldsymbol{\mathcal{U}}}_W e^{i\theta} + \hat{\boldsymbol{\mathcal{U}}}_W^{\dagger}\hat{\boldsymbol{\mathcal{B}}}_W^{\dagger}e^{-i\theta}\Big]\boldsymbol{\xi} = \Big[\hat{\boldsymbol{\mathcal{A}}}_W + \hat{\boldsymbol{\mathcal{B}}}_W + \hat{\boldsymbol{\mathcal{U}}}_W^{\dagger}\hat{\boldsymbol{\mathcal{B}}}_W^{\dagger}\hat{\boldsymbol{\mathcal{U}}}_W\Big]\boldsymbol{\xi} = \boldsymbol{0} \quad (3.24)$$

3. Special solution $\hat{\boldsymbol{\mathcal{G}}}(0)\boldsymbol{\tau}_z = \boldsymbol{0}$, $\boldsymbol{\tau}_z = \boldsymbol{e}_z \times \tilde{\boldsymbol{r}}$.

   First, $\boldsymbol{e}_z \times \Big(\hat{\boldsymbol{\mathcal{U}}}\boldsymbol{r}\Big) = \hat{\boldsymbol{\mathcal{U}}}\Big(\boldsymbol{e}_z \times \boldsymbol{r}\Big)$. Indeed,

$$\hat{\boldsymbol{\mathcal{U}}}\boldsymbol{\tau}_z = \begin{pmatrix} \cos\theta & \sin\theta & 0 \\ -\sin\theta & \cos\theta & 0 \\ 0 & 0 & 1 \end{pmatrix}\begin{pmatrix} -y \\ x \\ 0 \end{pmatrix} = \begin{pmatrix} x\sin\theta - y\cos\theta \\ x\cos\theta + y\sin\theta \\ 0 \end{pmatrix}$$

$$\boldsymbol{e}_z \times \begin{pmatrix} x\cos\theta + y\sin\theta \\ -x\sin\theta + y\cos\theta \\ 0 \end{pmatrix} = \begin{pmatrix} x\sin\theta - y\cos\theta \\ x\cos\theta + y\sin\theta \\ 0 \end{pmatrix}$$

The same can be proved for $\hat{\boldsymbol{\mathcal{U}}}^{\dagger}$. Thus

$$\boldsymbol{0} = \hat{\boldsymbol{\mathcal{A}}}\Big[\boldsymbol{e}_z \times \boldsymbol{r}\Big] + \hat{\boldsymbol{\mathcal{B}}}\Big[\boldsymbol{e}_z \times \Big(\hat{\boldsymbol{\mathcal{U}}}\boldsymbol{r}\Big)\Big] + \hat{\boldsymbol{\mathcal{U}}}^{\dagger}\hat{\boldsymbol{\mathcal{B}}}^{\dagger}\hat{\boldsymbol{\mathcal{U}}}\Big[\boldsymbol{e}_z \times \Big(\hat{\boldsymbol{\mathcal{U}}}^{\dagger}\boldsymbol{r}\Big)\Big] = \Big[\hat{\boldsymbol{\mathcal{A}}} + \hat{\boldsymbol{\mathcal{B}}}\hat{\boldsymbol{\mathcal{U}}} + \hat{\boldsymbol{\mathcal{U}}}^{\dagger}\hat{\boldsymbol{\mathcal{B}}}^{\dagger}\hat{\boldsymbol{\mathcal{U}}}\hat{\boldsymbol{\mathcal{U}}}^{\dagger}\Big]\Big(\boldsymbol{e}_z \times \boldsymbol{r}\Big) =$$
$$\hat{\boldsymbol{M}}^{1/2}\hat{\boldsymbol{\mathcal{G}}}(0)\hat{\boldsymbol{M}}^{1/2}\Big[\boldsymbol{e}_z \times \big(\hat{\boldsymbol{M}}^{-1/2}\tilde{\boldsymbol{r}}\big)\Big] = \hat{\boldsymbol{M}}^{1/2}\hat{\boldsymbol{\mathcal{G}}}(0)\big(\boldsymbol{e}_z \times \tilde{\boldsymbol{r}}\big) = 0 \quad (3.25)$$

As long as $\boldsymbol{e}_z \times \big(\hat{\boldsymbol{M}}^{-1/2}\tilde{\boldsymbol{r}}\big) = \hat{\boldsymbol{M}}^{-1/2}\big(\boldsymbol{e}_z \times \tilde{\boldsymbol{r}}\big)$.

Those special solutions correspond to so-called *acoustic bands*. In perfluoroalkane stranded structure one can expect four acoustic bands: one band $\omega_1(0) = 0$ corresponding to the rotational symmetry (special solution 3); two bands corresponding to translational symmetry (special solution 1), such that $\omega_2(0) = 0$ and $\omega_2(\phi) = \omega_3(2\pi - \phi)$; and one peculiar band $\omega_4(\theta) = 0$ (special solution 2).

In alkane chain with pure translational symmetry the matrix $\hat{\boldsymbol{\mathcal{U}}}$ is an identity matrix and $\hat{\boldsymbol{\mathcal{G}}}_0(\phi) = \hat{\boldsymbol{\mathcal{A}}}_W + \hat{\boldsymbol{\mathcal{B}}}_W e^{i\phi} + \hat{\boldsymbol{\mathcal{B}}}_W^{\dagger} e^{-i\phi}$. There are three special solutions corresponding to translational symmetry of the Hessian, such that

$$\hat{\boldsymbol{\mathcal{G}}}(0)\tilde{\boldsymbol{e}}_x = \hat{\boldsymbol{\mathcal{G}}}(0)\tilde{\boldsymbol{e}}_y = \hat{\boldsymbol{\mathcal{G}}}(0)\tilde{\boldsymbol{e}}_z = \mathbf{0}$$

and one band $\omega_1(0) = 0$ corresponding to the rotational symmetry (special solution 3): four acoustic bands as well.

Practically, the Hessian obtained from DFT-calculations does not reveal ideal translational and rotational symmetry, also the non-zero elements we neglect increase[6] the effect of violation $\hat{\boldsymbol{\mathcal{G}}}(q)$ matrix symmetry properties. It may affect the low-frequency modes, though at the same time mentioned slight symmetry violation has no impact on high-frequency optical modes [20], so the acoustic modes can barely be calculated straightforward from the realistic Hessian, especially in vicinity of $q = 0$. Thus we cannot determine speed of sound for acoustic modes using numerical derivative $d\omega(q)/dq$ at $q = 0$. However some estimate can be done using equation we are to derive below.

---

[6]Even with the next-neighbor interaction and beyond.

3.4 Acoustic velocity

Two solutions with $\omega(0) = 0$ correspond to acoustic modes with acoustic velocities $v = d\omega/dq$, $q = \phi/a = 0$. To find these values we don't need to solve Eq. (3.14) for arbitrary ϕ and take the derivative, the only required numerical calculation is solving eigenvector problem for matrix $\hat{\boldsymbol{\mathcal{G}}}(0)$. To show it we need to consider equation $\hat{\boldsymbol{\mathcal{G}}}(\phi)\boldsymbol{\eta} = \lambda(\phi)\boldsymbol{\eta}$ in vicinity of $\phi = 0$, treating ϕ as a perturbation parameter. For the sake of simplicity, below we omit subscript W for the "weighted" matrices and vectors.

$$\begin{aligned}
\hat{\boldsymbol{\mathcal{G}}}(\phi) &\simeq \hat{\boldsymbol{\mathcal{G}}}_0 + \phi\hat{\boldsymbol{\mathcal{G}}}_1 + \phi^2\hat{\boldsymbol{\mathcal{G}}}_2 \\
\lambda_i(\phi) &\simeq \lambda_i^{(0)} + \phi\lambda_i^{(1)} + \phi^2\lambda_i^{(2)} \\
\boldsymbol{\eta}_i &\simeq |i\rangle + \phi\boldsymbol{\eta}_i^{(1)} + \phi^2\boldsymbol{\eta}_i^{(2)}
\end{aligned} \tag{3.26}$$

where we use the following notations:

$$\begin{aligned}
\hat{\boldsymbol{\mathcal{G}}}_0 &= \hat{\boldsymbol{\mathcal{A}}} + \hat{\boldsymbol{\mathcal{B}}}\hat{\boldsymbol{\mathcal{U}}} + \hat{\boldsymbol{\mathcal{U}}}^\dagger\hat{\boldsymbol{\mathcal{B}}}^\dagger \\
\hat{\boldsymbol{\mathcal{G}}}_1 &= i\left[\hat{\boldsymbol{\mathcal{B}}}\hat{\boldsymbol{\mathcal{U}}} - \hat{\boldsymbol{\mathcal{U}}}^\dagger\hat{\boldsymbol{\mathcal{B}}}^\dagger\right] \\
\hat{\boldsymbol{\mathcal{G}}}_2 &= -\frac{1}{2}\left[\hat{\boldsymbol{\mathcal{B}}}\hat{\boldsymbol{\mathcal{U}}} + \hat{\boldsymbol{\mathcal{U}}}^\dagger\hat{\boldsymbol{\mathcal{B}}}^\dagger\right]
\end{aligned} \tag{3.27}$$

for matrices and $|i\rangle$ for eigenvectors of $\hat{\boldsymbol{\mathcal{G}}}(0)$. The eigenvectors of acoustic modes of interest are

$$\begin{aligned}
|1\rangle &= \frac{\boldsymbol{e}_z}{|\boldsymbol{e}_z|} \\
|2\rangle &= \frac{\boldsymbol{\tau}_z}{|\boldsymbol{\tau}_z|}
\end{aligned} \tag{3.28}$$

with the rest of eigenvectors of $\hat{\boldsymbol{\mathcal{G}}}_0$ $|i\rangle$, $i = 5..n$, corresponding to the optical bands, for certainty ordered as $\lambda_5^{(0)} < \lambda_6^{(0)} < .. < \lambda_{18}^{(0)}$. As long as $\omega_i(\phi) = \sqrt{\lambda_i(\phi)}$, to derive acoustic velocities we are particularly interested in the corrections to λ_1 and

λ_2. As it already shown, $\lambda_1^{(0)} = \lambda_2^{(0)} = 0$, so we are to deal with two-fold degenerated eigenvectors.

To proceed further we need to supplement the symmetry relations Eqs. (3.17), (3.19) with one more condition. If the considered unit cell is in the middle (for simplicity we can consider a unit cell with number $k = 0$ of an infinite chain), any deformation on the left will cause identical energy changes as the same deformation one the right. Considering translational and rotational deformations we obtain the condition:

$$\begin{aligned} \hat{\boldsymbol{\mathcal{B}}}\boldsymbol{e}_z &= \hat{\boldsymbol{\mathcal{U}}}^\dagger \hat{\boldsymbol{\mathcal{B}}}^\dagger \hat{\boldsymbol{\mathcal{U}}} \boldsymbol{e}_z \\ \hat{\boldsymbol{\mathcal{B}}}\boldsymbol{\tau}_z &= \hat{\boldsymbol{\mathcal{U}}}^\dagger \hat{\boldsymbol{\mathcal{B}}}^\dagger \hat{\boldsymbol{\mathcal{U}}} \boldsymbol{\tau}_z \end{aligned} \tag{3.29}$$

Now we can calculate the important matrix elements of $\hat{\boldsymbol{\mathcal{G}}}_1$. By definition of $\hat{\boldsymbol{\mathcal{G}}}_1$ all its diagonal elements are equal to zero, $\left(\hat{\boldsymbol{\mathcal{G}}}_1\right)_{12} = 0$ by property Eq. (3.29).

$$\langle i|\hat{\boldsymbol{\mathcal{G}}}_1|i\rangle = \langle 1|\hat{\boldsymbol{\mathcal{G}}}_1|2\rangle = 0 \tag{3.30}$$

From perturbation theory it can be shown [69] that

$$\begin{aligned} \lambda_1^{(1)} &= \lambda_2^{(1)} = \left|\langle 1|\hat{\boldsymbol{\mathcal{G}}}_1|2\rangle\right| = 0 \\ \lambda_i^{(2)} &= \langle i|\hat{\boldsymbol{\mathcal{G}}}_2|i\rangle - \sum_{j=5}^{n} \frac{\left|\langle i|\hat{\boldsymbol{\mathcal{G}}}_1|j\rangle\right|^2}{\lambda_j^{(0)}}, \quad i = 1, 2 \end{aligned} \tag{3.31}$$

Thus in vicinity of of $\phi = 0$ acoustic mode frequency $\omega = \phi\sqrt{\lambda^{(2)}}$ so that the group velocity is

$$v_i = a\sqrt{\frac{1}{2}\langle i|\hat{\boldsymbol{\mathcal{A}}}|i\rangle - \sum_{j=5}^{n} \frac{\left|\langle i|\hat{\boldsymbol{\mathcal{G}}}_1|j\rangle\right|^2}{\langle j|\hat{\boldsymbol{\mathcal{G}}}_0|j\rangle}}, \quad i = 1, 2 \tag{3.32}$$

where we replaced $\hat{\boldsymbol{\mathcal{G}}}_2$ with $\hat{\boldsymbol{\mathcal{A}}}$ using Eqs. (3.23), (3.25).

The estimates for C_{16} perfluoroalkane compound (see Fig. 3.1 and Sec. 3.6) are $v_1 \simeq 9.1$ km/s and $v_2 \simeq 1.8$ km/s.

3.5 Long-order interaction

Eq. (3.14) obtained for the case of interaction between adjacent unit cells can be generalized as long as the same symmetry assumptions are preserved. Consider a chain with $2N+1$ ($N \longrightarrow \infty$) unit cells. Introduce the following notations:

1. $\hat{\boldsymbol{\mathcal{H}}}_{mn}$ - part of the Hessian, related to the interaction between unit cells m and n, so that $\hat{\boldsymbol{\mathcal{H}}}_{mm}$ describes interaction between atoms in the unit cell m;
2. for the central unit cell $\hat{\boldsymbol{\mathcal{A}}} = \hat{\boldsymbol{\mathcal{H}}}_{00}$;
3. $\hat{\boldsymbol{\mathcal{B}}}_n = \hat{\boldsymbol{\mathcal{H}}}_{0n}$, $n = \pm 1.. \pm N$
4. the dispersion equation $\hat{\boldsymbol{\mathcal{G}}}(aq)\boldsymbol{\eta}_q = \omega_q^2 \boldsymbol{\eta}_q$ with new definition[7]

$$\hat{\boldsymbol{\mathcal{G}}}(\phi) = \hat{\boldsymbol{\mathcal{A}}} + \sum_n \left[\hat{\boldsymbol{\mathcal{B}}}_n \hat{\boldsymbol{\mathcal{U}}}^n e^{in\phi} + \left(\hat{\boldsymbol{\mathcal{U}}}^\dagger\right)^n \hat{\boldsymbol{\mathcal{B}}}_n^\dagger e^{-in\phi} \right] \tag{3.33}$$

Eq. (3.32) will be preserved with

$$\begin{aligned} \hat{\boldsymbol{\mathcal{G}}}_0 &= \hat{\boldsymbol{\mathcal{G}}}(0) \\ \hat{\boldsymbol{\mathcal{G}}}_1 &= i \sum_n n \left[\hat{\boldsymbol{\mathcal{B}}}_n \hat{\boldsymbol{\mathcal{U}}}^n - \left(\hat{\boldsymbol{\mathcal{U}}}^\dagger\right)^n \hat{\boldsymbol{\mathcal{B}}}_n^\dagger \right] \\ \hat{\boldsymbol{\mathcal{G}}}_2 &= -\frac{1}{2} \sum_n n^2 \left[\hat{\boldsymbol{\mathcal{B}}}_n \hat{\boldsymbol{\mathcal{U}}}^n + \left(\hat{\boldsymbol{\mathcal{U}}}^\dagger\right)^n \hat{\boldsymbol{\mathcal{B}}}_n^\dagger \right] \end{aligned} \tag{3.34}$$

in form

$$v_i = a \sqrt{ \left\langle i \middle| \hat{\boldsymbol{\mathcal{G}}}_2 \middle| i \right\rangle - \sum_{j=5}^{n} \frac{\left| \left\langle i \middle| \hat{\boldsymbol{\mathcal{G}}}_1 \middle| j \right\rangle \right|^2}{\left\langle j \middle| \hat{\boldsymbol{\mathcal{G}}}_0 \middle| j \right\rangle} }, \quad i = 1, 2 \tag{3.35}$$

---

[7] As in Sec. 3.4 we omit subscript W

3.6 Numerical calculation of symmetry parameters

We assume the following symmetry in the long enough perfluoroalkane chain: every elementary cell might be obtained from the previous one by translation along z-axis (lattice period a) and rotation by constant angle θ. The optimized geometry and the Hessian matrix were obtained from DFT-calculation for perfluoroalkane compound C_{16} with CO_2H and CF_2H complexes on the ends [16], `B3LYP` hybrid functional and `6-31(d, p)` basis sets were used, as implemented in a Gaussian 09 software package [68]. To reduce boundary effects, seven elementary cells were picked, starting with the third carbon atom from carbolic acid side (Fig. 3.1). To determine parameters a and θ from this geometry one can use mean least square method.

Introduce matrix $\hat{\boldsymbol{\mathcal{U}}}$ - generator of rotations by angle θ around z-axis:

$$\hat{\boldsymbol{\mathcal{U}}} = \begin{pmatrix} \cos\theta & \sin\theta & 0 \\ -\sin\theta & \cos\theta & 0 \\ 0 & 0 & 1 \end{pmatrix} \tag{3.36}$$

To estimate the parameters one needs minimize function

$$\mathcal{S}(a,\theta) = \sum_{k=1}^{n-1}\sum_{i=1}^{6}\left[\boldsymbol{r}_{k+1}^{i} - \hat{\boldsymbol{\mathcal{U}}}\boldsymbol{r}_{k}^{i} - a\boldsymbol{e}_z\right]^{\dagger}\left[\boldsymbol{r}_{k+1}^{i} - \hat{\boldsymbol{\mathcal{U}}}\boldsymbol{r}_{k}^{i} - a\boldsymbol{e}_z\right] \tag{3.37}$$

where k is number of the unit cell and i is number of the atom into the unit cell. To simplify the calculations one can consider $\alpha = \cos\theta$, $\beta = \sin\theta$ as two independent

parameters with constrain $\alpha^2 + \beta^2 - 1 = 0$. The matrix (3.36) becomes

$$\begin{pmatrix} \alpha & \beta & 0 \\ -\beta & \alpha & 0 \\ 0 & 0 & 1 \end{pmatrix}$$

So introducing Lagrange multiplier λ one can obtain the solution from

$$\tilde{\mathcal{S}}_\lambda = \mathcal{S}(a, \alpha, \beta) + \lambda \left[\det \left(\hat{\boldsymbol{u}}^\dagger \hat{\boldsymbol{u}} \right) - 1 \right] \longrightarrow \min \tag{3.38}$$

Introduce coefficients

$$A = \sum_{k=1}^{n-1} \sum_{i=1}^{6} \left(x_{k+1}^i x_k^i + y_{k+1}^i y_k^i \right) \tag{3.39}$$

$$B = -\sum_{k=1}^{n-1} \sum_{i=1}^{6} \left((x_k^i)^2 + (y_k^i)^2 \right) \tag{3.40}$$

$$C = \sum_{k=1}^{n-1} \sum_{i=1}^{6} \left(x_{k+1}^i y_k^i - y_{k+1}^i x_k^i \right) \tag{3.41}$$

and obtain parameters:

$$a = \frac{1}{6(n-1)} \sum_{k=1}^{n-1} \sum_{i=1}^{6} \left(z_{k+1}^i - z_k^i \right) \tag{3.42}$$

$$\alpha = \pm \frac{A}{\sqrt{A^2 + C^2}} \tag{3.43}$$

$$\beta = \pm \frac{C}{\sqrt{A^2 + C^2}} \tag{3.44}$$

The sign $\pm$ corresponds to the right or left twist.

The numerical values obtained for perfluoroalkane chain are $a = 2.6\,\text{Å}$ and $\theta = 29°$. This approach obviously can be applied for any helix-structured periodic polymer.

3.7 Energy bands theory application for ballistic energy transport in alkane oligomers

As it was mentioned above, even minor deviations from ideal structure in Hessian matrix lead to difficulties in numerical study of acoustic modes. At the same time slight symmetry violation has no impact on high-frequency optical modes. In this section we present an example of practical energy bands theory application for study of ballistic transport in alkane chains.

In the recent paper [20] there were reported results of study by relaxation-assisted two-dimensional infrared spectroscopy of the intramolecular transport of vibrational energy in oligomers featuring alkane chains of various length. The transport was initiated by exciting various end-group modes (tags) such as different modes of the azido ν(N≡N) and ν(N=N), carboxylic acid ν(C=O), and succinimide ester ν_{as}(C≡O) with short mid-IR laser pulses. It was shown that the transport via alkane chains is ballistic and the transport speed is dependent on the type of the tag mode that initiates the transport. The transport speed of 8.0 Å/ps was observed when initiated by either ν(C=O) or ν_{as}(C≡O). When initiated by ν(N≡N) and ν(N=N), the transport speed of 14.4 ± 2 and 11 ± 4 Å/ps was observed. Analysis of the vibrational relaxation channels of different tags, combined with the results for the group velocity evaluation, permitted identification of the chain bands predominantly contributing to the transport for different cases of the transport initiation. In the present discussion we will concentrate on group velocity evaluation.

Some refinement for the involvement of different chain bands can be obtained from the comparison of the group velocities supported by each chain band with the experimental transport speeds. Previously the band structure was evaluated for alkane chains using semi-empirical force field methods [76] and these results are consistent

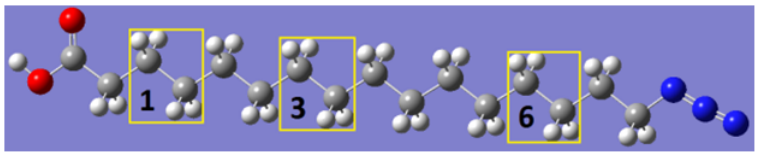

(a) projection on X-Z plane

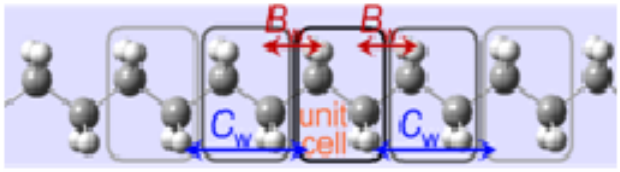

(b) unit cell with the nearest and the next neighbor interaction

Figure 3.2: Alkane compound C_{15} with CO_2H and N_3 complexes on the ends: (a) projection on X-Z plane, the unit cells are shown; (b) unit cell with the nearest and the next neighbor interaction.

with our DFT analysis. The Hessian matrix of force constants for the alkane chain was obtained from the DFT normal-mode analysis for CH15-a: the optimized geometry and the Hessian matrix were obtained from DFT calculations for alkane chain consisting of 15 carbon atoms with carboxylic acid and N_3 azido group on the sides (Fig. 3.2(a)). The Gaussian09 software was used, `B3LYP` calculation method with `6-311+G(d.p)` basis sets. To reduce boundary effects we picked out 6 unit cells starting with the 3rd carbon atom (from carbolic acid side) and applied Eq. (3.14) to the 3rd and 4-th unit cells in the middle of the chain (with identical results, as expected) with some corrections for matrix $\hat{\boldsymbol{\mathcal{G}}}$:

$$\hat{\boldsymbol{\mathcal{G}}}(aq) = \hat{\boldsymbol{\mathcal{A}}}_W + (\hat{\boldsymbol{\mathcal{B}}}_W + \hat{\boldsymbol{\mathcal{B}}}_W^\dagger)\cos(aq) + i(\hat{\boldsymbol{\mathcal{B}}}_W - \hat{\boldsymbol{\mathcal{B}}}_W^\dagger)\sin(aq) + (\hat{\boldsymbol{\mathcal{C}}}_W + \hat{\boldsymbol{\mathcal{C}}}_W^\dagger)\cos(2aq) + i(\hat{\boldsymbol{\mathcal{C}}}_W - \hat{\boldsymbol{\mathcal{C}}}_W^\dagger)\sin(2aq) \quad (3.45)$$

The difference with Eq. (3.15) is that $\hat{\boldsymbol{\mathcal{U}}}$ is identity matrix as long as $\theta = 0$ and we use the next-neighbor approximation with $\hat{\boldsymbol{\mathcal{C}}} = \hat{\boldsymbol{H}}_{kk+2}$ (see Fig. 3.2(b) and Sec. 3.5). This short range approximation is justified by relation $|\hat{\boldsymbol{H}}_{kk\pm3}|/|\hat{\boldsymbol{H}}_{kk\pm1}| \lesssim 6 \cdot 10^{-3}$.

The lattice period was estimated as $a = 2.56\,\text{Å}$ (see Sec. 3.6).

The optical bands, shown in Fig. 3.3, appear in pairs and are represented by the lines of the same color. For example, the two rocking modes are shown with black lines, where the first band spans from 733 to 804 cm^{-1} and the second band spans from 804 to 1082 cm^{-1}. It is sufficient to plot the band in the wave-vector (q) region from 0 to π/a; for the finite chain length, this portion of the band contains the number of states equal to the number of unit cells. Due to central symmetry of the unit cell, the two bands of the same motion nature have the same energy at $q = \pi/a$ and continuous derivative. Thick lines are used in Fig. 3.3 to identify the bands of the same motion type. Each thick line comprises two optical bands, one in the wave-vector region from 0 to π/a, another from π/a to $2\pi/a$ (Fig. 3.3).

The group velocity for a narrow range of frequencies centered at $\omega(q_0)$ is determined as $v(q_0) = (d\omega/dq)_{q=q_0}$. Because the velocity is different for different ranges of wave-vectors (frequencies), the mean group velocity over selected range of wave-vectors from q_1 to q_2 is computed as

$$\langle v_b \rangle = \frac{1}{q_2 - q_1} \int_{q_1}^{q_2} |v(q)| dq \tag{3.46}$$

The mean group velocity corresponding to the whole i-th band is defined by Eq. (3.16):

$$\langle v_i \rangle = \frac{1}{\pi} \int_{0}^{\pi/a} |v_i(q)| dq$$

According to Eq. (3.46) the frequency width of the wave packet affects its group velocity. Therefore, the group velocities were computed for each chain band for the frequency range corresponding to the $1/e$ peak width of the two stretching transitions initiating the wave packet, ν(N=N) and ν(N−C), and the results are given

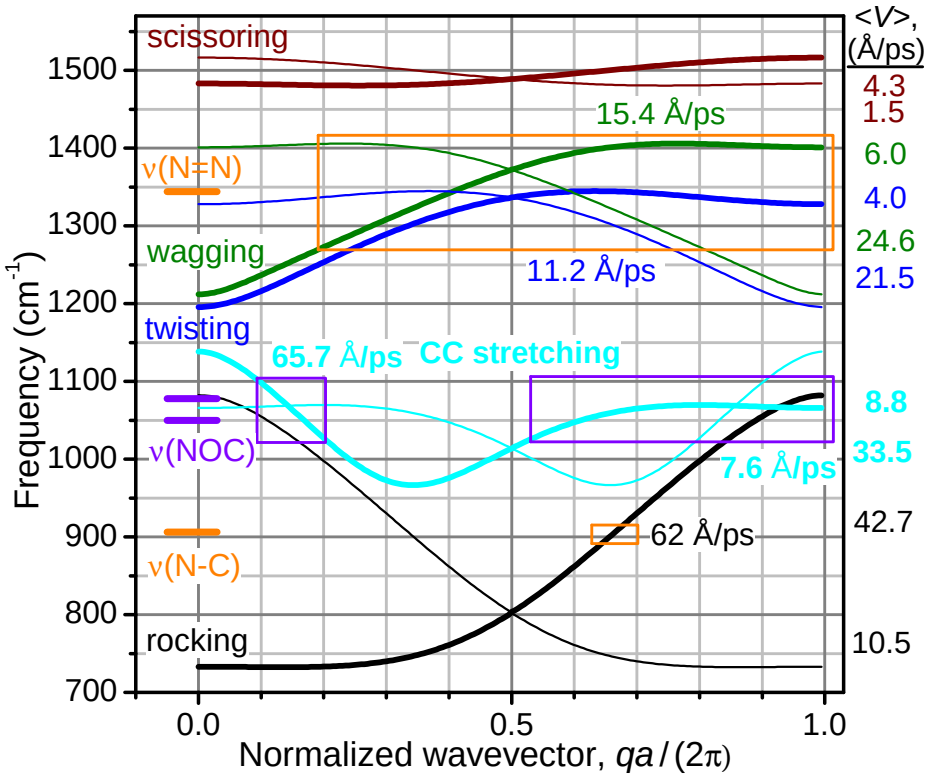

Figure 3.3: Structure of 10 lowest-energy optical bands obtained as eigenvalues of matrix from Eq. (3.45) for the alkane chain (labeled) as a function of a normalized wave-vector. The boxes match the width of the azido-group stretching modes, ν(N=N) and ν(C−N) and the ν(NOC) (orange) of the succinimide ester (violet). Mean group velocities computed with Eq. (3.16) are shown on the right. Velocities in the boxes are computed with Eq. (3.46).

in Fig. 3.3. The experimentally measured transport speed of 14.4 Å/ps is close to those calculated for the CH_2 wagging (15.4 Å/ps) and twisting (11.2 Å/ps) bands. The group velocity supported by the CH_2 rocking band is significantly larger than the experimental value. Small density of states in this band results in a low quality of the formed wave packet and reduces its throughput. Thus, it was concluded that the CH_2 twisting and wagging bands contribute most to the transport initiated by the ν(N≡N) mode.

3.8 Conclusion

In this chapter we developed semi-classical method for investigation of energy ballistic transport in oligomers, based on solution of dispersion equations with parameters obtained from quantum mechanical calculations. This method is applicable for long polymer chains of different structure (perfluoroalkane, alkane, PEG etc.), if their optimized geometry and interatomic interaction possess translational-rotational symmetry. Practically, it is difficult to investigate acoustic bands in the molecules, because of sensitivity of low-frequency modes to deviations from ideal geometry, though it can be possible with development of Hessian modeling based on exact DFT-calculations. We also considered a practical example of the recently reported energy bands study in alkane chain.

Appendices

Appendix A

Derivations for the Liouville-Bloch equation

A.1 White noise in the quantum Liouville - Bloch equation

In this section derive *quantum Bloch-Liouville* equation with decoherence as a result of dynamical energy fluctuations. The Hamiltonian used in Section 1.2 is

$$\hat{\boldsymbol{\mathcal{H}}} = \sum_m \omega_m \hat{b}_m^\dagger \hat{b}_m + \frac{1}{2} \sum_{mn} \Delta_{mn} \left(\hat{b}_m^\dagger \hat{b}_n + \hat{b}_m \hat{b}_n^\dagger \right) \tag{A.1}$$

with non-diagonal matrix elements Δ_{mn}:

$$\Delta_{mn} = \Delta_{mn} \left(\delta_{mn+1} + \delta_{mn-1} \right) \tag{A.2}$$

for the nearest-neighbor interaction. The diagonal matrix elements are delta - correlated:

$$\langle \delta\omega_m(t_1) \delta\omega_n(t_2) \rangle = \frac{W}{2} \delta_{mn} \delta(t_1 - t_2) \tag{A.3}$$

Off-diagonal matrix elements are also delta-correlated. We split the elements Δ_{mn} into real and imaginary parts:

$$\begin{aligned} \Delta_{mn} &= \alpha_{mn} + i\beta_{mn} \\ \alpha_{nm} &= \alpha_{mn} \\ \beta_{nm} &= -\beta_{mn} \end{aligned} \tag{A.4}$$

and introduce the fluctuations separately:

$$\langle \delta\alpha_{mn}(t_1)\delta\alpha_{kl}(t_2)\rangle = \frac{\tilde{W}}{4}\left(\delta_{mk}\delta_{nl} + \delta_{ml}\delta_{nk}\right)\left(\delta_{mn+1} + \delta_{mn-1}\right)\delta(t_1 - t_2) \tag{A.5}$$

preserving the Hamiltonian and its fluctuation as hermitian operators.

$$\langle \delta\beta_{mn}(t_1)\delta\beta_{kl}(t_2)\rangle = \frac{\tilde{W}}{4}\left(\delta_{mk}\delta_{nl} - \delta_{ml}\delta_{nk}\right)\left(\delta_{mn+1} + \delta_{mn-1}\right)\delta(t_1 - t_2) \tag{A.6}$$

Thus the correlation of the off-diagonal elements is given by

$$\begin{aligned} \langle \delta\Delta_{mn}(t_1)\delta\Delta_{kl}(t_2)\rangle &= \langle \delta\alpha_{mn}(t_1)\delta\alpha_{kl}(t_2)\rangle - \langle \delta\beta_{mn}(t_1)\delta\beta_{kl}(t_2)\rangle = \\ &\frac{\tilde{W}}{4}\Big[\left(\delta_{mk}\delta_{nl} + \delta_{ml}\delta_{nk}\right) - \left(\delta_{mk}\delta_{nl} - \delta_{ml}\delta_{nk}\right)\Big]\left(\delta_{mn+1} + \delta_{mn-1}\right)\delta(t_1 - t_2) = \\ &\frac{\tilde{W}}{2}\delta_{ml}\delta_{nk}\left(\delta_{mn+1} + \delta_{mn-1}\right)\delta(t_1 - t_2) \end{aligned} \tag{A.7}$$

Also, the average values of diagonal and off-diagonal elements are:

$$\begin{aligned} \langle \omega_m(t)\rangle &= \omega \\ \langle \Delta_{mn}(t)\rangle &= \Delta \end{aligned} \tag{A.8}$$

Hence it is natural to introduce following notations splitting the Hamiltonian into

regular and irregular parts:

$$\begin{aligned}
\omega_m(t) &= \omega + \delta\omega_m(t) \\
\Delta_{mn}(t) &= \Delta + \delta\Delta_{mn}(t) \\
\hat{\boldsymbol{\mathcal{H}}} &= \left\langle \hat{\boldsymbol{\mathcal{H}}} \right\rangle + \delta\hat{\boldsymbol{\mathcal{H}}}
\end{aligned} \tag{A.9}$$

The quantum Liouville equation (also called von Neumann equation) is

$$\frac{\partial \rho}{\partial t} = -\frac{i}{\hbar}\Big[\hat{\boldsymbol{\mathcal{H}}}, \rho\Big] \tag{A.10}$$

We are to derive equation for $\langle \partial\rho/\partial t \rangle$, for the sake of simplicity we will omit $< .. >$ in the left part, assuming below that the notation ρ stands for the average value of the density matrix with respect to the fluctuations. The regular part of Eq. (A.10) has a form of

$$-\frac{i}{\hbar}\Big[\left\langle \hat{\boldsymbol{\mathcal{H}}} \right\rangle, \rho\Big]_{mn} = i\Delta\Big\{\rho_{mn+1} + \rho_{mn-1} - \rho_{m+1n} - \rho_{m-1n}\Big\} \tag{A.11}$$

and the irregular part

$$-\frac{i}{\hbar}\left\langle \Big[\delta\hat{\boldsymbol{\mathcal{H}}}, \rho\Big] \right\rangle_{mn} = i\left\langle \Big\{\delta\omega_n - \delta\omega_m\Big\}\rho_{mn} \right\rangle + i\sum_k \Big\{ \langle \rho_{mk}\delta\Delta_{kn}\rangle - \langle \delta\Delta_{mk}\rho_{kn}\rangle \Big\} \tag{A.12}$$

First, consider the diagonal part.

$$\begin{aligned}
\langle \delta\omega_m \rho_{mn}\rangle &= \int_{t-\delta t}^{t} d\tau \left\langle \delta\omega_m(t)\frac{\partial \rho_{mn}}{\partial \tau} \right\rangle \\
&\simeq i\int_{t-\delta t}^{t} d\tau \left\langle \delta\omega_m(t)\Big\{\delta\omega_m(\tau) - \delta\omega_n(\tau)\Big\} \right\rangle \rho_{mn} = i\frac{W}{2}\left(1 - \delta_{mn}\right)\rho_{mn}
\end{aligned}$$

Thus the first order correction due to the energy fluctuations is

$$-\frac{i}{\hbar}\left\langle\left[\delta\hat{\boldsymbol{\mathcal{H}}},\rho\right]\right\rangle_{mn}^{diag}=-W(1-\delta_{mn})\rho_{mn} \tag{A.13}$$

In the same way consider off-diagonal part:

$$\sum_k\langle\rho_{mk}\delta\Delta_{kn}\rangle=\sum_k\int\limits_{t-\delta t}^{t}d\tau\left\langle\frac{\partial\rho_{mk}}{\partial\tau}\delta\Delta_{kn}(t)\right\rangle\simeq$$

$$\simeq i\sum_k\sum_p\int\limits_{t-\delta t}^{t}d\tau\Big\{\rho_{mp}\left\langle\delta\Delta_{kn}(t)\delta\Delta_{pk}(\tau)\right\rangle-\left\langle\delta\Delta_{kn}(t)\delta\Delta_{mp}(\tau)\right\rangle\rho_{pk}\Big\}=$$

$$=i\frac{\tilde{W}}{2}\sum_k\sum_p\Big\{\rho_{mp}\delta_{kk}\delta_{np}-\delta_{kp}\delta_{nm}\rho_{pk}\Big\}\Big(\delta_{kn+1}+\delta_{kn-1}\Big)=$$

$$i\frac{\tilde{W}}{2}\sum_k\Big\{\rho_{mn}\delta_{kk}-\delta_{mn}\rho_{kk}\Big\}\Big(\delta_{kn+1}+\delta_{kn-1}\Big)=i\frac{\tilde{W}}{2}\Big\{2\rho_{mn}-\delta_{mn}\Big(\rho_{mm-1}+\rho_{mm+1}\Big)\Big\}$$

$$\sum_k\langle\delta\Delta_{mk}\rho_{kn}\rangle=\sum_k\int\limits_{t-\delta t}^{t}d\tau\left\langle\delta\Delta_{mk}(t)\frac{\partial\rho_{kn}}{\partial\tau}\right\rangle\simeq$$

$$\simeq i\sum_k\sum_p\int\limits_{t-\delta t}^{t}d\tau\Big\{\rho_{kp}\left\langle\delta\Delta_{mk}(t)\delta\Delta_{pn}(\tau)\right\rangle-\left\langle\delta\Delta_{mk}(t)\delta\Delta_{kp}(\tau)\right\rangle\rho_{pn}\Big\}=$$

$$=i\frac{\tilde{W}}{2}\sum_k\sum_p\Big\{\rho_{kp}\delta_{mn}\delta_{kp}-\delta_{mp}\delta_{kk}\rho_{pn}\Big\}\Big(\delta_{km+1}+\delta_{km-1}\Big)=$$

$$i\frac{\tilde{W}}{2}\sum_k\Big\{\rho_{kk}\delta_{mn}-\delta_{kk}\rho_{mn}\Big\}\Big(\delta_{km+1}+\delta_{km-1}\Big)=-i\frac{\tilde{W}}{2}\Big\{2\rho_{mn}-\delta_{mn}\Big(\rho_{mm-1}+\rho_{mm+1}\Big)\Big\}$$

Thus the first order correction due to the off-diagonal energy fluctuations is

$$-\frac{i}{\hbar}\left\langle\left[\delta\hat{\boldsymbol{\mathcal{H}}},\rho\right]\right\rangle_{mn}^{offdiag}=-2\tilde{W}(1-\delta_{mn})\rho_{mn}+\tilde{W}\delta_{mn}(\rho_{m-1m-1}-2\rho_{mm}+\rho_{m+1m+1}) \tag{A.14}$$

Combining Eqs. (A.10), (A.13), (A.14) we obtain quantum Liouville-Bloch equation:

$$\frac{\partial \rho_{mn}}{\partial t} = i\Delta\Big\{\rho_{mn+1} + \rho_{mn-1} - \rho_{m+1n} - \rho_{m-1n}\Big\} - \\ - (W + 2\tilde{W})(1 - \delta_{mn})\rho_{mn} + \tilde{W}\delta_{mn}\Big\{\rho_{m-1m-1} - 2\rho_{mm} + \rho_{m+1m+1}\Big\} \quad \text{(A.15)}$$

As one can see above the physical source of the decoherence is the fluctuation of energy; mathematically it appears in the equation (causing the irreversibility) as a result of transition to a "rough" time scale with some typical time step δt (so-called coarse-graining [63]), within which many "collisions" occur so that the noise can be considered as delta-correlated. By replacing two constants W, $\tilde{W}$ with one decoherence rate $W : W + 2\tilde{W} \longrightarrow W$ and by neglecting additional channel $\tilde{W}\delta_{mn}\Big\{\rho_{m-1m-1} - 2\rho_{mm} + \rho_{m+1m+1}\Big\}$ due to its week contribution to the coherent transport for assumption $W \ll \Delta$, we represent Eq. (A.15) in a form of

$$\frac{\partial \rho_{mn}}{\partial t} = -i\Delta\left\{\rho_{m-1n} + \rho_{m+1n} - \rho_{mn-1} - \rho_{mn+1}\right\} - W\left(1 - \delta_{mn}\right)\rho_{mn} \quad \text{(A.16)}$$

which corresponds to Eq. (1.6) with $\gamma = 0$ (see Section 1.2).

A.2 Derivation of the exact solution

We are to solve quantum *Liouville-Bloch equation*

$$\frac{\partial \rho_{mn}}{\partial t} = -i\Delta \left\{ \rho_{m-1n} + \rho_{m+1n} - \rho_{mn-1} - \rho_{mn+1} \right\} - (W+\gamma)\rho_{mn} + W\delta_{mn}\rho_{mn} \quad \text{(A.17)}$$

$$\rho_{mn}(0) = \delta_{0m}\delta_{0n} \quad \text{(A.18)}$$

The solution of Eq. (1.6) for the diagonal elements of the density matrix can be obtained in the exact form in the continuous limit, $N \gg 1$. This limit is equivalent to evaluating the *inverse Fourier transform* of the solution in the momentum representation obtained in Ref. [26]. Importantly this solution can be evaluated in the analytical form in space-time representation. The probability of finding the excitation on the n-th site is given by the expression

$$P_n(t) = e^{-(W+\gamma)t} \Bigg\{ \mathrm{J}_n^2(2\Delta t) + \frac{W}{4\Delta} \Bigg[\mathrm{I}_0 \left(W\sqrt{t^2 - \frac{n^2}{4\Delta^2}} \right) + \mathrm{L}_0 \left(W\sqrt{t^2 - \frac{n^2}{4\Delta^2}} \right) \Bigg] \theta\left(t^2 - \frac{n^2}{4\Delta^2} \right) \Bigg\} \quad \text{(A.19)}$$

where J_n and I_0 are the n-th order and zero-order Bessel functions, respectively, and L_0 is the zero-order Struve function. [41] The derivation of Eq. (A.19) is given below.

A.2.1 General approach

Applying the *Fourier transform*, $\tilde{\rho}(p,k;t) = \sum \rho_{mn} \exp\{ia(pn - km)\}$, to Eq. (A.17) with respect to both indices, m and n, we obtain

$$\dot{\tilde{\rho}}(p,k;t) = -i2\Delta \left\{ \cos(pa) - \cos(ka) \right\} \tilde{\rho}(p,k;t) - (W+\gamma)\tilde{\rho}(k,p;t) + W\tilde{P}(p-k;t) \quad \text{(A.20)}$$

where

$$\tilde{P}(q) = \sum_n e^{iaqn} \rho_{nn} \tag{A.21}$$

is the *Fourier transform* of the site-diagonal density matrix characterizing transport of the excitation density and a is the average distance between two adjacent monomers.

If one can manage to find $\tilde{P}(q)$, then the diagonal components of the density matrix can be found as the *inverse Fourier transform*:

$$\rho_{nn}(t) = \left(\frac{a}{2\pi}\right)^2 \int_{-\pi/a}^{+\pi/a} dp \int_{-\pi/a}^{+\pi/a} dk e^{-i(p-k)an} \tilde{P}(p-k;t) \tag{A.22}$$

After applying a *Laplace transform* to Eq. (A.20) with respect to time

$$\tilde{\rho}(z) = \mathcal{L}_z \left[\tilde{\rho}(z)\right] = \int_0^{+\infty} dt e^{-zt} \tilde{\rho}(t) \tag{A.23}$$

one can represent the density matrix in terms of its diagonal part as

$$\tilde{\rho}(p,k;z) = \frac{1 + W\tilde{P}(p-k;z)}{z + i2\Delta\left[\cos(pa) - \cos(ka)\right] + W + \gamma} \tag{A.24}$$

where $2\Delta\cos(pa)$ describes the spectrum of optical phonons within the band. The group velocity for the specific wave vector p is given by $2a\Delta\sin(pa)$. The maximum velocity corresponds to $p = \pi/(2a)$ and is given by $v_{\max} = 2a\Delta$. We will show below that this is the actual velocity of the *ballistic* transport. Using the relation between $\tilde{P}$ and $\tilde{\rho}$

$$\tilde{P}(q) = \frac{a}{2\pi} \int_{-\pi/a}^{+\pi/a} dp \int_{-\pi/a}^{+\pi/a} dk \delta(p-k-q) \tilde{\rho}(p,k) \tag{A.25}$$

and the identity

$$\frac{a}{2\pi}\int\limits_{-\pi/a}^{+\pi/a} dp \int\limits_{-\pi/a}^{+\pi/a} dk \frac{\delta(p-k-q)}{z+W+\gamma+i2\Delta\left[\cos(pa)-\cos(ka)\right]} = \frac{1}{\sqrt{\left[z+W+\gamma\right]^2+\left[4\Delta\sin(qa/2)\right]^2}} \quad \text{(A.26)}$$

one can solve Eq. (A.24) for $\tilde{P}$ in z-representation:

$$\tilde{P}(q;z) = \frac{1}{\sqrt{\left[z+W+\gamma\right]^2+\left[4\Delta\sin(qa/2)\right]^2}-W} \quad \text{(A.27)}$$

To obtain the probability of finding excitation on the n-th site, $P_n(t) = \rho_{nn}(t)$, we need to apply the *inverse Fourier transform* and the *inverse Laplace transform* to Eq. (A.27). Before doing that we will split Eq. (A.27) in two components, $\tilde{P} = \tilde{P}_B + \tilde{P}_D$, defined below in Eqs. (A.28) and (A.29) and discuss their physical meaning. The first component

$$\tilde{P}_B(q) = \frac{1}{\sqrt{\left[z+W+\gamma\right]^2+\left[4\Delta\sin(qa/2)\right]^2}} \quad \text{(A.28)}$$

is responsible for the *ballistic* transport. Indeed, if we consider transport to large distance so that q is small and $\sin(qa/2) \simeq qa/2$, then Eq. (A.28) corresponds to the running wave-packet with the group velocity $v = 2a\Delta$ and dumping rate $W+\gamma$. The *diffusive* part takes the form

$$\tilde{P}_D(q;z) = \frac{W\tilde{P}_B(q;z)}{\sqrt{\left[z+W+\gamma\right]^2+\left[4\Delta\sin(qa/2)\right]^2}-W} \quad \text{(A.29)}$$

In the case of energy conservation and long distance - long time limit it can be expressed in the form of a diffusion pole $\tilde{P}_D(q;z) \sim 1/(z+2Dq^2)$, where $D = a^2\Delta/W$ is a diffusion coefficient. Next we will consider *ballistic* and *diffusive* components of

the solution separately.

A.2.2 Purely ballistic transport

Based on the property of the *inverse Laplace transform* one can see that the *ballistic* component is given by $\exp\{-(W+\gamma)t\}\rho^0_{nn}(t)$, where $\rho^0_{mn}(t)$ is a solution of Eq. (A.17) in a purely coherent case, $W = \gamma = 0$. $\rho^0_{mn}(t)$ can be found as a tensor product of wave-functions, $\boldsymbol{\rho}^0 = \psi \otimes \psi$, which can be obtained as a solution of the *Schrödinger equation*

$$i\hbar\frac{\partial\psi}{\partial t} = \hat{\boldsymbol{\mathcal{H}}}\psi \tag{A.30}$$

Introducing as a basis set the states $|n\rangle$, corresponding to the excitation on the n-th site, such that $\psi(t) = \sum C_n(t)\,|n\rangle$ and $\rho^0_{mn} = C^*_m C_n$, we can rewrite the Eq. (A.30) as

$$i\dot{C}_n = \omega C_n + \Delta\left(C_{n-1} + C_{n+1}\right) \tag{A.31}$$

with initial condition $C_n(0) = \delta_{n0}$. Respectively introducing a function $F_n(t) = C_n(t)e^{-i\omega t}$ and a new variable $y = -i2\Delta t$ we can reduce the Eq. (A.31) to

$$\frac{dF_n}{dy} = \frac{1}{2}\left(F_{n-1}(y) + F_{n+1}(y)\right) \tag{A.32}$$

which is an identity for the modified Bessel function [41] $\mathrm{I}_n(y)$. Using definition [41] of the modified Bessel function

$$\mathrm{I}_n(y) = e^{-i\frac{\pi n}{2}}\mathrm{J}_n(iy) \tag{A.33}$$

we obtain the solution of the *Schrödinger equation* as

$$C_n(t) = e^{-i\omega t}e^{-i\frac{n\pi}{2}}\mathrm{J}_n(2\Delta t) \tag{A.34}$$

which also satisfies the initial condition. Thus the ballistic component of the probability to find the excitation on the n-th site (in agreement with Ref. [27]) is given by

$$P_n^B(t) = e^{-(W+\gamma)t} \mathrm{J}_n^2(2\Delta t) \tag{A.35}$$

A.2.3 Purely Diffusive transport (approximate solution)[1]

Another approximate solution of Eq. A.17 can be found for $W \gg \Delta$ for sufficiently large time scale ($t > W^{-1}$). This condition allows to assume

$$\begin{aligned} \dot{\rho}_{mn} &\simeq 0, \quad m \neq n \\ \rho_{mn} &\simeq 0, \quad |m-n| > 1 \end{aligned} \tag{A.36}$$

so that

$$\begin{aligned} 0 \simeq \dot{\rho}_{m-1m} &\simeq -i\Delta\left(\rho_{mm} - \rho_{m-1m-1}\right) - W\rho_{m-1m} \\ 0 \simeq \dot{\rho}_{m+1m} &\simeq -i\Delta\left(\rho_{mm} - \rho_{m+1m+1}\right) - W\rho_{m+1m} \\ 0 \simeq \dot{\rho}_{mm-1} &\simeq i\Delta\left(\rho_{mm} - \rho_{m-1m-1}\right) - W\rho_{mm-1} \\ 0 \simeq \dot{\rho}_{mm+1} &\simeq i\Delta\left(\rho_{mm} - \rho_{m+1m+1}\right) - W\rho_{mm+1} \end{aligned} \tag{A.37}$$

Here we omit $-\gamma\rho_{mn}$ term for the sake of simplicity, final expression is to be corrected by $\boldsymbol{\rho}(t) \longrightarrow e^{-\gamma t}\boldsymbol{\rho}(t)$, as we did it in Section A.2.2. Thus, plugging Eq. (A.37) into expression for time derivative of diagonal components of the density matrix, one obtain for probability to find excitation on the m-th site $P_m = \rho_{mm}$ a discreet diffusion

[1]This section is useful for the analysis and better understanding of the equation, yet the exact solution for diffusive component of Eq. (A.17) will be obtained in the Section A.2.4 so the current section can be skipped.

equation:

$$\frac{\partial P_m}{\partial t} = \frac{2\Delta^2}{W}\left(P_{m+1} - 2P_m + P_{m-1}\right) \tag{A.38}$$

This equation with substitution $P_m(t) = \exp\{-4\Delta^2 t/W\}F_m(4\Delta^2 t/W)$ can be reduced to the modified Bessel function identity Eq. (A.32). Thus, the approximate solution for purely diffusive regime is given by expression

$$P_m^{\text{approx}}(t) = \mathrm{I}_m\left(\frac{4\Delta^2}{W}t\right)\exp\left\{-\left(\frac{4\Delta^2}{W} + \gamma\right)t\right\} \tag{A.39}$$

Eq. (A.38) with $-\gamma P_m$ term can be also rewritten in continuous limit $x = na$ as

$$\frac{\partial P(x,t)}{\partial t} = D\frac{\partial^2 P}{\partial x^2} - \gamma P \tag{A.40}$$

which is a diffusion equation with dissipation, where diffusion coefficient $D = \frac{4\Delta^2 a^2}{W}$, and a is the lattice constant. Its solution [33] for $P(x,t)$, a probability to find excitation on the interval $x, x + dx$,

$$P(x,t) = \frac{1}{\sqrt{2\pi Dt}}e^{-\frac{x^2}{2Dt} - \gamma t} \tag{A.41}$$

describes both *diffusion* and *directed diffusion* regimes (see Section 1.3. The latter expression can also be obtained from Eq. (A.39) using asymptotic properties of Bessel function (see Section A.3.2).

A.2.4 Diffusive transport (exact solution)

For the *diffusive* component the double integral in Eq. (A.22) can be reduced to

$$P_n^D(t) = \mathcal{L}_t^{-1}\left[\frac{a}{4\pi}\int_{-2\pi/a}^{+2\pi/a} dq\tilde{P}_D(q;z)e^{-iqan}\right] \tag{A.42}$$

where $\mathcal{L}_t^{-1}$ denotes the $z \longrightarrow t$ *inverse Laplace transform.* We will expand Eq. (1.10) into a series with respect to the number of scattering events on the stochastic random potential $\delta\omega(t)$ associated with the decoherence and express the solution as

$$P_n^D(t) = \sum_{k=1}^{\infty} \rho_{nn}^k(t) \tag{A.43}$$

where

$$\rho_{nn}^k(t) = \frac{a}{4\pi}\frac{W^k}{2\pi i}\int_{-i\infty}^{+i\infty} dz \int_{-2\pi/a}^{+2\pi/a} dq \frac{e^{-iqan}e^{(z+\delta)t}}{\left[(z+\delta+W+\gamma)^2 + (4\Delta\sin(qa/2))^2\right]^{\frac{k-1}{2}+1}} \tag{A.44}$$

with $\delta \to 0$. For long distances, $n \gg 1$, which are the target of our consideration, one can expand $\sin(qa/2) \simeq qa/2$ and set all integration limits to infinity, which corresponds to the exact limit of the continuous model.

Applying those assumptions and introducing new variables,

$$z_\pm = z \pm i2\Delta q + W + \gamma$$

we obtain

$$\rho_{nn}^k(t) = \frac{W^k}{4\Delta}\mathcal{U}\left(t - \frac{n}{2\Delta}\right)\mathcal{U}\left(t + \frac{n}{2\Delta}\right)e^{-(W+\gamma)t} \tag{A.45}$$

where

$$\mathcal{U}(\tau) = \frac{1}{2\pi i}\lim_{\delta\to 0}\int_{-i\infty}^{+i\infty} dz \frac{e^{\frac{1}{2}(z+\delta)\tau}}{(z+\delta)^{\frac{k-1}{2}+1}} = \mathcal{L}_{\tau/2}^{-1}\left[\frac{1}{z^{\frac{k-1}{2}+1}}\right] = \frac{\left(\frac{\tau}{2}\right)^{\frac{k-1}{2}}}{\Gamma(\frac{k-1}{2}+1)}\theta(\tau) \tag{A.46}$$

and $\theta(\tau)$ is a Heaviside step function.

Introducing $x = W\sqrt{t^2 - n^2/(2\Delta)^2}$ we rewrite Eq. (A.43) as

$$P_n^D(t) = e^{-(W+\gamma)t}\theta\left(t^2 - \frac{n^2}{4\Delta^2}\right)\frac{W}{4\Delta}\sum_{k=0}^{\infty}\frac{\left(\frac{x}{2}\right)^k}{\Gamma^2\left(\frac{k}{2}+1\right)} \tag{A.47}$$

To evaluate the series we need to split it in two sub-series $k = 2m$ and $k = 2m+1$. Using the definitions [41]

$$\mathrm{I}_0(x) = \sum_{m=0}^{\infty}\frac{\left(\frac{x}{2}\right)^{2m}}{\Gamma^2(m+1)}; \quad \mathrm{L}_0(x) = \sum_{m=0}^{\infty}\frac{\left(\frac{x}{2}\right)^{2m+1}}{\Gamma^2\left(m+\frac{3}{2}\right)} \tag{A.48}$$

we obtain the expression for the *diffusive* component as

$$P_n^D(t) = e^{-(W+\gamma)t}\frac{W}{4\Delta}\left[\mathrm{I}_0\left(W\sqrt{t^2 - \frac{n^2}{4\Delta^2}}\right) + \mathrm{L}_0\left(W\sqrt{t^2 - \frac{n^2}{4\Delta^2}}\right)\right]\theta\left(t^2 - \frac{n^2}{4\Delta^2}\right) \tag{A.49}$$

Composing Eqs. (A.35), (A.49) we obtain the final analytical solution of Eq. (A.19).

A.3 Asymptotic limits of the solution

Here we derive asymptotic limits based on asymptotic behavior of Bessel functions.

A.3.1 Ballistic component

To find ballistic regime approximation one needs to consider asymptotics of Bessel function $\mathrm{J}_n(z)$ for large z. We will use integral representation:

$$\mathrm{J}_n(z) = \frac{1}{\pi}\int\limits_0^{\pi} d\theta \cos\left(z\sin\theta - n\theta\right) = \frac{1}{2\pi}\int\limits_0^{\pi} d\theta e^{iz\sin\theta - in\theta} + \text{c. c.} = \frac{e^{-in\pi/2}}{2\pi}\int\limits_{-\pi/2}^{+\pi/2} d\theta e^{iz\cos\theta - in\theta} + \text{c. c.} \quad \text{(A.50)}$$

Assuming the integral is defined by vicinity of maximum of function $z\cos\theta - n\theta$ for $z \gg 1$ (saddle point method), we can estimate

$$\frac{e^{-in\pi/2}}{2\pi}\int\limits_{-\pi/2}^{+\pi/2} d\theta e^{iz\cos\theta - in\theta} \simeq \frac{e^{-in\pi/2}}{2\pi}\int\limits_{-\infty}^{+\infty} d\varepsilon e^{iz\cos\theta_0 - in\theta_0 - \frac{iz}{2}\varepsilon^2} = \frac{1}{2\pi} e^{-in\pi/2 + iz\cos\theta_0 - in\theta_0}\sqrt{\frac{2\pi}{iz\cos\theta_0}} \quad \text{(A.51)}$$

where θ_0 is defined by $z\sin\theta_0 + n = 0$, so that

$$\cos\theta_0 = \sqrt{1 - \left(\frac{n}{z}\right)^2}, \quad \theta_0 = \arcsin\left(\frac{n}{z}\right)$$

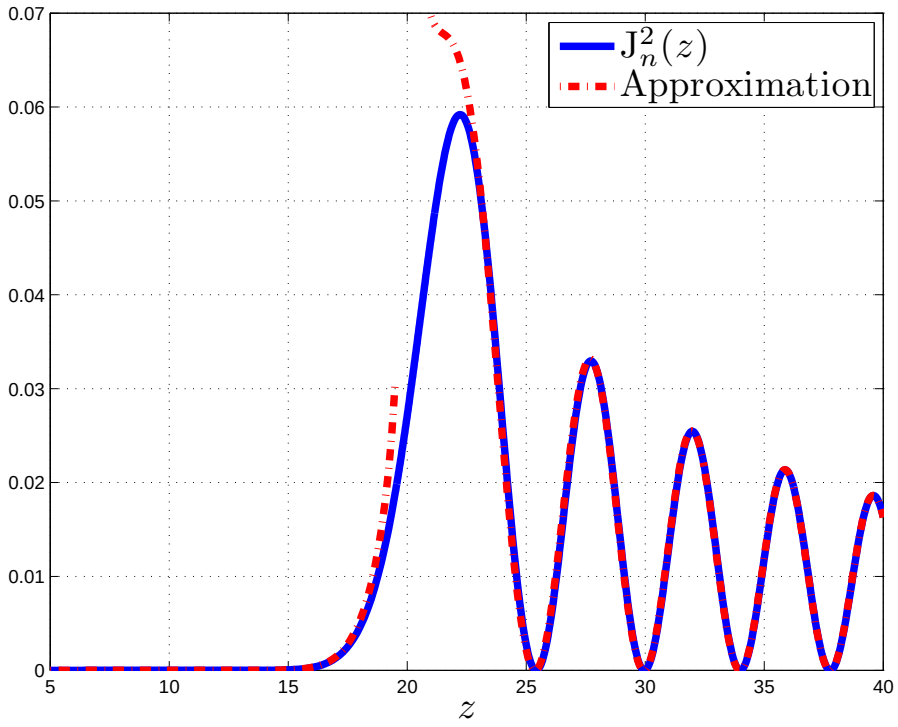

Figure A.1: Bessel function $\mathrm{J}_n^2(x)$ (blue solid line) and its approximation by Eq. (A.52) (red dashed-dotted line) for n = 20. As one can see, the approximation works very well everywhere except of the most interesting vicinity of the first maximum.

Finally, the main asymptotics of Bessel function for $|z| \gg 1$ is given by expression:[2]

$$\mathrm{J}_n(z) \simeq \sqrt{\frac{2}{\pi(z^2-n^2)^{1/2}}}\cos\left[\sqrt{z^2-n^2} - \frac{n\pi}{2} - \frac{\pi}{4} + n\arcsin\left(\frac{n}{z}\right)\right] \qquad \text{(A.52)}$$

The approximation for $J_n^2(z)$ with $n = 20$ is shown on Fig. A.1. As one can see it is not good approximation for the most important vicinity of the first maximum while the first maximum of $J_n^2(z)$ defines $T_{\max}$ in the *ballistic regime*.

There is an interesting observation. The first maximum of $\mathrm{J}_n(z)$ lies in vicinity of $z \sim n$. The asymptotic expression for large n can be found similarly to Eq. (A.51).

---

[2]This expression is slightly more accurate than the one presented in Ref. [41].

Expanding $n\sin\theta \pm n\theta$ in vicinity of its maximum

$$n\sin(\theta_0+\varepsilon) \pm n(\theta_0+\varepsilon) \simeq -\frac{in\varepsilon^3}{3!}, \quad \theta_0 = 0 \tag{A.53}$$

we can approximate

$$\begin{aligned}
\mathrm{J}_n(n) = \frac{1}{\pi}\int\limits_0^\pi d\theta \cos\left(n\sin\theta - n\theta\right) = \frac{1}{2\pi}\int\limits_0^\pi d\theta e^{in\sin\theta - in\theta} + \text{c. c.} \simeq \\
\frac{1}{2\pi}\int\limits_0^{+\infty} d\varepsilon \exp\Big\{-\frac{in\varepsilon^3}{3!}\Big\} + \text{c. c.} = \frac{1}{3\cdot 2\pi}\int\limits_0^{+\infty} d\xi \xi^{\frac{1}{3}-1}\exp\Big\{-\frac{in}{3!}\xi\Big\} + \text{c. c.} = \\
\frac{1}{6\pi}\left(\frac{in}{6}\right)^{-\frac{1}{3}}\Gamma\left(1/3\right) + \text{c. c.} = \frac{n^{-1/3}}{3\pi}6^{1/3}\Gamma\left(1/3\right)\frac{e^{-i\pi/6}+e^{i\pi/6}}{2} = \\
\frac{n^{-1/3}}{3}\frac{6^{1/3}}{\Gamma\left(2/3\right)\sin\left(\pi/3\right)}\cos\left(\pi/6\right) = \lambda n^{-1/3}, \quad \lambda = \left(\frac{2}{9}\right)^{1/3}\frac{1}{\Gamma\left(2/3\right)}
\end{aligned} \tag{A.54}$$

Above we used definition and properties of Gamma-function $\Gamma(z)$ [41]:

$$\begin{aligned}
\Gamma(z) &\stackrel{\text{def}}{=} \int\limits_0^\infty d\xi \xi^{1-z}e^{-\xi} \\
k^{-z}\Gamma(z) &= \int\limits_0^\infty d\xi \xi^{1-z}e^{-k\xi} \\
\Gamma(z)\Gamma(1-z) &= \frac{\pi}{\sin(\pi z)}
\end{aligned} \tag{A.55}$$

We may assume (though not prove, unfortunately) the same $n^{-1/3}$ rule is valid for the Bessel function in its first maximum. So in ballistic regime $W < 2\Delta/n$ the amplitude of the signal might be estimated as

$$P_{\max}(n) \sim n^{-2/3}e^{-\frac{W+\gamma}{2\Delta}n} \tag{A.56}$$

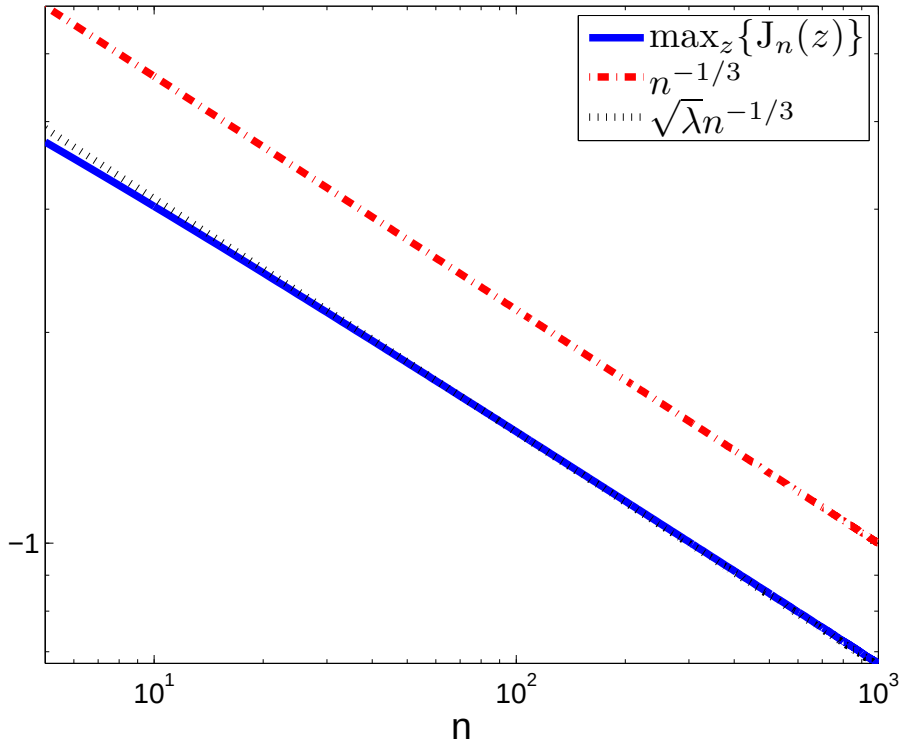

Figure A.2: Log-Log representation of maximum of Bessel function J_n (solid blue line) and $n^{-1/3}$ (red dashed-dotted line) vs n. Dotted black line represents $\sqrt{\lambda}n^{-1/3}$, $\lambda = (2/9)^{1/3}/\Gamma(2/3)$.

The latter assumption is confirmed by numerical calculations. Moreover, if we substitute pre-factor λ by its square root we very good approximation even for the amplitude, not for its slop only (black dashed line on Fig. (A.2)).

Now we can estimate $T_{\max}$ for entirely ballistic regime. Introduce X_* such that $J_n(X_*) \longrightarrow \max$. In fact $X_* \simeq n + C_0$, $C_0 \ll n$. Now we wish to estimate the correction to X_* corresponding to low decoherence and relaxation.

$$e^{-(\gamma+W)t} J_n^2(2\Delta t) \longrightarrow \max, \quad \text{so that} \quad -\frac{\gamma+W}{2\Delta} J_n(2\Delta t) + 2J_n'(2\Delta t) = 0$$

with assumption $(\gamma + W) \ll \Delta$ we may expand the function in vicinity of X_*:

$$-\frac{\gamma + W}{2\Delta}\left(\mathrm{J}_n(X_*) + \mathrm{J}'_n(X_*)\varepsilon + \frac{1}{2}\mathrm{J}''_n(X_*)\varepsilon^2\right) + 2\mathrm{J}'_n(X_*) + 2\mathrm{J}''_n(X_*)\varepsilon \simeq 0 \qquad \text{(A.57)}$$

$$\begin{aligned} \mathrm{J}_n(X_*) &= An^{-1/3} \\ \mathrm{J}'_n(X_*) &= 0 \\ \mathrm{J}''_n(X_*) &= -B/2, \quad B > 0 \end{aligned} \qquad \text{(A.58)}$$

A is a square root of pre-factor in Eq. (A.54), coefficient B corresponds to width of the first peak and almost doesn't depend on n as well as A. Neglecting ε^2 term in Eq. (A.57) we obtain

$$T_{\max} \simeq \frac{X_*}{2\Delta} - \frac{A}{B}\frac{\gamma + W}{4\Delta^2}n^{-1/3} = \frac{n}{2\Delta} + C_0 - \frac{C}{n^{1/3}}\frac{\gamma + W}{4\Delta^2}, \quad C_0 \simeq \Delta^{-1} \qquad \text{(A.59)}$$

Finally, the main asymptotics for ballistic regime:

$$\begin{aligned} T^B_{\max}(W) &\simeq T_0 - \alpha W, \quad \alpha \sim \frac{n^{-1/3}}{4\Delta^2} \\ T^B_{\max}(n) &\simeq \frac{n}{2\Delta} \xrightarrow{x=na} \frac{x}{2a\Delta} \end{aligned} \qquad \text{(A.60)}$$

From the first expression one can see that for large n $T_{\max}$ does not depend on decoherence rate (see also Fig. 1.3 in Section 1.3). The second expression suggest propagation of energy with constant speed

$$v = 2a\Delta \qquad \text{(A.61)}$$

where a is a lattice constant.

A.3.2 Diffusive component

To consider asymptotic limit of diffusive component Eq. (A.49) one needs to consider asymptotic behavior of modified Bessel functions for large large values of the argument. The main asymptotics can be obtained applying saddle point method to the integral representation of I_n:

$$\mathrm{I}_n(z) = \frac{1}{\pi}\int\limits_0^{\pi} d\theta e^{z\cos\theta}\cos(n\theta) = \frac{1}{2\pi}\int\limits_{-\pi}^{+\pi} d\theta e^{z\cos\theta}\cos(n\theta) = \frac{1}{2\pi}\int\limits_{-\pi}^{+\pi} d\theta e^{z\cos\theta+in\theta} \simeq$$
$$\frac{e^z}{2\pi}\int\limits_{-\infty}^{+\infty} d\theta e^{-\frac{z\theta^2}{2}+in\theta} = \frac{e^z e^{-\frac{n^2}{2z}}}{2\pi}\sqrt{\frac{2\pi}{z}} = \frac{e^z}{\sqrt{2\pi z}}e^{-\frac{n^2}{2z}} \quad \text{(A.62)}$$

Asymptotic behavior of Struve function $\mathrm{L}_0(\alpha)$ to that of $\mathrm{I}_n(\alpha)$:

$$\mathrm{L}_0(z) - \mathrm{I}_0(z) = -\frac{2}{\pi}z^{-1} \longrightarrow 0, \quad |z| \gg 1 \quad \text{(A.63)}$$

so that Eq. (A.49) can be approximated by

$$P_n^D(t) \xrightarrow{t\gg W^{-1}}$$
$$\frac{W}{2\Delta}e^{-(W+\gamma)t}\mathrm{I}_0\left(W\sqrt{t^2-\frac{n^2}{4\Delta^2}}\right) \longrightarrow \frac{W}{2\Delta}\frac{1}{\sqrt{2\pi Wt}}e^{-\gamma t - Wt + W\sqrt{t^2-\frac{n^2}{4\Delta^2}}} \simeq$$
$$\sqrt{\frac{W}{8\pi\Delta^2 t}}\exp\left\{-\frac{Wn^2}{8\Delta^2 t}-\gamma t\right\} \xrightarrow{x=na}$$
$$\frac{a}{\sqrt{2\pi Dt}}e^{-\frac{x^2}{2Dt}-\gamma t} \quad \text{(A.64)}$$

where a is a lattice constant, and $D = 4\Delta^2 a^2/W$. Function

$$P(x,t) = \frac{1}{\sqrt{2\pi Dt}}e^{-\frac{x^2}{2Dt}-\gamma t}$$

is a probability to find excitation in continuous limit on the interval $x, x+dx$, identical to Eq. (A.41). Applying Eq. (A.62) to the approximate solution Eq. (A.39) one gains the same result. Constant D has a physical meaning of *diffusion coefficient*. To estimate $T_{\max}(n)$ - time required to reach maximum intensity on n-th site we need to apply to $P_n^D(t)$ condition:

$$e^{-(W+\gamma)t}\frac{\exp\left\{W\sqrt{t^2-\frac{n^2}{4\Delta^2}}\right\}}{\left(t^2-\frac{n^2}{4\Delta^2}\right)^{1/4}} \longrightarrow \max \tag{A.65}$$

We will consider the case of $\gamma \ll \Delta/n$. In such a situation the maximum will be reached at $t \gg n/\Delta$ so we can simplify the exponent and deal with equation

$$\frac{d}{dt}\left\{\left(t^2-\frac{n^2}{4\Delta^2}\right)^{-1/4} e^{-\gamma t-\frac{Wn^2}{8\Delta^2 t}}\right\} = 0 \tag{A.66}$$

which leads to

$$2\gamma t^2 + t - (W+2\gamma)\frac{n^2}{4\Delta^2} + \frac{Wn^4}{16\Delta^4}t^{-2} = 0 \tag{A.67}$$

where the last term is to be neglected. Indeed, with dividing Eq. (A.67) by t one can see $\sim (n^4/\Delta^4)t^{-3}$ is the term we have already neglected in asymtotics of $\sqrt{t^2 - n^2/(2\Delta)^2}$. Therefore we get a simple quadratic equation:

$$2\gamma t^2 + t - (W+2\gamma)\frac{n^2}{4\Delta^2} = 0 \tag{A.68}$$

and finally:

$$T_{\max} = \frac{\sqrt{1+2\frac{n^2}{\Delta^2}(W+2\gamma)\gamma}-1}{4\gamma}, \quad \gamma \ll \Delta/n \tag{A.69}$$

For purely *diffusive regime*

$$T_{\max} \xrightarrow{\gamma\longrightarrow 0} T_{\max}^D = \frac{n^2}{4\Delta^2}W \xrightarrow{x=na} \frac{x^2}{D} \tag{A.70}$$

and corresponding amplitude $P^D_{\max}$ can be obtained by plugging $T^D_{\max}$ into Eq. (A.64):

$$P^D_{\max}(x) = (2\pi e)^{-1/2} x^{-1} e^{-\frac{\gamma}{D}x^2} \tag{A.71}$$

Another interesting asymptotic regime can be obtained from Eq. (A.69) when n becomes sufficiently large and the term $2(n^2/\Delta^2)(W + 2\gamma)\gamma \gg 1$ so the main asymptotics of $T_{\max}$ becomes

$$T^{DD}_{\max}(n) = \frac{n}{2\Delta}\sqrt{1 + \frac{W}{2\gamma}} - \frac{1}{4\gamma} \sim \frac{n}{2\Delta}\sqrt{\frac{W}{2\gamma}} \xrightarrow{x=na} \frac{x}{\sqrt{2\gamma D}} \tag{A.72}$$

This is so-called *directed diffusive* regime (see also Section 1.3), characterized, unlike purely diffusive regime, by constant speed

$$\tilde{v} = \sqrt{\frac{8\Delta^2\gamma}{a^2 W}} = \sqrt{2\gamma D} \tag{A.73}$$

Corresponding amplitude $P^{DD}_{\max}$ can be obtained by plugging $T^{DD}_{\max}$ into Eq. (A.64):

$$P^{DD}_{\max}(x) = \left(\frac{\gamma}{2\pi^2 D}\right)^{1/4} x^{-1/2} e^{-\frac{\tilde{v}}{D}x} \tag{A.74}$$

Appendix B

Derivations for electronic sound through cumulene chain

B.1 Derivation of the hydrogen torsional mode frequency as a function of molecule length

Consider the following model for carbyne molecule: a long spring with two 'whiskers" on the sides. The potential energy depends on the spring torsion (gradient of angle $\theta(z)$) and the torsion of the 'whiskers" (angles ϕ_l, ϕ_r) with respect to the spring.

$$\mathcal{L} = \frac{1}{2}J_l\dot{\phi}_l^2 + \frac{1}{2}J_r\dot{\phi}_r^2 + \frac{1}{2}\int_{z_l}^{z_r} dz j_e\dot{\theta}^2 - \frac{1}{2}\int_{z_l}^{z_r} dz\left\{\kappa\left(\frac{\partial\theta}{\partial z}\right)^2 + \epsilon(z-z_l)\Big[\phi_l - \theta(z)\Big]^2 + \epsilon(z-z_r)\Big[\phi_r - \theta(z)\Big]^2\right\} \quad \text{(B.1)}$$

with $J_l = J_r = J_{2H} = J/2$, where J - moment of inertia along main axis, determined entirely by hydrogen atoms on the sides, where j_e - linear density of electronic moment of inertia, assumed $j_e = J_e/L$, L - length of the molecule (see Fig. 2.3

and Sec. 2.4). The integration limits $z_{l,r} = \mp L/2$. The dynamical equations from Lagrangian Eq. (B.1) are

$$\begin{cases} \dfrac{J}{2}\ddot{\phi}_l = -\displaystyle\int_{z_l}^{z_r} dz\epsilon(z-z_l)\Big[\phi_l - \theta(z)\Big] \\ \dfrac{J}{2}\ddot{\phi}_r = -\displaystyle\int_{z_l}^{z_r} dz\epsilon(z-z_r)\Big[\phi_r - \theta(z)\Big] \\ j_e\ddot{\theta} = \kappa\dfrac{\partial^2\theta}{\partial z^2} + \epsilon(z-z_l)\Big[\phi_l - \theta\Big] + \epsilon(z-z_r)\Big[\phi_r - \theta\Big] \end{cases} \tag{B.2}$$

For antisymmetric solution the boundary conditions are

$$\begin{cases} \phi_r = \phi = -\phi_l \\ \theta(z_r) = \theta_0 = -\theta(z_l) \end{cases} \tag{B.3}$$

The simplest model for function $\epsilon(z)$ is

$$\epsilon(z) = \epsilon_0\delta(z) \tag{B.4}$$

The time-depended solution is to be sought as $\theta(t,z) = \exp\{i\omega_\tau t\}\theta(z)$, $\phi(t) = \exp\{i\omega_\tau t\}\phi$

With those conditions the equations into Eq. (B.2) are reduced to

$$\frac{J\omega_\tau^2}{2} = \epsilon_0\left(\phi - \theta_0\right) \tag{B.5}$$

and

$$-j_e\omega_\tau^2\theta = \kappa\frac{\partial^2\theta}{\partial z^2}, \quad -\frac{L}{2} < z < \frac{L}{2}, \quad -\theta\left(-\frac{L}{2}\right) = \theta\left(\frac{L}{2}\right) = \theta_0 \tag{B.6}$$

There is one more boundary condition which can be obtained from the third equation in Eq. (B.2). Apply integration in vicinity the right boundary: $\int_{z_r-\varepsilon}^{z_r+\varepsilon} dz$. While the

function θ is continuous on the boundary as well as everywhere, its derivative has a jump. Indeed

$$\int_{z_r-\varepsilon}^{z_r+\varepsilon} dz\theta(z) \overset{\varepsilon\longrightarrow 0}{\longrightarrow} 0$$

$$\int_{z_r-\varepsilon}^{z_r+\varepsilon} dz\frac{\partial^2\theta}{\partial z^2} = \frac{\partial\theta}{\partial z}\bigg|_{z_r+\varepsilon}^{z_r-\varepsilon} = 0 - \frac{\partial\theta}{\partial z}\Big|_{z=z_r+\varepsilon} \overset{\varepsilon\longrightarrow 0}{\longrightarrow} -\frac{\partial\theta}{\partial z}\Big|_{z=z_r}$$

so finally

$$\kappa\frac{\partial\theta}{\partial z}\Big|_{z=L/2} = \epsilon_0\left(\phi - \theta_0\right) \tag{B.7}$$

The solution of Eq. (B.6) is

$$\theta(z) = \theta_0\frac{\sin\left(q_* z\right)}{\sin\left(q_* L/2\right)}, \quad q_* = \omega_\tau\sqrt{\frac{j_e}{\kappa}} \tag{B.8}$$

Combining Eqs. (B.5), (B.7), (B.8) we obtain a system determining the connection between torsion mode frequency ω_τ and force constants ϵ_0 and κ:

$$\begin{cases} J\omega_\tau^2\phi = \epsilon_0(\phi - \theta_0) \\ \theta_0\omega_\tau\sqrt{j_e\kappa} = \epsilon_0(\phi - \theta_0)\tan\left(\dfrac{\omega_\tau L}{2}\sqrt{\dfrac{j_e}{\kappa}}\right) \end{cases} \tag{B.9}$$

The transcendent equation can be simplified by the long-wave approximation

$$\frac{q_* L}{2} = \frac{\omega_\tau L}{2}\sqrt{\frac{j_e}{\kappa}} \ll 1 \tag{B.10}$$

One can get the same approximation simply neglecting electronic kinetic energy, which is reasonable while $J_e \ll J$, and setting the Laplacian in Eq. (B.6) to zero.

Finally,

$$\omega_\tau^2 = \frac{4\kappa}{J}\frac{1}{L + \frac{2\kappa}{\epsilon_0}} \tag{B.11}$$

With approximation $\epsilon_0 \gg \kappa/L$ Eq. (B.11) is simplified so that $\omega_\tau \sim 1/\sqrt{L}$ and

$$\omega_\tau^2 = \frac{4\kappa}{J}\frac{1}{L} \tag{B.12}$$

B.2 Zero-point atomic vibrations

In this section we deduce detailed derivations of the correction $-\alpha\theta^2/(2L)$ to the potential energy in Eq. (2.1) due to the zero-point atomic vibrations:

$$\mathcal{L}_e = \frac{1}{2}\int_{z_l}^{z_r} dz \left\{ j_e \left(\frac{d\theta}{dt}\right)^2 - \kappa \left(\frac{\partial\theta}{\partial z}\right)^2 - \alpha\frac{\theta^2}{L} \right\} \tag{B.13}$$

and describe numerical calculations of *torsiton* spectrum $\Delta\omega = \sqrt{\alpha/j_e L}$ (see Sec. 2.7).

B.2.1 Analytical derivation of energy correction

All the normal modes in the molecule, which don't include motion of hydrogen atoms with respect to the adjacent carbon atoms, can be either longitudinal or transverse. We assume the coordinate system with the origin at the central carbon atom, z-axis is the principal axis of the chain and (X-Z) and (Y-Z)-plains coincide with the plains of two orthogonal CH_2 groups. Thus, any normal mode of interest has only one Cartesian component (x, y for transverse and z for longitudinal modes) and one can apply Cartesian symmetry operations to the Hamiltonian recorded in the normal modes representation. Anharmonic constant A_{abc} in normal mode representation, where a, b, c are normal modes numbers, can be rewritten as $V_{\alpha_i\beta_j\gamma_k}$, where indexes $\{\alpha, \beta, \gamma\}$ correspond to Cartesian coordinates $\{x, y, z\}$ and subscripts $\{i, j, k\}$ enumerate the harmonics in the corresponding directions.

The symmetry point group we consider is D_{2d}, which consist of C_2, S_4 and σ_d symmetry operations. It described above explicit Cartesian coordinates those

operations take form of

$$\begin{aligned}
&(x,y,z) \xrightarrow{\sigma_{yz}} (-x,y,z), \quad (x,y,z) \xrightarrow{\sigma_{xz}} (x,-y,z) \\
&(x,y,z) \xrightarrow{C_2} (-x,-y,z) \\
&(x,y,z) \xrightarrow{S_4} (y,-x,-z), \quad (x,y,z) \xrightarrow{S_4^3} (-y,x,-z)
\end{aligned} \tag{B.14}$$

To posses such symmetries Hamiltonian should be constructed from combinations

$$u_{x_i}^2 + u_{y_i}^2, \quad u_{z_i}^2 \tag{B.15}$$

in harmonic approximation and

$$(u_{x_i}u_{x_j} - u_{y_i}u_{y_j})u_{z_k} \tag{B.16}$$

for the 3-d order anharmonicity, where u_{x_i}, u_{y_i}, u_{z_i} stand for displacements in normal modes representation.

From Eq. (B.15) one can see that the harmonic Hamiltonian should be double-generate,[1] so that

$$\hbar\omega_{x_i} = \frac{\partial^2 H}{\partial u_{x_i}^2} = \frac{\partial^2 H}{\partial u_{y_i}^2} = \hbar\omega_{y_i} = \hbar\omega_i \tag{B.17}$$

Also, the rotation along z-axis by angle θ transforms the coordinates

$$\begin{aligned}
x &\xrightarrow{\theta} x' = x\cos\theta + y\sin\theta \\
y &\xrightarrow{\theta} y' = -x\sin\theta + y\cos\theta \\
z &\xrightarrow{\theta} z' = z
\end{aligned} \tag{B.18}$$

---

[1] Actually, cumulene molecules $H_2 = C_n = H_2$ with even number of carbon atoms are planar and belong to a symmetry point group D_{2h}, so that $\omega_{x_i} \neq \omega_{y_i}$, however this is entirely effect of the sides while in our consideration pi-bond symmetry is of the interest.

so that the combination of displacements transforms accordingly:

$$u_{x_i}u_{x_j} + u_{y_i}u_{y_j} \xrightarrow{\theta} \big(u_{x_i}\cos\theta + u_{y_i}\sin\theta\big)\big(u_{x_j}\cos\theta + u_{y_j}\sin\theta\big) + \\ \big(-u_{x_i}\sin\theta + u_{y_i}\cos\theta\big)\big(-u_{x_j}\sin\theta + u_{y_j}\cos\theta\big) = u_{x_i}u_{x_j} + u_{y_i}u_{y_j} \quad \text{(B.19)}$$

and the harmonic Hamiltonian

$$\hat{\boldsymbol{\mathcal{H}}}_2 = \frac{1}{2}\sum_i \omega_{x_i}\left(p_{x_i}^2 + u_{x_i}^2\right) + \frac{1}{2}\sum_i \omega_{y_i}\left(p_{y_i}^2 + u_{y_i}^2\right) + \frac{1}{2}\sum_k \omega_{z_k}\left(p_{z_k}^2 + u_{z_k}^2\right) \quad \text{(B.20)}$$

is axially symmetric, so that axial symmetry violation is entirely anharmonic effect.

From Eq. (B.16) one can see that the only non-zero 3rd-order anharmonic constants are

$$V_{x_i x_j z_k} = -V_{y_i y_j z_k} = V_{ijz_k} \quad \text{(B.21)}$$

and the corredtion to Hamiltonian Eq. (B.20) can be represented as

$$\hat{\boldsymbol{\mathcal{V}}}_3 = \sum_k \left\{ \frac{1}{2}\sum_i V_{iiz_k}\Big(u_{x_i}^2 - u_{y_i}^2\Big) + \sum_{i<j} V_{ijk}\Big(u_{x_i}u_{x_j} - u_{y_i}u_{y_j}\Big) \right\} u_{z_k} \quad \text{(B.22)}$$

where subscripts i, j enumerate transverse modes while subscript k is related to longitudinal modes only. Ground state of Hamiltonian $\hat{\boldsymbol{\mathcal{H}}} = \hat{\boldsymbol{\mathcal{H}}}_2 + \hat{\boldsymbol{\mathcal{V}}}_3$ can be found using perturbation theory:

$$|\psi_0\rangle = |0\rangle + \sum_k \sum_i \Big(A_{ik}^x \left|2_i^x 1_k^z\right\rangle + A_{ik}^y \left|2_i^y 1_k^z\right\rangle \Big) + \\ 2\sum_k \sum_{i<j} \Big(B_{ijk}^x \left|1_i^x 1_j^x 1_k^z\right\rangle + B_{ijk}^y \left|1_i^y 1_j^y 1_k^z\right\rangle \Big) \quad \text{(B.23)}$$

where

$$
\begin{aligned}
A^x_{ik} &= -\frac{\langle 0|\,\hat{\boldsymbol{\mathcal{V}}}_3\,|2^x_i 1^z_k\rangle}{\hbar(2\omega_{x_i}+\omega_{z_k})} = -\frac{1}{4\hbar}\frac{V_{iiz_k}}{2\omega_i+\omega_{z_k}}\\
A^y_{ik} &= -\frac{\langle 0|\,\hat{\boldsymbol{\mathcal{V}}}_3\,|2^y_i 1^z_k\rangle}{\hbar(2\omega_{y_i}+\omega_{z_k})} = +\frac{1}{4\hbar}\frac{V_{iiz_k}}{2\omega_i+\omega_{z_k}}\\
B^x_{ijk} &= -\frac{\langle 0|\,\hat{\boldsymbol{\mathcal{V}}}_3\,|1^x_i 1^x_j 1^z_k\rangle}{\hbar(\omega_{x_i}+\omega_{x_j}+\omega_{z_k})} = -\frac{1}{\hbar\sqrt{8}}\frac{V_{ijz_k}}{\omega_i+\omega_j+\omega_{z_k}}\\
B^y_{ijk} &= -\frac{\langle 0|\,\hat{\boldsymbol{\mathcal{V}}}_3\,|1^y_i 1^y_j 1^z_k\rangle}{\hbar(\omega_{y_i}+\omega_{y_j}+\omega_{z_k})} = +\frac{1}{\hbar\sqrt{8}}\frac{V_{ijz_k}}{\omega_i+\omega_j+\omega_{z_k}}
\end{aligned}
\tag{B.24}
$$

Here we calculate matrix elements applying secondary quantization formalism:

$$
u_{\alpha_i} = \frac{\hat{b}_{\alpha_i}+\hat{b}^\dagger_{\alpha_i}}{\sqrt{2}},\quad \langle 0^\alpha_i|\,u_{\alpha_i}\,|1^\alpha_i\rangle = \frac{1}{\sqrt{2}},\quad \langle 0^\alpha_i|\,u^2_{\alpha_i}\,|2^\alpha_i\rangle = \frac{1}{\sqrt{2}} \tag{B.25}
$$

where $\alpha = x, y, z$. Finally,

$$
\begin{aligned}
|\psi_0\rangle = |0\rangle - \frac{1}{4\hbar}\sum_k\sum_i \frac{V_{iiz_k}}{2\omega_i+\omega_{z_k}}\Big(|2^x_i 1^z_k\rangle - |2^y_i 1^z_k\rangle\Big) -\\
\frac{1}{\hbar\sqrt{2}}\sum_k\sum_{i<j}\frac{V_{ijz_k}}{\omega_i+\omega_j+\omega_{z_k}}\Big(\big|1^x_i 1^x_j 1^z_k\big\rangle - \big|1^y_i 1^y_j 1^z_k\big\rangle\Big)
\end{aligned}
\tag{B.26}
$$

The rotation along z-axis by angle θ transforms displacements combination

$$
\begin{aligned}
u_{x_i}u_{x_j} - u_{y_i}u_{y_j} \xrightarrow{\theta} u'_{x_i}u'_{x_j} - u'_{y_i}u'_{y_j} =\\
\big(u_{x_i}\cos\theta + u_{y_i}\sin\theta\big)\big(u_{x_j}\cos\theta + u_{y_j}\sin\theta\big) -\\
\big(-u_{x_i}\sin\theta + u_{y_i}\cos\theta\big)\big(-u_{x_j}\sin\theta + u_{y_j}\cos\theta\big) =\\
\big(u_{x_i}u_{x_j} - u_{y_i}u_{y_j}\big) - 2\big(u_{x_i}u_{x_j} - u_{y_i}u_{y_j}\big)\sin^2\theta +\\
2\big(u_{x_i}u_{y_j} + u_{y_i}u_{x_j}\big)\sin\theta\cos\theta
\end{aligned}
\tag{B.27}
$$

so that the Hamiltonian changes in diabatic approximation by

$$\delta\hat{\boldsymbol{\mathcal{H}}}(\theta) = \hat{\boldsymbol{\mathcal{H}}}(\theta) - \hat{\boldsymbol{\mathcal{H}}}(0) = \\ -\sum_k \left\{ \sum_i V_{iiz_k}\left(u_{x_i}^2 - u_{y_i}^2\right) + 2\sum_{i<j} V_{ijz_k}\left(u_{x_i}u_{x_j} - u_{y_i}u_{y_j}\right) \right\} u_{z_k} \sin^2\theta + \\ 2\sum_k \left\{ \sum_i V_{iiz_k} u_{x_i}u_{y_i} + \sum_{i<j} V_{ijz_k}\left(u_{x_i}u_{y_j} + u_{y_i}u_{x_j}\right) \right\} u_{z_k} \sin\theta\cos\theta \quad \text{(B.28)}$$

The correction to classical energy is defined by

$$\delta E(\theta) = \langle\psi_0|\, \delta\hat{\boldsymbol{\mathcal{H}}}\, |\psi_0\rangle \quad \text{(B.29)}$$

Applying Eqs. (B.26), (B.28) and

$$\langle\psi_0|\left(u_{x_i}^2 - u_{y_i}^2\right)u_{z_k}|\psi_0\rangle = -\frac{1}{2\hbar}\frac{V_{iiz_k}}{2\omega_i + \omega_{z_k}}$$

$$\langle\psi_0|\left(u_{x_i}u_{y_i}u_{z_k}|\psi_0\rangle = 0$$

$$\langle\psi_0|\left(u_{x_i}u_{x_j} - u_{y_i}u_{y_j}\right)u_{z_k}|\psi_0\rangle = -\frac{1}{\hbar}\frac{V_{ijz_k}}{\omega_i + \omega_j + \omega_{z_k}}$$

$$\langle\psi_0|\left(u_{x_i}u_{y_j} + u_{y_i}u_{x_j}\right)u_{z_k}|\psi_0\rangle = 0$$

finally we get for classical energy correction $\delta E(\theta) = \alpha\theta^2/2$,

$$\alpha = \sum_k \left\{ \sum_i \frac{|V_{iiz_k}|^2}{\hbar(2\omega_i + \omega_{z_k})} + \sum_{i<j} \frac{4|V_{ijz_k}|^2}{\hbar(\omega_i + \omega_j + \omega_{z_k})} \right\} \quad \text{(B.30)}$$

assuming $\sin\theta \simeq \theta$.

B.2.2 Numerical estimate of the gap

To apply Eq. (B.30) for spectrum gap estimate $\Delta\omega = \sqrt{\alpha/j_e L}$ we performed DFT-calculations with anharmonic analysis, using `B3LYP` hybrid functional and `6-31`

basis set [68, 73] for cumulene molecule $H_2C_5H_2$. The symmetry requirement was loosen to secure D_{2d} point group in the optimized geometry.

For linear chain of 5 atoms one expects 4 longitudinal and 3×2 double-degenerate transverse vibrational modes. In the Gaussian output normal modes with numbers 14, 9, 6, 5 were identified as longitudinal modes u_{z_k}, and pairs $\{21, 20\}$, $\{19, 18\}$, $\{17, 16\}$ as transverse modes $\{u_{x_i}, u_{y_i}\}$. The corresponding frequencies and 3rd order non-zero anharmonic constants are presented in Table B.1. Plugging those data into Eq. (B.30) we obtain $\alpha \simeq 119$ cm^{-1}. If $[\alpha] = \text{cm}^{-1}$ and $[j_e L] = \text{u}\cdot\text{Å}^2$, then to keep $\Delta\omega$ in cm^{-1} one has to multiply $\Delta\omega = \sqrt{\alpha / j_e L}$ by factor $\sqrt{\hbar/(2\pi c\beta)}$, where

$$
\begin{aligned}
&1\,u = 1.66 \cdot 10^{-27}\,\text{kg} \\
&\hbar = 1.05 \cdot 10^{-34}\,\text{J}\cdot\text{s} \\
&\text{c} = 3 \cdot 10^{10}\,\text{cm/s} \\
&\beta = 1.66 \cdot 10^{-27}\,\text{kg}\cdot\text{u}^{-1} \cdot 10^{-20}\,\text{m}\cdot\text{Å}^{-2}
\end{aligned}
$$

and

$$
\sqrt{\frac{\hbar}{2\pi c\beta}} = 5.77 \cdot \sqrt{\frac{\text{u}\cdot\text{Å}^2}{\text{cm}}}
$$

The electronic moment of inertia is $j_e L \simeq 5 \cdot 10^{-3}$ u·Å^2. Finally

$$
\Delta\omega = 5.77 \cdot \sqrt{\frac{119}{5 \cdot 10^{-3}}} \simeq 890\,\text{cm}^{-1} \tag{B.31}
$$

Table B.1: The list of frequencies and the third-order anharmonic constants for $H_2{=}C_5{=}H_2$ related to purely longitudinal and transverse vibrations. The numbers in the first three columns enumerate the corresponding normal modes in the Gaussian output.

X_i	X_j	Z_k	ω_{x_i}, cm^{-1}	ω_{x_j}, cm^{-1}	ω_{z_k}, cm^{-1}	$V_{x_i x_j z_k}$, cm^{-1}
21	21	9	151.9	151.9	1354	-24.84
21	21	6	151.9	151.9	1973	-128.9
19	19	9	351.7	351.7	1354	52.98
19	19	6	351.7	351.7	1973	-177.3
17	17	9	590.1	590.1	1354	-42.66
17	17	6	590.1	590.1	1973	-3.77
21	19	9	151.9	351.7	1354	105.9
21	19	6	151.9	351.7	1973	-196.3
21	17	9	151.9	590.1	1354	-36.14
21	17	6	151.9	590.1	1973	-7.79
19	17	9	351.7	590.1	1354	56.28
19	17	6	351.7	590.1	1973	-46.14
Y_i	Y_j	Z_k	ω_{y_i}, cm^{-1}	ω_{y_j}, cm^{-1}	ω_{z_k}, cm^{-1}	$V_{y_i y_j z_k}$, cm^{-1}
20	20	9	151.9	151.9	1354	24.84
20	20	6	151.9	151.9	1973	128.9
18	18	9	351.7	351.7	1354	177.3
18	18	6	351.7	351.7	1973	177.3
16	16	9	590.1	590.1	1354	42.66
16	16	6	590.1	590.1	1973	3.77
20	18	9	151.9	351.7	1354	-105.9
20	18	6	151.9	351.7	1973	196.3
20	16	9	151.9	590.1	1354	36.14
20	16	6	151.9	590.1	1973	7.79
18	16	9	351.7	590.1	1354	-56.28
18	16	6	351.7	590.1	1973	46.14

References

[1] Chang, C.; Okawa, D.; Majumdar, A.; Zettl, A. *Science* **2006**, *314*, 1121–1124.

[2] Yu, C.; Shi, L.; Yao, Z.; Li, D.; Majumdar, A. *Nano Lett.* **2005**, *5*, 1842–1846.

[3] Pernot, G. et al. *Nature materials* **2010**, *9*, 491–495.

[4] Majumdar, S.; Sierra-Suarez, J. A.; Schiffres, S. N.; Ong, W.-L.; Higgs III, C. F.; McGaughey, A. J.; Malen, J. A. *Nano letters* **2015**, *15*, 2985–2991.

[5] Nitzan, A.; Ratner, M. A. *Science* **2003**, *300*, 1384–1389.

[6] Tian, Z.; Marconnet, A.; Chen, G. *Applied Physics Letters* **2015**, *106*, 211602.

[7] Losego, M. D.; Grady, M. E.; Sottos, N. R.; Cahill, D. G.; Braun, P. V. *Nature materials* **2012**, *11*, 502–506.

[8] Shen, S.; Henry, A.; Tong, J.; Zheng, R.; Chen, G. *Nat. Nanotechnol.* **2010**, *5*, 251–255.

[9] Henry, A.; Chen, G. *Phys. Rev. Lett.* **2008**, *101*, 235502.

[10] Nitzan, A. *Science* **2007**, *317*, 759–760.

[11] Yue, Y.; Grusenmeyer, T.; Ma, Z.; Zhang, P.; Schmehl, R. H.; Beratan, D. N.; Rubtsov, I. V. *Dalton Transactions* **2015**, *44*, 8609–8616.

[12] Lin, Z.; Lawrence, C. M.; Xiao, D.; Kireev, V. V.; Skourtis, S. S.; Sessler, J. L.; Beratan, D. N.; Rubtsov, I. V. *J. Am. Chem. Soc.* **2009**, *131*, 18060–18062.

[13] Delor, M.; Scattergood, P. A.; Sazanovich, I. V.; Parker, A. W.; Greetham, G. M.; Meijer, A. J.; Towrie, M.; Weinstein, J. A. *Science* **2014**, *346*, 1492–1495.

[14] Schreier, W. J.; Aumüller, T.; Haiser, K.; Koller, F. O.; Löweneck, M.; Musiol, H.-J.; Schrader, T. E.; Kiefhaber, T.; Moroder, L.; Zinth, W. *Peptide Science* **2013**, *100*, 38–50.

[15] Schade, M.; Moretto, A.; Crisma, M.; Toniolo, C.; Hamm, P. *The Journal of Physical Chemistry B* **2009**, *113*, 13393–13397.

[16] Rubtsova, N. I.; Rubtsov, I. V. *Chem. Phys.* **2013**, *422*, 16–21.

[17] Rubtsova, N. I.; Nyby, C. M.; Zhang, H.; Zhang, B.; Zhou, X.; Jayawickramarajah, J.; Burin, A. L.; Rubtsov, I. V. *The Journal of chemical physics* **2015**, *142*, 212412.

[18] Segal, D.; Nitzan, A.; Hänggi, P. *J. Chem. Phys.* **2003**, *119*, 6840–6855.

[19] Leitner, D. M. *Phys. Rev. B* **2001**, *64*, 094201.

[20] Yue, Y.; Qasim, L. N.; Kurnosov, A. A.; Rubtsova, N. I.; Mackin, R. T.; Zhang, H.; Zhang, B.; Zhou, X.; Jayawickramarajah, J.; Burin, A. L.; Rubtsov, I. V. *J. Phys. Chem. B* **2015**, *119 (21)*, 6448–6456.

[21] Rubtsova, N. I.; Qasim, L. N.; Kurnosov, A. A.; Burin, A. L.; Rubtsov, I. V. *Acc. Chem. Res.* **2015**, *48 (9)*, 2547–2555.

[22] Kurnosov, A. A.; Rubtsov, I. V.; Burin, A. L. *J. Chem. Phys.* **2015**, *142*, 011101.

[23] Kurnosov, A. A.; Rubtsov, I. V.; Maksymov, A. O.; Burin, A. L. *J. Chem. Phys.* **2016**, *145*, 034903.

[24] Joachim, C.; Ratner, M. A. *Proc. Natl. Acad. Sci. U. S. A.* **2005**, *102*, 8801–8808.

[25] Wang, J.; Wang, J.-S. *Appl. Phys. Lett.* **2006**, *88*, 111909–111909.

[26] Haken, H.; Strobl, G. *Z. Phys.* **1973**, *262*, 135–148.

[27] Schwarzer, E. *Z. Phys. B Con. Mat.* **1975**, *20*, 185–193.

[28] Yu, X.; Leitner, D. M. *J. Phys. Chem. B* **2003**, *107*, 1698–1707.

[29] Schwarzer, D.; Kutne, P.; Schröder, C.; Troe, J. *J. Chem. Phys.* **2004**, *121*, 1754–1764.

[30] Schröder, C.; Vikhrenko, V.; Schwarzer, D. *J. Phys. Chem. A* **2009**, *113*, 14039–14051.

[31] Wang, Z.; Carter, J. A.; Lagutchev, A.; Koh, Y. K.; Seong, N.-H.; Cahill, D. G.; Dlott, D. D. *Science* **2007**, *317*, 787–790.

[32] Lin, Z.; Rubtsov, I. V. *Proc. Natl. Acad. Sci. U. S. A.* **2012**, *109*, 1413–1418.

[33] Tesar, S. L.; Kasyanenko, V. M.; Rubtsov, I. V.; Rubtsov, G. I.; Burin, A. L. *J. Phys. Chem. A* **2013**, *117*, 315–323.

[34] Benderskii, V. A.; Kats, E. I. *JETP Lett.* **2011**, *94*, 459–464.

[35] Benderskii, V. A.; Kotkin, A. S.; Rubtsov, I. V.; Kats, E. I. *JETP Lett.* **2013**, *98*, 219–222.

[36] Rubtsova, N. I.; Kurnosov, A. A.; Burin, A. L.; Rubtsov, I. V. *J. Phys. Chem. B* **2014**, *118*, 8381–8387.

[37] Rubtsov, I. V. *Acc. Chem. Res.* **2009**, *42*, 1385–1394.

[38] Kurochkin, D. V.; Naraharisetty, S. R. G.; Rubtsov, I. V. *Proc. Natl. Acad. Sci. U. S. A.* **2007**, *104*, 14209–14214.

[39] Skinner, J.; Hsu, D. *J. Phys. Chem.* **1986**, *90*, 4931–4938.

[40] Bulatov, A.; Kuklov, A.; Birman, J. L. *Chem. Phys. Lett.* **1998**, *289*, 261–266.

[41] Abramowitz, M.; Stegun, I. A. *Handbook of mathematical functions: with formulas, graphs, and mathematical tables*; Courier Dover Publications, 1972.

[42] Debye, P. *Math. Ann.* **1909**, *67*, 535–558.

[43] Watson, G. N. *A treatise on the theory of Bessel functions*; Cambridge university press, 1995.

[44] Chishtie, F.; Rao, K.; Kotsireas, I.; Valluri, S. *Int. J. Mod. Phys. D* **2008**, *17*, 1197–1212.

[45] Glowacki, D. R.; Rose, R. A.; Greaves, S. J.; Orr-Ewing, A. J.; Harvey, J. N. *Nature Chem.* **2011**, *3*, 850–855.

[46] Gruebele, M.; Wolynes, P. *Acc. Chem. Res.* **2004**, *37*, 261–267.

[47] Li, N.; Ren, J.; Wang, L.; Zhang, G.; Hänggi, P.; Li, B. *Rev. Mod. Phys.* **2012**, *84*, 1045.

[48] Weidinger, D.; Gruebele, M. *Mol. Phys.* **2007**, *105*, 1999–2008.

[49] Davydov, A. S. *Theory of molecular excitons*; McGraw-Hill Book Co.: New York, 1962.

[50] Lewis, F. D.; Zhang, L.; Liu, X.; Zuo, X.; Tiede, D. M.; Long, H.; Schatz, G. C. *J. Am. Chem. Soc.* **2005**, *127*, 14445–14453.

[51] Burin, A. L.; Armbruster, M. E.; Hariharan, M.; Lewis, F. D. *Proc. Natl. Acad. Sci. U. S. A.* **2009**, *106*, 989–994.

[52] Piseri, L.; Zerbi, G. *J. Chem. Phys.* **1968**, *48*, 3561–3572.

[53] Jishi, R.; Venkataraman, L.; Dresselhaus, M.; Dresselhaus, G. *Chem. Phys. Lett.* **1993**, *209*, 77–82.

[54] Liu, M.; Artyukhov, V. I.; Lee, H.; Xu, F.; Yakobson, B. I. *Acs Nano* **2013**, *7*, 10075–10082.

[55] Hasmy, A.; Rincón, L.; Hernández, R.; Mujica, V.; Márquez, M.; González, C. *Phys. Rev. B* **2008**, *78*, 115409.

[56] Dai, L.; Sow, C.; Lim, C.; Tan, V. In *Nanowires - Fundamental Research*; Abbass, H., Ed.; INTECH Open Access Publisher, 2011; Chapter 9, pp 183 – 202.

[57] Tereshko, V.; Gorchakov, A.; Tereshko, I.; Abidzina, V.; Red'ko, V. In *Advances in Biomaterials Science and Biomedical Applications*; Pignatello, R., Ed.; INTECH Open Access Publisher, 2013; Chapter 1, pp 2 – 21.

[58] Larade, B.; Taylor, J.; Mehrez, H.; Guo, H. *Phys. Rev. B* **2001**, *64*, 075420.

[59] Cretu, O.; Botello-Mendez, A. R.; Janowska, I.; Pham-Huu, C.; Charlier, J.-C.; Banhart, F. *Nano Lett.* **2013**, *13*, 3487–3493.

[60] Banhart, F. *Beilstein J. Nanotechnol.* **2015**, *6*, 559–569.

[61] Fischer, H. In *The chemistry of alkenes*; Patai, S., Ed.; John Wiley & Sons, 1964; Vol. 1; Chapter 13, pp 1025–1159.

[62] Landau, L. D.; Lifshitz, E. M. *Theory of Elasticity*, 3rd ed.; Pergamon Press, 1986.

[63] Nitzan, A. *Chemical Dynamics in Condensed Phases: Relaxation, Transfer and Reactions in Condensed Molecular Systems*; Oxford University Press, 2006.

[64] Cahangirov, S.; Topsakal, M.; Ciraci, S. *Phys. Rev. B* **2010**, *82*, 195444.

[65] Engel, G. S.; Calhoun, T. R.; Read, E. L.; Ahn, T.-K.; Mančal, T.; Cheng, Y.-C.; Blankenship, R. E.; Fleming, G. R. *Nature* **2007**, *446*, 782–786.

[66] Panitchayangkoon, G.; Hayes, D.; Fransted, K. A.; Caram, J. R.; Harel, E.; Wen, J.; Blankenship, R. E.; Engel, G. S. *Proc. Natl. Acad. Sci. U. S. A.* **2010**, *107*, 12766–12770.

[67] Borysenko, K.; Mullen, J.; Li, X.; Semenov, Y.; Zavada, J.; Nardelli, M. B.; Kim, K. W. *Phys. Rev. B* **2011**, *83*, 161402.

[68] Frisch, M. J. et al. Gaussian 09 Revision A.02. 2009; Gaussian Inc. Wallingford CT.

[69] Landau, L. D.; Lifshitz, E. M. *Quantum mechanics: non-relativistic theory*, 3rd ed.; Pergamon Press, 1977.

[70] Kittel, C. *Quantum theory of solids*; Wiley New York, 1963.

[71] Dziarmaga, J.; Smerzi, A.; Zurek, W.; Bishop, A. *Phys. Rev. Lett.* **2002**, *88*, 167001.

[72] Wilson, E. B.; Decius, J. C.; Cross, P. C. *Molecular vibrations: the theory of infrared and Raman vibrational spectra*; McGraw-Hill Book Company, Inc., 1955.

[73] Barone, V. *J. Chem. Phys.* **2005**, *122*, 014108.

[74] Januszewski, J. A.; Tykwinski, R. R. *Chem. Soc. Rev.* **2014**, *43*, 3184–3203.

[75] Chalifoux, W. A.; Tykwinski, R. R. *Nature Chem.* **2010**, *2*, 967–971.

[76] Tasumi, M.; Shimanouchi, T.; Miyazawa, T. *Journal of Molecular Spectroscopy* **1962**, *9*, 261–287.

Biography

Arkady Albertovich Kurnosov was born in 1981 in Petropavlovsk-Kamchatsky, Russia, on the Pacific Ocean coast. Graduated from a Shevah-Mofet high school in Tel Aviv, Israel in 1998. In 2004 graduated with Master Degree in Physics from the Lomonosov Moscow State University, Moscow, Russia. For a number of years worked as high school teacher at Liceum "Vtoraya Shkola" (School #2) in Moscow, Russia; won a "Dynasty" Foundation grand competition for physics and math young teachers in 2007, 2009. In 2009–2016 studied PhD program on the Department of Chemistry, Tulane University, New Orleans, LA, USA.